Assessing the role of digital aerial photogrammetry for characterizing forest structure and enhancing forest inventories

by

Tristan Robert Heinrich Goodbody

B.Sc. The University of British Columbia, 2014

A THESIS SUBMITTED IN PARTIAL FULFILLMENT OF

THE REQUIREMENTS FOR THE DEGREE OF

DOCTOR OF PHILOSPHY

in

THE FACULTY OF GRADUATE AND POSTDOCTORAL STUDIES

(Forestry)

THE UNIVERSITY OF BRITISH COLUMBIA

(Vancouver)

March 2019

© Tristan Robert Heinrich Goodbody, 2019

The following individuals certify that they have read, and recommend to the Faculty of Graduate and Postdoctoral Studies for acceptance, the dissertation entitled:

Assessing the role of digital aerial photogrammetry for characterizing forest structure and enhancing forest inventories

submitted by Tristan R.H. Goodbody in partial fulfillment of the requirements for

the degree of Doctor of Philosophy

in Forestry

Examining Committee:

Nicholas C. Coops
Supervisor

Peter Marshall
Supervisory Committee Member

Bruce Larsen
Supervisory Committee Member

Cindy Prescott
University Examiner

Mark Johnson
University Examiner

Additional Supervisory Committee Members:

Ken Day
Supervisory Committee Member

Supervisory Committee Member

Abstract

In order to sustainably manage forest resources, a contemporary, dynamic, and consistent description of their state and extent must exist. As well, there is a need for reliable information on the change to the forested land base to support future policy development and to act informatively on new and emerging issues. Experimentation and technological innovation have spurred remote sensing research to better characterize and inventory forests globally. This dissertation examines how, and to what extent, digital aerial photogrammetry (DAP) and associated spatial products are capable of informing forest planning and management. Alongside innovation in DAP, unmanned aerial systems (UAS) are becoming viable management tools for acquiring stereo-imagery. Fast operationalization, cost-effectiveness, and their ability to acquire high spatial and temporal resolution data sets makes UAS a niche operational inventory tool. To assess the capacity of these technologies, forests of differing stages of structural development, including post-harvest regeneration, and mature managed forest landscapes, were examined. DAP data from these sites were analyzed to determine how, and to what extent, standard and novel inventory attributes can be accurately derived under specific image capture and data model circumstances. I advocate and provide evidence throughout this dissertation that DAP is a technology with ample potential for integration into enhanced forest inventory (EFI) frameworks. This work elaborates on where, and under what conditions, DAP data is successful and limited in characterizing forests with the ultimate goal of improving information for operational, tactical, and strategic decision-making.

Lay Summary

Forest inventories are expensive, time consuming, and complex. Forest managers require datasets that will improve efficiency and cost-effectiveness of developing and updating forest inventories, while providing data that inform management decision making. The acquisition of aerial imagery and use of photogrammetry over forested landscapes has been commonplace in conventional forest inventory frameworks for decades. Emergent technologies such as digital aerial photogrammetry (DAP), where digital imagery are processed using computer algorithms to provide three-dimensional characterizations of forest structure, have shown promise for enhancing forest inventory data. In this dissertation, DAP data characterizing varying forest structures were analyzed to assess the potential of DAP to provide data products and analytical methods that can improve forest inventories. The role of DAP, with reference to its areas of success, limitation, and future directions, is discussed to provide insight into its potential use in enhancing forest inventories and improving forest resources management.

Preface

The research questions and objectives of this dissertation were originally conceived from discussion between my supervisory committee and myself. Chapters of this dissertation are derived from a variety of co-authored studies in peer-reviewed journals. Co-authors Ken Day, Patrick Crawford, Gaetan Pelletier, Grant McCartney, and David A. MacLean were responsible for providing data and context for case studies. I performed the primary research, data analysis and interpretation, and preparation of final manuscripts. Text and information in the dissertation are derived from the following sources:

Chapter 1/2: **Goodbody, T.R.H**., Coops, N.C., White, J.C., 2018. Digital aerial photogrammetry for updating area-based forest inventories: A review of opportunities, issues, and future directions. Current Forestry Reports. (*In Press)*

Chapter 3/8: **Goodbody, T.R.H**., Coops, N.C., Marshall, P., Tompalski, P., Crawford, P., 2017. Unmanned aerial systems for precision forest inventory purposes a review and case study. For. Chron. 93, 71–81.

Chapter 4: **Goodbody, T.R.H**., Coops, N.C., Hermosilla, T., Tompalski, P., Pelletier, G., 2018. Vegetation Phenology Driving Error Variation in Digital Aerial Photogrammetrically Derived Terrain Models. Remote Sens. 10, 1554.

Chapter 5: **Goodbody, T.R.H**., Coops, N.C., Hermosilla, T., Tompalski, P., Crawford, P., 2018. Assessing the status of forest regeneration using digital aerial photogrammetry and unmanned aerial systems. Int. J. Remote Sens. 39, 5246–5264.

Chapter 6: **Goodbody, T. R.H**., Coops, N. C., Hermosilla, T., Tompalski, P., McCartney, G., & MacLean, D. A. 2018. Digital aerial photogrammetry for assessing cumulative spruce budworm defoliation and enhancing forest inventories at a landscape level. ISPRS Journal of Photogrammetry and Remote Sensing, 142, 1-11.

Chapter 7: **Goodbody, T.R.H**., Coops, N.C., Tompalski, P., Crawford, P., Day, K.J.K., 2016. Updating residual stem volume estimates using ALS- and UAV-acquired stereo-photogrammetric point clouds. Int. J. Remote Sens. 1161.

Table of Contents

Abstract ..... **iii**

Lay Summary ..... **iv**

Preface ..... **v**

Table of Contents ..... **vi**

List of Tables ..... **x**

List of Figures ..... **xii**

List of Abbreviations ..... **xviii**

Acknowledgements ..... **xx**

Dedication ..... **xxii**

Chapter 1: Rationale and foundation for research 1

1.1 Forest inventory needs 1

1.2 Inventory update 2

1.3 Airborne laser scanning and enhanced forest inventories 4

1.4 Enhanced forest inventories: Challenges and opportunities 8

1.5 Objectives and fundamental dissertation themes 10

1.6 Research questions 11

1.7 Dissertation overview 13

Chapter 2: Digital aerial photogrammetry and its role in updating area-based forest inventories 15

2.1 Photogrammetry and digital aerial photogrammetry 15

2.2 Area-based EFI update using DAP data 33
2.3 DAP data for forest inventory: A summary of quantitative findings..... 33
2.4 Summary 40
Chapter 3: Unmanned aerial systems and their growing role in forest management 41
3.1 Unmanned aerial systems 41
3.2 UAS applications for forestry 49
3.3 Summary 52
Chapter 4: Vegetation phenology driving error variation in digital aerial photogrammetrically derived terrain models..... 54
4.1 Background and motivation 54
4.2 Materials and methods 57
4.3 Results 65
4.4 Discussion 72
4.5 Conclusions 76
Chapter 5: Assessing the status of forest regeneration using digital aerial photogrammetry and unmanned aerial systems..... 77
5.1 Background and motivation 77
5.2 Study sites 79
5.3 Methods 81
5.4 Object based image analysis 85
5.5 Results 88
5.6 Discussion 95
5.7 Conclusions 101

Chapter 6: Digital aerial photogrammetry for assessing cumulative spruce budworm defoliation and enhancing forest inventories at a landscape level 103
6.1 Background and motivation 103
6.2 Methods 108
6.3 Sampling stratification 114
6.4 Field measurements 115
6.5 Cumulative defoliation analysis 116
6.6 Area-based approach for estimating forest inventory attributes 118
6.7 Results 119
6.8 Discussion 123
6.9 Conclusions 128
Chapter 7: Updating residual stem volume estimates using ALS and DAP point clouds 130
7.1 Background and motivation 130
7.2 Materials and methods 133
7.3 Results 138
7.4 Discussion 145
7.5 Conclusion 150
Chapter 8: Updating individual tree heights and volumes using DAP 151
8.1 Background and motivation 151
8.2 Results 154
8.3 Discussion 157
8.4 Conclusions 162
Chapter 9: Conclusions 163

9.1 Dissertation objectives 163

9.2 Research innovations 168

9.3 Research limitations 169

9.4 Future directions 173

9.5 Closing statement 180

Bibliography 181

Appendices 216

List of Tables

Table 1: Imagery acquisition dates and corresponding mean flight altitude (above ground level), mean ground sample distance, mean sun angle from nadir, and mean DAP point density. 61

Table 2: Summary statistics of the differential error per flight for the entire study site as well as only the road validation section of the analysis. 69

Table 3: Total number of samples for each class within each classification along with mean and standard deviations within and among classifications for the Nakusp Site. 88

Table 4: Total number of samples for each class within each classification along with mean and standard deviations within and among classifications for the Quesnel Site. 88

Table 5: Confusion matrices comparing reference and classification data for the Nakusp site for (a) 5 YSP, (b) 10 YSP, and (c) 15 YSP. 90

Table 6: Confusion matrices comparing reference and classification data for the Quesnel site for (a) 5 YSP, (b) 10 YSP, and (c) 15 YSP. 91

Table 7: Most frequently selected metrics, their type, and the number of times they were selected in Random Forest classifications. 95

Table 8: Imagery acquisition parameters. 110

Table 9: Spectral vegetation indices produced using raw imagery bands (B1 = Red, B2 = Green, B3 = Blue, B4 = NIR). Spectral type of index is listed as visible (Vis), near infrared (NIR), or a combination of the two (Vis-NIR). 113

Table 10: Description and codification of features extracted by FETEX 2.0 taken from Appendix A of Ruiz et al. (2011). GLCM refers to the grey level co-occurrence matrix produced within the FETEX 2.0 software. Listed spectral and textural metrics were computed for each of the raw

bands and vegetation indices. Semivariogram metrics were computed using the raw NIR band. Further documentation on computational procedures can be found in Ruiz et al. (2011). 114

Table 11: Summary of PLS_{spec}, PLS_{struc}, and PLS_{comb} cumulative defoliation models. Coefficient of determination for each model were determined based on the inclusion of components. Best iterations of each model are displayed in bold with their associated explained variability (%), cumulative explained variability (%) with the addition of consecutive components, and cross-validated predicted root mean squared error (RMSE). Number of predictors is the number of spectral and/or structural metrics included in the final PLS models following variable elimination. 120

Table 12: Descriptive statistics produced for ALS and DAP point clouds. Elevation and strata metrics are comprised using combinations of first and all returns. 138

Table 13: Linear parameters and metrics used for T_1 ALS and T_2 DAP predictive volume models and $\Delta V_{Indirect}$ and ΔV_{Direct} volume change models. 144

List of Figures

Figure 1: Conceptual diagram outlining the structure of this dissertation. DAP – Digital aerial photogrammetry; UAS – Unmanned aerial systems; EFI – Enhanced forest inventory 12

Figure 2: Point cloud cross-section comparison of ALS (light green) and DAP (dark blue). ALS points can be seen characterizing internal forest structure and the ground surface, while DAP is limited to the outer canopy envelope. 16

Figure 3: Comparison between ALS (left) and DAP (right) point clouds from the same sample plot near Williams Lake, BC. These data are described in detail in Chapter 7. 18

Figure 4: Flowchart listing the order of a theoretical digital photogrammetric workflow with associated research gaps for each stage. 24

Figure 5: Simplified visualization example of how DAP point clouds are generated from stereo-imagery. Point cloud generated using Pix4D software. These data were acquired near Nakusp, BC, and are described in detail in Chapter 5. 30

Figure 6: Schematic visualizing how normalization of T_1 ALS and T_2 DAP point clouds is conducted. ALS data is normalized using points classified as ground (top) to remove terrain influence. When the same concept is applied to DAP data (middle), however using DAP points classified as ground, data are prone to errors due to lack of accurate ground characterization by DAP. To solve this issue, ground points from T_1 ALS data are merged with T_2 DAP (bottom) and are used for normalization. 32

Figure 7: Result of literature review comparing %RMSE for ALS and DAP for the estimation of Volume, Height, Basal Area, and Diameter. Standard deviation (SD) % of ALS and DAP are presented for each attribute. Mean differences ($Diff_{mean}$) between ALS and DAP all indicate the average %RMSE difference for the attribute of estimation. %RMSE for DAP was higher for all

comparisons except for dominant height in Navarro et al. (2018), and basal area in Iqbal et al. (2019). Blank spaces indicate that a comparison of ALS and DAP for estimating that particular attribute did not take place for that study. Bohlin et al. 2012 [A], [B], [C] as well as Nurminen et al. (2013) [A], [B] are separate analyses conducted within the same study with varying acquisition parameters. Iqbal et al. (2019) compared small- [A], and medium-format [B] digital sensors. 36

Figure 8: Number of publications annually in the ISI Web of Knowledge for a general search on ["Unmanned Aerial System", "Unmanned Aerial Vehicle"] conducted in November 2018. 42

Figure 9: Aeryon Skyranger quadcopter operated by FYBR inc. - https://www.fybrsolutions.com/ 47

Figure 10: UAS-acquired imagery using SUNEX MT9F002 red-green-blue (RGB; true-colour) sensor at 100 m (a) and 200 m (b) above ground level 49

Figure 11: Methodological flow chart of photogrammetric processing, point cloud processing, and time series DTM analysis. 58

Figure 12: Study area on (a) 2017-05-25, (b) 2017-06-27, and (c) 2017-09-15, displaying the sparsely forested site used for DTM analysis and road validation area. The smaller, upper-most portion of the low cover forest area is comprised of short understory regeneration, while the larger section is sparsely forested with approximately 50 stems per hectare of juvenile mixed wood. Imagery used was acquired using a Sequoia multi-spectral camera and is displayed in a false colour composite of near infra-red, red, green. 59

Figure 13: Visualized error (m) for each DAP derived DTM listed by day of year relative to the reference ALS DTM. Grey colour indicates the full extent of the reference DTM. 67

Figure 14: Boxplots of DTM error by day of year, coloured by acquisition year. 68

Figure 15: Generalized additive mixed models for (a) vegetation cover, (b) mean error, and (c) proportional DAP coverage. Solid smoothed lines indicate the fitted GAMM models and dashed lines indicate standard error bounds. Green backdrop from day 178 to 281 indicate locations where mean DTM error exceeded 0.15 m. 71
Figure 16: Results of the best available terrain pixel analysis including (a) the optimal DTM, (b) composite error map, (c) donor pixel map, and (d) cumulative donor pixel frequency indicating the days of year with the least to highest frequency of donated pixels. Light grey colour indicates the full extent of the reference DTM, delineating areas with consistent 100% vegetation coverage. 72
Figure 17: Upper section: study area map detailing locations of Nakusp and Quesnel within British Columbia, Canada (a); Aeryon SkyRanger UAS used for imagery acquisition (b); example plot centre delineated with red spray-paint (c). Lower section: Quesnel stands 5 years since planting (YSP) (d), 10 YSP (e), and 15 YSP (f) and Nakusp stands 5 YSP (g), 10 YSP (h), and 15 YSP (i). Plot locations within each stand are delineated by black points. 81
Figure 18: Flow diagram detailing the methodological process used for field sample and imagery data acquisition, OBIA and classification, and structural, spectral, and temporal analysis. Graphical representation of RGB, visible vegetation indices, and canopy height model layer stack with UAS acquired imagery of a 3.99m radius sample plot in the Nakusp site on 13 June 2016 with red X plot centre demarcation (a), segmented object product of same layer stack with zoom inset (b), and final classified objects (c). 83
Figure 19: Scatter plot detailing the Spearman's correlation (r_s) between field measured representative height (m) and the maximum height from DAP plot point clouds. Solid diagonal represents the 1:1 line. 89

Figure 20: Aggregated plot level forest cover proportions in the Quesnel (a) and Nakusp (b) at 5, 10, and 15 YSP. 92
Figure 21: Mean height of conifer, deciduous, and ground features in Nakusp (a) and Quesnel (b) for 5, 10, and 15 YSP. 93
Figure 22: Distribution of object area coverage (m^2) and mean height (m) for 5, 10, and 15 YSP stands in the Nakusp site. The height of each bar represents the area of the canopy of trees with a mean height that fall within the range of the heights labelled on either side of the bars. 93
Figure 23: Mean brightness values for the green band (a, b) and the mean NGRDI (c, d) for 5, 10, and 15 YSP stands in the Nakusp and Quesnel sites. 94
Figure 24: Comparison of (a) UAS-acquired ortho imagery and (b) wall-to-wall classification for 5 years since planting stand in the Quesnel site. 97
Figure 25: Study area map detailing location of Kapuskasing within Ontario, Canada and landscape level extents of the Gordon Cosens Forest study area. Land cover and species information taken from a 2008 enhanced forest resource inventory and road features were provided courtesy of RYAM Forest Management. Current defoliation features for 2014 and 2015 were derived from annual sketch mapping surveys conducted by the Ontario MNRF Northeast Biodiversity and Monitoring Section. Final sample plot locations (n=30) are marked with triangles. 109
Figure 26: Analysis workflow starting with imagery acquisition, processing, implementation of stratified sampling, field measurement data collection, and forest modelling approaches and associated outcomes. Cumulative defoliation modeling, the primary objective of the study is outlined in bold. 112

Figure 27: Scatterplots for the PLSspec (a), PLSstruc (b), and PLScomb (c) PLS regression models. Solid diagonal line represents the 1:1 line..... 119
Figure 28: Circles of correlation comparing the first two components for the PLS_{spec} (a), PLS_{struc} (b), and PLS_{comb} cumulative defoliation PLS models. Metrics included in the model are written in bold with associated vectors indicating direction and magnitude of coefficient weights on the final model. Field measured cumulative defoliation samples are classified into three colour coded classes (low: 0 – 25%, moderate: 26 – 75 %, and severe: > 75%). The cumulative defoliation (CD) response variable with its associated correlation vector is depicted in blue, indicating direction and magnitude of correlation to the associated model predictor variables..... 122
Figure 29: Scatterplots for the predictive linear regression models for basal area (a) and volume (b). Solid diagonal represents the 1:1 line. 123
Figure 30: a) Landscape level prediction of cumulative defoliation (%) derived from the PLS_{spec} model. Zoom extents for areas A1 and A2 for cumulative defoliation (b,c), volume (m^3 ha^{-1}) (d,e), and basal area (m^2 ha^{-1}) (f,g). 124
Figure 31: Study area southeast of Williams Lake, BC (a) with UAS-acquired orthomosaic of compartment B (b) with inlay (d), and sub canopy image (c). 133
Figure 32: Framework for indirect and direct modelling approaches..... 138
Figure 33: Cartographical representation of (a, i) ALS derived canopy height model in 2013 (CHM_{T1}), (b, ii) UAS stereo-photogrammetric canopy height model in 2015 (CHM_{T2}), and (c, iii) their difference (CHM_{diff}) for compartment B. 141
Figure 34: Comparison of ALS and DAP metrics for (a) 5^{th}, (b) 25^{th}, (c) 50^{th}, (d) 75^{th}, (e) 95^{th} percentile of height (m), (f) mean height (m), (g) standard deviation of height (m), and (h) proportion of points above 2 m (%). 1:1 line is shown in each plot. 142

Figure 35: (a) T_1 ALS and (b) T_2 DAP predictive volume models. 1:1 line is shown in each plot. 143
Figure 36: (a) Indirect and (b) direct predictive volume difference models. 1:1 line is shown in each plot. 143
Figure 37: (a, i) T_1 ALS and (b, ii) T_2 DAP predictive volume wall-to-wall outputs for compartment B. 147
Figure 38: Canopy height model (CHM) height profile (m) of 2013 ALS (dark grey) and 2015 DAP (light grey) and associated point clouds denoted by circles. Treetops can clearly be identified in both data sets, outlining how the CHM local maxima were used to delineate crown extents and estimate heights. 154
Figure 39: Histogram of all 171 individually matched trees with their 2013 CHM gross volume (m^3) estimates (dark grey) and corresponding gross volume (m^3) increment estimates (light grey). The sum of the gross volume and increment equates to the CHM gross volume estimate for 2015. 155
Figure 40: Comparison of tree heights (m) for all ALS and DAP trees from the CHM (dark grey) and 95th percentile of height (light grey) along with tree growth statistics. 1:1 line shown. 156
Figure 41: Comparison of gross volumes (m^3) for all ALS and DAP trees from the CHM (dark grey) and 95th percentile of height (light grey) along with volume increase statistics. 1:1 line shown 156
Figure 42: Summary of where additional research is warranted to improve the potential of DAP for characterizing forest structure and enhancing forest inventories. 174

List of Abbreviations

ALS - Airborne Laser Scanning

AFRF - Alex Fraser Research Forest

ABA - Area Based Approach

BATP - Best Available Terrain Pixel

BC - British Columbia

CC - Canopy Cover

CHM - Canopy Height Model

CD - Cumulative Defoliation

DBH - Diameter at Breast Height

DAP - Digital Aerial Photogrammetry

DSM - Digital Surface Model

DTM - Digital Terrain Model

EFI - Enhanced Forest Inventory

GAMM - Generalized Additive Mixed Model

GPS - Global Positioning System

GCF - Gordon Cosens forest

GLI_x - Green Leaf Indices

GSD - Ground Sample Distance

NIR - Near-Infrared

NGRDI - Normalized Green Red Difference Index

OBIA - Object Based Image Analysis

PLS - Partial Least Squares

RGB - Red Green Blue

RMSE - Root Mean Squared Error

3D - Three-Dimensional

T_1; T_2 - Time 1; Time 2

UAS (a.k.a. Drones, UAV) - Unmanned Aerial Systems

VIP - Variable Importance for Projection

$VARI_g$ - Visible Atmospherically Resistant Index

VVI - Visible Vegetation Index

V_{T1}; V_{T2} - Volume Time 1; Volume Time 2

YSP - Years Since Planting

Acknowledgements

I first want to thank my supervisor and friend Dr. Nicholas C. Coops for his unrelenting support. I am extremely grateful to have had the opportunity to have been taught remote sensing theory from him in my undergraduate degree, and then have the ability to apply that knowledge at a graduate level. Nicholas is an exceptionally hard working scientist, who has provided me with superb guidance, knowledge, experience, and patience throughout my time as his student. Apart from remote sensing knowledge, Nicholas has helped me to learn more about teaching, time and people management, and the importance of being able to have a good time at work. Nicholas always made himself available to me when I needed advice and was prompt to provide constructive criticism to improve my work.

I am also extremely indebted to Dr. Piotr Tompalski and Dr. Txomin Hermosilla, whom I have considered mentors throughout my time as a graduate student. I have been very fortunate to be able to learn about remote sensing from these exceptionally knowledgeable scientists and friends. I applaud their patience with me throughout the learning process and being willing to share their expertise. You both embody the virtue of altruism.

Thank you to my parents Ruth and Quentin, and my sister Emma, for their unrelenting support and interest in my work. Your endless support, advice, and love have helped me to make it this far. Special thanks also goes out to my dog, Kyra, who offered me nothing but unconditional love at the beginning and end to each day. Thanks also to all my friends, particularly Dane, Mike, Austin, and Craig, who were supportive and interested throughout my graduate studies.

I thank Patrick Crawford and Mike Wilcox for their help, willingness to share data for numerous projects, friendship, and ongoing support. Further thanks to an anonymous

organization for providing funding for a portion of this research, and to NSERC for considering it worthy of scholarship.

Dedication

To my family, friends, and colleagues

Apologies for the jargon

Chapter 1:

Rationale and foundation for research

This chapter establishes the context for the greater body of work within this dissertation and outlines overall objectives and research questions. The contemporary needs of forest inventories are discussed, as well as opportunities and rationale for their continued modernization.

Rationale

1.1 Forest inventory needs

It is well known that forests are highly dynamic ecosystems undergoing perpetual successional changes through growth and natural disturbance (Forest et al., 1990; Oliver and Larson, 1996). Forest management information needs are increasingly complex and wide ranging including biodiversity, habitat, timber and non-timber values, riparian management, evolving forest practices legislation, and climate change amongst others (Corona, 2016). These needs place pressure on forest inventories to supply data that is timely, spatially detailed, accurate, and able to characterize forest composition, structure, and condition (Holopainen et al., 2014). The inherent complexity of forest ecosystems incentivizes the argument that routine data acquisitions to generate and update inventories are needed to capture and integrate knowledge of forest dynamics, improve forest

stewardship, and ultimately provide data driven justifications for forest and environmental policy (Franklin, 2001; Fridman et al., 2014; Gillis and Leckie, 1996)

As with other resource management fields, the demand for, and expectations of, inventory quality and content have compounded. Challenges like high up-front costs, complexity in data acquisition, and ongoing uncertainty surrounding the future state and condition of forests due to climate change are principle motivators for improving forest inventory frameworks (Barrett et al., 2016; Kangas et al., 2018; MacDicken, 2015). Globally, forest inventories at various spatial scales are continuing to shift toward multi-attribute, spatially-explicit polygon data derived from photo-interpretation and field measurement campaigns (Tomppo et al., 2010). Conventional methods involving combinations of aerial photography and reconnaissance sketch mapping missions, satellite imagery, and field surveys are common (Gillis and Leckie, 1996). Acquired inventory data, geographic information systems analysis, and statistical modelling outcomes focus on the provision of information on the current status, and projected condition of timber and non-timber resources.

1.2 Inventory update

While traditional methods have been effective, opportunities exist to modernize forest inventory frameworks (Holopainen et al., 2014). Ensuring completeness and currency, as well as designing adaptable frameworks that facilitate the routine updating of previously acquired data, is essential to enhancing inventory systems. Informed management decisions require data to be as current as possible (Tompalski et al., 2018).

The periodic updating of inventories for the purposes of improving projections is critical to understanding stand growth and development patterns, formulating viable economic projections, comprehending current and future socio-economic reliance on forest ecosystems, and framing forest policy initiatives. Organized monitoring and scheduled inventory updating is inherent to the effective stewardship of timber and non-timber forest values (Bolton et al., 2018; Gillis and Leckie, 1996; Hilker et al., 2008).

Inventory update is the process of detecting, collecting, and adding changes to an inventory resulting from disturbances causing depletions (harvesting, fire, insect defoliation etc.), as well as changes to the forest causing accretions (Gillis and Leckie, 1996). Bonnor and Magnussen (1987) add that depletions and accretions from land-use change need also be integrated. The two main data sources that facilitate updates are information that can be observed and mapped, such as harvesting boundaries and fire damage, and information that must be sampled and/or modelled such as permanent sample plots detailing growth, health, and compositional change (Bonnor and Magnussen, 1987). In order to perform updates, mapping products and detection of minimum levels of disturbance and growth must have acceptable levels of accuracy, and the frequency and timing of data acquisitions must be established. Decisions to update are primarily driven by a need for current information to support management planning and decision making, as well as regulatory requirements and/or reporting obligations (Gillis and Leckie, 1996).

1.3 Airborne laser scanning and enhanced forest inventories

While the currency and spatial completeness of inventories is critical for establishing inventory reliability, the data content of these inventories is also fundamental. Photo-interpretation and field measure campaigns are indelible parts of forest inventory frameworks; however, opportunity and substantial scientific justification exists for their continued technological modernization (Holopainen et al., 2015; McRoberts and Tomppo, 2007).

Structural forest characterizations using technologies such as airborne laser scanning (ALS) have been conducted to establish statistical relationships between forest structure and standard forest inventory attributes (Næsset, 2014; Tompalski et al., 2016). ALS systems, which have traditionally been attached to manned aircraft, are comprised of a global navigation satellite system, an inertial measuring unit, and a laser sensor (Wehr and Lohr, 1999). The satellite system provides accurate geo-spatial tracking of the sensor, while the inertial measuring unit records physical movements to make pitch, roll, and yaw corrections. A single pulse from an ALS system can be reflected from a number of different objects, resulting in several recorded points, often referred to as first, intermediate and last returns. This combination of points, commonly referred to as a point cloud, forms a highly accurate three-dimensional (3D) representation of objects on the ground, including the forest canopy, and provides information on individual tree heights, structural complexity, and terrain elevation (Wulder et al., 2008).

Linking spatial and structural information from ALS with traditional forest inventory plot data has brought about a paradigm shift in the conceptualization and implementation of forest inventories (Næsset, 2014, 2002a). Advances in ALS technology, driven largely by developments in sensor specifications, quality of data sets, and innovative forest management research, have been used to enhance forest inventory value through realizing measurement and estimation efficiencies (White et al., 2013a), cost-effectiveness (McRoberts et al., 2018), provision of a diverse and ever-increasing compilation of inventory data (Wulder et al., 2012), modelling estimates (White et al., 2017), and finalized mapping products (McRoberts and Tomppo, 2007). Herein, I refer to these inventory systems as enhanced forest inventories (EFI) (Bechtold and Patterson, 2005; Goodbody et al., 2017b; Tompalski et al., 2014; White et al., 2016).

A common justification for landscape-level ALS acquisitions is realizing operational cost savings. Apart from providing information related to above-ground vegetation structure, ALS data also provide terrain information in the form of a digital terrain model (DTM). Terrain is assumed to change very slowly, increasing DTM shelf-life within inventories and the long-term value of ALS data. ALS derived DTMs can provide highly accurate topographic data at unprecedented spatial resolutions (Furze et al., 2017). These DTMs, often considered best available terrain products, are invaluable as they offer detailed sub-metre accuracy information that can improve planning and management activities, including designing optimal road and skid trail networks, locating and delineating riparian ecosystems (Tompalski et al., 2017), and guiding programs related to

archaeological overview assessments (Wulder et al., 2008). DTMs also allow ALS point clouds to be analyzed relative to ground height, facilitating landscape level inventory attribute estimation using the area-based approach (ABA) (Næsset, 2002a; White et al., 2017). Fekety et al. (2015) demonstrated the temporal transferability of the ABA, and how pooling data across time increases their availability for improving inventory predictions. For the purposes of this dissertation we use the terms prediction and estimation interchangeably. Chapters 2, 6, and 7 elaborate further on the ABA to attribute estimation. EFIs, as described above, involve combining traditional inventory data with ALS technology. The increasingly high spatial and temporal accuracy of EFI data products, and 3D representation of forests from tree top through to ground level, provides managers with informative, accurate, and highly customizable representations of operating areas (Bechtold and Patterson, 2005). When contrasted with traditional inventories, EFIs provide an abundance of advantageous, non-traditional, structural forest characterizations that can be utilized to better inform forest management practices. Novel examples of these products and their methodologies are presented in Chapters 4-8. Likewise, these data sets can be joined with existing conventional inventory frameworks to establish EFI baselines, which describe the initial state of the forest for use as inputs for future predictions, as well as a reference to evaluate management prescriptions (Gillis and Leckie, 1996).

EFI data products are commonly produced at a standard grid-cell size, providing spatially and temporally explicit attribute predictions. These cell-level predictions have the potential to be summarised to stand-level information typically used in forest inventories,

while maintaining within-stand variability often unavailable through other means (White et al., 2017; White et al., 2013a; Wulder et al., 2012). The inclusion of forest structural data such as height percentiles and crown cover within inventories also provides a means to characterize and segment forested landscapes objectively and derive high resolution estimates of forest attributes. Wall-to-wall (over the entire area of interest) coverage of forest parameter estimates, such as tree height, volume, basal area, growth and yield projections, and photo-interpreted imagery polygons, are becoming increasingly common (Mulverhill et al., 2018; Næsset, 2007; Økseter et al., 2015; Tompalski et al., 2015; White et al., 2017). These products can be used to guide forest planning and management decisions, impacting socio-economic and environmental outcomes.

Remote sensing and forest management research using ALS data has shown that structural characterization of forests serves to improve inventory accuracy, precision, and spatial objectivity (Magnussen et al., 2012; McRoberts et al., 2018; van Leeuwen and Nieuwenhuis, 2010; Vastaranta et al., 2013b; White et al., 2016; Wulder et al., 2008). Integrating ALS into inventories has been demonstrated to provide multi-scale information to improve knowledge on landscape ecology and guide forest planning and management activities (Guo et al., 2017; Mulverhill et al., 2018; Næsset, 2007; White et al., 2013a); however, these data should not be viewed as a panacea. Field measurements and validation of remote sensing products is essential for ensuring reliability and improving future products (Frazer et al., 2011; Strunk et al., 2012). As a result, these data and associated products are increasingly becoming adopted and utilized in industrial forest management as

a means of enhancing inventory content, as well as bridging gaps between strategic, tactical, and operational inventories (White et al., 2016; Woods et al., 2011; Wulder et al., 2008). ALS data and its benefits within forest inventories are further elaborated upon in Chapters 7 and 8.

1.4 Enhanced forest inventories: Challenges and opportunities

One challenge related to the use of ALS within an EFI framework is how these data maintain their utility as they age. McRoberts et al. (2018) found that the shelf-life of ALS datasets used in a model-assisted framework was at least 10 years, helping to reduce long-term inventory costs, as well as maintain the accuracy and applicability of predictive attribute models. Their findings indicate that ALS data can provide value for at least several years after acquisition related to the landscape level quantification of forest attributes, as well as immediate cost savings through the provision of high quality DTMs. It is important to bear in mind that data shelf-life may change with disturbance type (anthropogenic or non-anthropogenic) and rate of change, as well as forest type. While these data provide obvious benefits to inventory systems, reliance on a single ALS data acquisition does not provide information on how forest vegetation is changing through time, perhaps one of the most critical tactical and strategic management directives (Tomppo et al., 2010). This theme, which is fundamental to this dissertation, is repeatedly addressed to outline the importance of updatable EFI frameworks for establishing linkages between inventories and forest management strategies.

A possible method to better incorporate forest dynamics into EFIs, and achieve a more holistic inventory framework, is through repeated ALS acquisitions (Alonzo et al., 2017; Andersen et al., 2014; Zhao et al., 2018). A critical factor for re-acquisition of ALS is ensuring that growth increments for targeted forests exceed the noise (precision) of instruments and any bias associated with the measurements (Wulder et al., 2008). An operational limitation is that repeat ALS acquisitions are often economically infeasible and scale dependent (Dees et al., 2012; McRoberts et al., 2018; Ullah et al., 2017). For example, acquisitions over vast forest tenures, and oppositely, local operational scale (< 100 ha) openings are impractical (Wulder et al., 2008).

Given the difficult economics, alternate technologies must be integrated to provide a means of cost-effectively and efficiently updating pre-established EFIs (Goodbody et al., 2016; Tompalski et al., 2018; White et al., 2016). In particular, Chapters 2, 7 and 8 speak to these limitations and discuss approaches to effectively supplement baseline EFIs.

A technology that has garnered significant interest due to its similarities with ALS is digital aerial photogrammetry (DAP) (Figure 1; Rahlf et al., 2017; Stepper et al., 2017; White et al., 2015). DAP and its underlying technologies, which are thoroughly reviewed in Chapter 2, are capable of generating spatially continuous, 3D data derived from digital stereo-imagery (Rahlf et al., 2017). These data, which have been referred to as 3D vision, structure from motion, image-based point clouds, image point clouds, photogrammetric point clouds, and digital stereo imagery in the literature, is a technology capable of characterizing

vegetation structure analogous to ALS data (Goodbody et al., 2016; Leberl et al., 2010; Ullah et al., 2017; White et al., 2015).

The primary focus of this dissertation is to critically review, analyze, and discuss DAP and its role in an EFI context. Reviews and analyses herein illustrate how DAP data can be integrated to provide estimates of standard and novel inventory attributes at differing stages of stand structure, as well as their potential for incorporation into EFI frameworks. Additionally, I discuss the importance of the development of unmanned aerial systems (UAS) as a platform for acquiring stereo-imagery for DAP production. Innovation in UAS technology is happening at a rapid rate, and merits a review such as that presented in Chapter 3. While this thesis remains predominantly agnostic with regards to acquisition platform, the current and future role of UAS for improving cost-effectiveness, precision, and efficiency of imagery acquisitions in a forest management context is elaborated in significant detail.

1.5 Objectives and fundamental dissertation themes

Given the promise of DAP technology for integration into EFI frameworks, in this dissertation I:

- Review, examine, and report on DAP's successes and limitations for characterizing forests of varying structures.
- Determine the role of DAP in generating, extrapolating, and updating EFI data.
- Assess DAP-derived inventory products and datasets for their potential to monitor, update, and expand inventory knowledge, as well as inform multi-level forest management initiatives.

1.6 Research questions

To address the above themes, I pose the following research questions (Figure 1):

1. What is the state of DAP research with regard to enhancing forest inventories, and what is the capacity to create, update, and monitor EFIs in maturing stands using DAP?
2. How does seasonal timing of DAP acquisitions influence its ability to provide accurate terrain information in sparsely forested openings?
3. Can temporal and spatial knowledge of forest regeneration be improved using DAP?
4. What are the values of DAP spectral and structural metrics for spatially modelling biotically disturbed stands and standard inventory attributes?
5. What are the drivers for acquiring DAP data using UAS?

By addressing these research questions, I outline the potential of DAP to provide novel datasets and approaches for supplementing EFI data for various forest structure conditions.

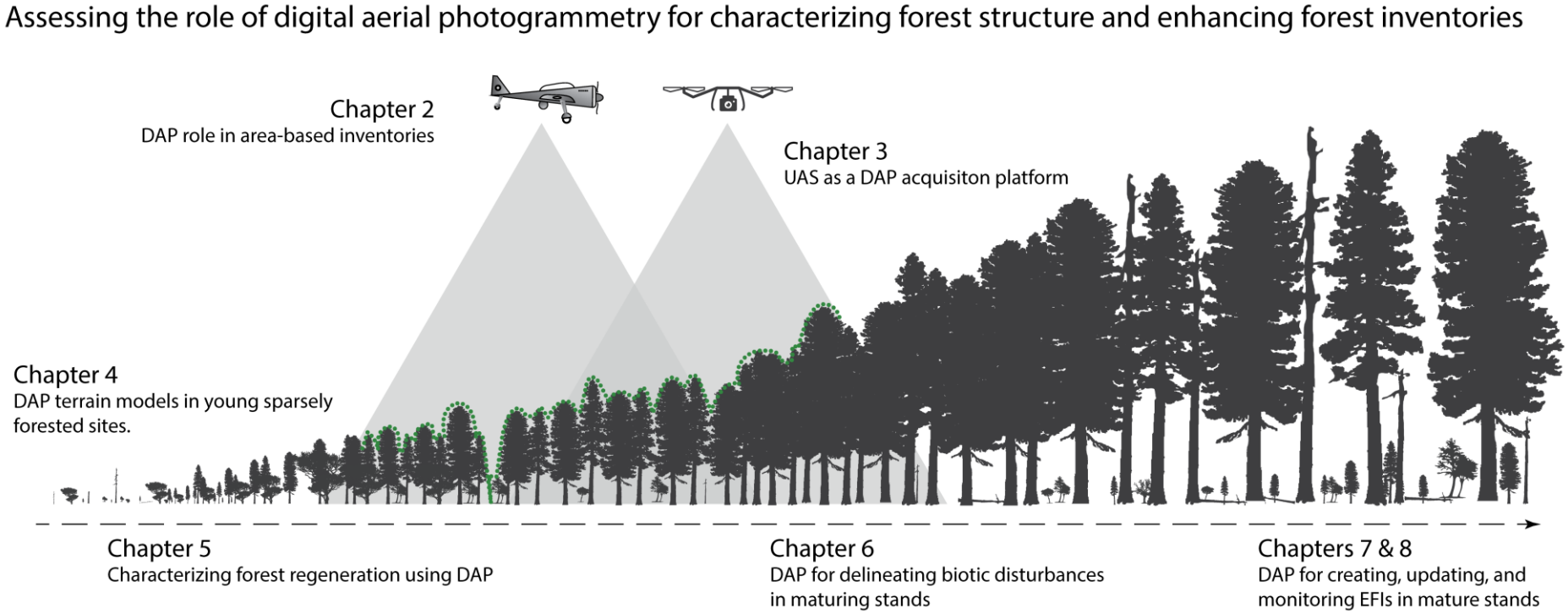

Figure 1: Conceptual diagram outlining the structure of this dissertation. DAP – Digital aerial photogrammetry; UAS – Unmanned aerial systems; EFI – Enhanced forest inventory

1.7 Dissertation overview

Chapter 2 reviews DAP technology and its integration into forest inventories to generate accurate and reliable data models and products. This chapter focuses on how DAP has major potential as a technology for updating ALS generated EFIs to form an effective inventory framework.

Chapter 3 reviews UAS as a viable platform to acquire forest inventory data, with a focus on stereo-imagery acquisition and DAP. UAS technology and its use within a forest management context is outlined to better understand the role this tool will play in future management and planning scenarios. Chapter 2 and 3 both look to establish a knowledge foundation for consequent analytical chapters.

Chapter 4, the first analytical chapter in this dissertation, focuses on how seasonality and vegetation phenology influence the ability of DAP to generate accurate terrain models in a sparsely forested, deciduous dominated stand. The potential of utilizing multi-temporal DAP data is addressed in this chapter, outlining the benefits of both DAP and UAS.

Chapter 5 assesses the potential of DAP and UAS to be used to spatially, structurally, and spectrally characterize forest regeneration to provide novel data products to improve silvicultural management strategies and establish a means of multi-temporal monitoring.

Chapter 6 compares the relative effectiveness of DAP's structural and spectral metrics for characterizing cumulative eastern spruce budworm (*Choristoneura fumiferana*) defoliation. The value of structural metrics for modelling standard forest inventory attributes at a landscape level is also explored. DAP's provision of both spectral and structural metrics are analyzed to determine the benefits of both data types from stereo-imagery acquisitions.

Chapters 7 and 8 use DAP as a means of updating an ALS EFI baseline. Chapter 7 approaches the potential of DAP to update residual timber volume estimates by applying the area-based approach (ABA), while Chapter 8 addresses the ability of DAP to update ALS EFIs at an individual tree level. These chapters outline the potential for synergy between ALS and DAP technologies to facilitate periodic and effective EFI updates.

Chapter 9 offers conclusions with reference to research themes and questions, outlines limitations, and presents future research opportunities for area-based EFI update using DAP data.

Chapter 2:

Digital aerial photogrammetry and its role in updating area-based forest inventories[1]

2.1 Photogrammetry and digital aerial photogrammetry

At its most basic level, application of photogrammetry in inventories involves identifying a common location, such as a tree or road intersection, in two or more overlapping images (McGlone et al., 2004). Typically, an aircraft with a mounted camera would follow a flight path to ensure total coverage of a given forest area while acquiring images with sufficient overlap (Tao et al., 2011). Upon completion, adjacent aerial images are overlaid and analyzed stereoscopically to outline timber resources and terrain characteristics in 3D.

DAP utilises this concept; however, instead of a photo interpreter identifying common objects manually, conjugate pixels are located in overlapping images with photogrammetric software. When conjugate pixel pairs are located, a line, or ray, is superimposed from the vantage point of the camera to their location for each image. The intersection of all rays for one pixel determines its 3D position. This is done for each pixel in all overlapping aerial images using an image-matching algorithm such as semi-global matching (Hirschmüller, 2005). Once complete, pixels are plotted in 3D space in the form of a point cloud (Figure 2). These point

[1] The content of this chapter has been adapted from:
Goodbody, T.R.H., Coops, N.C., White, J.C., (2018). Digital aerial photogrammetry for updating area-based forest inventories: A review of opportunities, issues, and future directions. Current Forestry Reports. (*In Review)*

clouds share multiple similarities to those produced using ALS; however, image pixels are used instead of directed light energy (White et al., 2015).

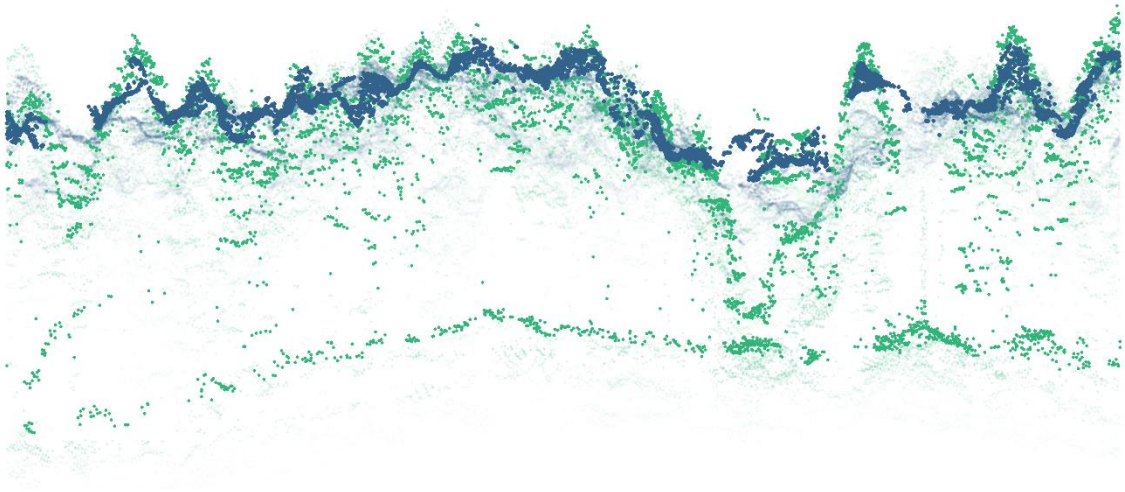

Figure 2: Point cloud cross-section comparison of ALS (light green) and DAP (dark blue). ALS points can be seen characterizing internal forest structure and the ground surface, while DAP is limited to the outer canopy envelope.

The incorporation of DAP for enhancing forest inventories is logical for a number of reasons:

- Stereo-photogrammetry has a long-standing history in forest management (Spurr, 1954), enabling characterization of terrain, forest cover, and species data, amongst others (McGlone et al., 2004; White et al., 2016).
- The use of aerial imagery for photo-interpretation of land cover and detailed forest cover is commonplace in forest inventory systems globally (Tomppo et al., 2010). These imagery datasets are integrated to provide spatially linked ecological information for the purposes of data driven resources management approaches as well as informing federal / international reporting obligations (Kangas et al., 2018).
- The advent of ALS data in the late 1990s challenged the utility of photographs as the data source of choice for forest applications (Baltsavias, 1999), however renewed interest and investment in digital photogrammetry has occurred largely as a function of its capacity to derive 3D information similar to ALS at a fraction of the cost (Rahlf et al., 2017; White et al., 2015).

- The historical prominence and ongoing development of photogrammetry in the field of forestry, and resources management more generally, provide structural, spatial, and spectral information for the purposes of enhancing and updating forest inventories (Goodbody et al., 2018).

The relative advantages of ALS and DAP were first summarized by Baltsavias (1999). For DAP, key strengths continue to be the ability to acquire data from higher altitudes at faster speeds, thereby enabling data acquisition over substantially larger areas relative to that of ALS, for a fixed number of flying hours. DAP workflows are becoming increasingly automated (Remondino et al., 2014), relative costs are low (White et al., 2013b), and in many jurisdictions, photos are routinely acquired for alternative mapping projects (Straub et al., 2013), potentially providing an already established and funded method for photogrammetric data acquisitions. Key considerations are that acquisition and processing benchmarks have yet to be established, and that DAP is strongly influenced by shadows and occlusions from objects that can prevent image matching. DAPs major difference from ALS in the context of EFIs is that it is limited to characterizing the forest surface (Figure 3), as opposed to internal forest structure (White et al., 2015). DAP is however effective for conventional forest inventory processes such as manual interpretation tasks or stand boundary delineation.

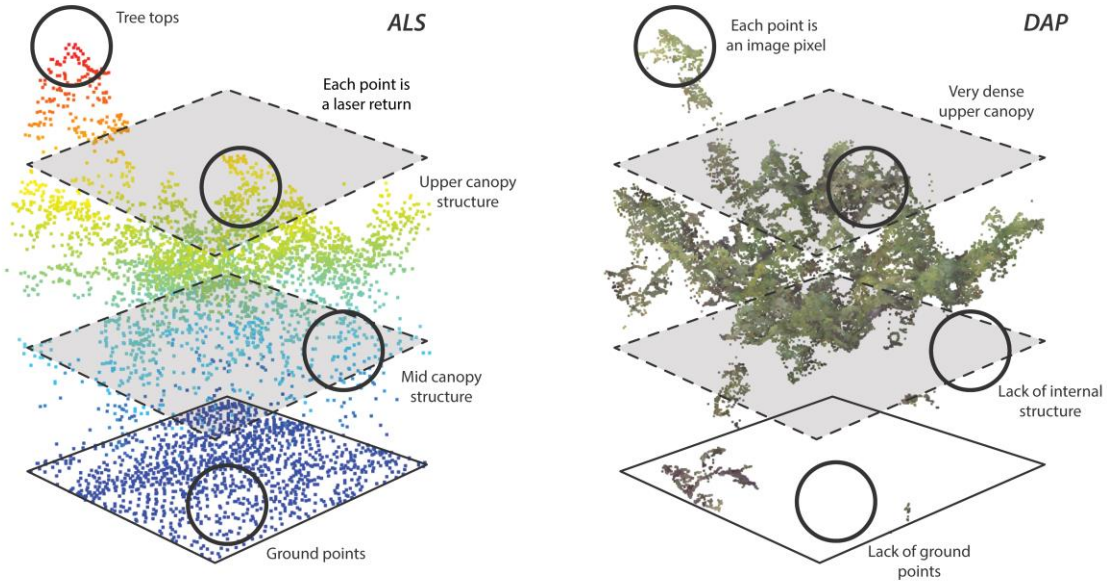

Figure 3: Comparison between ALS (left) and DAP (right) point clouds from the same sample plot near Williams Lake, BC. These data are described in detail in Chapter 7.

Like ALS, DAP point clouds also have the capability to generate DTMs; however, due to the fact that the technology is based on images, mapping accuracy declines under canopy (Holopainen et al., 2015). Consequently, it is recommended that ALS derived DTMs be used in forested areas if available. As elaborated upon in Chapter 3, due to the high cost of conventional aerial imagery from airplanes or helicopters, UAS are increasingly being used in the acquisition of high spatial resolution imagery for local operational tasks (Pajares, 2015). Low long-term capital costs, ease of use, and fast data acquisition are major drivers for their adoption (Tao et al., 2011). UAS have been proven to provide valuable data for surveillance, mapping, and 3D modelling applications at operational scales (Nex and Remondino, 2013).

2.1.1 Enabling technologies

A digital photogrammetric system or framework is comprised of computer hardware and software designed to generate photogrammetric products from digital stereo-imagery using a

combination of manual and automatic techniques. Rapid technological advancements and cost reductions for computer/platform hardware components have lowered the barriers-to-entry to conduct photogrammetric processing routines at spatial and temporal frequencies that were once cost-restrictive (Nolan et al., 2015). Increased availability and cost-effectiveness of high quality computer hardware has shifted the competitive edge of digital photogrammetry systems to being software driven with a variety of commercial and open source software available (Stone et al., 2016).

Although digital frame scanners (area-array sensors) have been predominantly used for photogrammetric surveying, some linear-array architecture sensors, also known as pushbroom or three-line scanners, have shown promise for stereo-image acquisitions (Table 1, Pepe et al., 2018; Pitt et al., 2014). These sensors incorporate forward, nadir- and backward-oriented overlapping panchromatic scenes that allow derivation of 3D products (Gruen and Li, 2002). Additional linear arrays have also been added to provide multispectral, as well as true and false-colour imagery (Petrie and Walker, 2007). Studies such as Haala et al. (2000), which compared the ability of frame and pushbroom sensors to generate DTMs and orthoimagery, found that both technologies are equally capable of generating accurate products, and that the choice of sensor type is more dependent on overall hardware and software costs, as well as performance of commercially available processing suites. In depth summaries and examples of contemporary linear- and area-array sensors can be found in Lemmens (2008) and Pepe et al. (2018).

Digital sensors provide improved radiometric performance, eliminate film processing costs, decrease physical storage space requirements, and facilitate highly automated workflows that greatly reduce the time needed to generate photogrammetric products (Kang et al., 2008; Leberl et al. 2010). Digital sensor technologies have also improved ground sample distances

(GSD) and image capture rates. These technological advancements have increased the number and quality of images being acquired, and consequently improved the potential for increased imagery overlaps. This means that more stereo-images are being captured at no additional cost, improving rates of successful image matching and survey cost-effectiveness. Increased image overlaps have also acted to reduce the need for dense ground control due to reductions in systematic and pseudo-systematic errors influencing photogrammetric measurement accuracy (Kraus, 2004). It must be added that although increases in along-track overlap can be realized without any added cost to surveying (Leberl et al., 2010), increasing across-track overlap would require more flight lines, driving up cost. This is why a high-overlap/flight efficiency trade-off exists, and must be balanced according to image parameter requirements.

Significant advancements in the quality and quantity of imagery through direct geo-referencing from high-quality onboard global positioning system (GPS)-derived positions and inertial navigation systems have led to improved accuracy of photogrammetric processing (Cramer et al., 2000). Unlike frame cameras, linear array systems must rely on GPS and inertial navigation systems for accurate position information. These components add cost to the overall image system (Haala et al., 1998; Meng et al., 2012). These technological innovations have provided a means of generating high density and accuracy point clouds for forest surveying (Leberl et al., 2010), while realized economic efficiencies can be attributed to imagery digitization.

2.1.2 Image-matching algorithms

Image matching algorithms are diverse, with a variety having been used to generate point clouds for the purposes of estimating structural attributes of vegetation and timber (Goodbody et al., 2018; Haala, 2014; Melin et al., 2017; Næsset, 2002b; Stepper et al., 2017; Ullah et al.,

2017). Algorithms can be separated into two distinct streams: feature- and area-based methods (Lowe, 2004; Remondino et al., 2014; Remondino and Menna, 2008; Zitová and Flusser, 2003). Feature-based methods, the simpler of the two types, use rudimentary cartographic points and lines to find image matches, while area-based methods use a moving window approach that analyzes pixel differences to find matching points (Kukkonen et al., 2017). A thorough history and description of the development, testing, and implementation of image matching algorithms can be found in Remondino et al. (2012, 2014). The performance of contemporary algorithms has invoked a renewed interest in aerial photography due to their provision of high resolution imagery and structural information at lower costs than ALS (Stone et al., 2016).

Software robustness, reliability, and speed is a rapidly advancing field, increasing competition amongst software developers (Hirschmüller, 2005; Smith et al., 2015; Stone et al., 2016). The proprietary nature of some algorithms however, raises challenges related to their functionality, where "black-box" transparency restrictions limit knowledge of the assumptions of inner workings of the algorithms, and reduce algorithm focused reporting (Remondino et al., 2012). A secondary challenge in using these algorithms is that they have not been purposefully developed to reconstruct vegetation for forest inventory purposes (Baltsavias et al., 2008), an area where continued research into algorithm refinement and benchmarking is warranted. The degree to which software can be parameterized is important for forest environments (among others). Parameters are often determined by trial and error and many are software specific. This poses challenges for large area implementations.

Many software packages implement some form of the semi-global matching algorithm (Hirschmüller, 2008, 2005). Semi-global matching is a fast and efficient image matching algorithm, and has been demonstrated to provide accurate image matching results with low

processing times (Dall'Asta, 2016; Hirschmüller, 2011). The inter-comparison of selected algorithms for the purposes of producing point clouds for forest attribute estimation has typically focused on a comparison of two software packages, rather than a systematic evaluation. Ullah et al. (2017) and Kukkonen et al. (2017) compared software in the context of the ABA for forest attribute estimation, for canopy cover estimation by Granholm et al. (2017), and for miscellaneous targets in Remondino et al. (2014). Both Ullah et al. (2017) and Kukkonen et al. (2017) found that image matching techniques were capable of generating standard forest inventory estimates such as timber volume with accuracies comparable to those of ALS.

In Ullah et al. (2017) the semi-global matching algorithm was found to outperform the enhanced automatic terrain extraction algorithm for generating information layers or thematic map products to aid forest management. Semi-global matching was found to be the simpler of the two algorithms, with less user defined parameters, faster processing speed, and higher overall accuracy. Kukkonen et al. (2017) compared semi-global matching to the next-generation automatic terrain extraction algorithm (Zhang, 2006), finding negligible differences in generated digital surface models (DSM), and indicated that both algorithms were capable and accurate at providing forest attribute estimates with the pre-condition that an ALS DTM was available. Granholm et al. (2017) compared the MATCH-T and SURE algorithms for estimating vertical canopy cover and found differences in point cloud outputs, but not in generated metrics. All studies, however, were cautious in their recommendation of a particular algorithm due to the potential differences that could arise from software tuning, forest type, and solar illumination.

2.1.3 Digital photogrammetric workflow

Prior to image acquisition and consequent photogrammetric processing, a number of factors must be considered for successful imagery acquisitions (Figure 4). Mission planning in

aerial photogrammetric projects is the primary and critical step to ensure success in consequent acquisition and processing stages (Pepe et al., 2018). Flight planning is likely the area that would most benefit from parameter benchmarking studies as it would help to improve overall cost-effectiveness and efficiency of acquisitions, while ensuring that consequent point cloud products are best suited to area-based estimation approaches. Pepe et al. (2018) provide an in-depth review of flight planning considerations for a variety of platforms, sensors, as well as commercially available and open source flight planning software. Similarly, Osborn et al. (2017) detail photographic componentry and settings, imaging sensors and platforms, and flight planning details with their advantages and disadvantages for photogrammetric mapping to support forest inventories. Research gaps presented in Figure 4 are discussed and elaborated upon in Chapter 9.

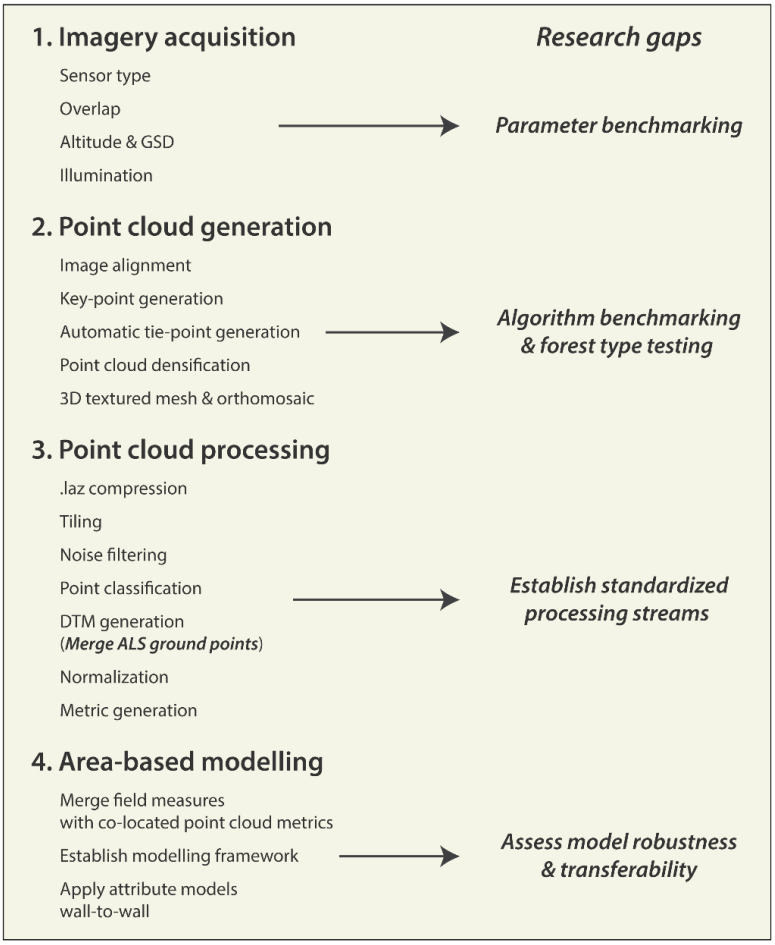

Figure 4: Flowchart listing the order of a theoretical digital photogrammetric workflow with associated research gaps for each stage.

2.1.4 Imagery acquisition

Landscape level imagery acquisitions for the purposes of forest inventory related photogrammetric analyses have been proven capable and effective for providing structural and spectral forest inventory information (Bohlin et al., 2012; Granholm et al., 2015; Honkavaara et al., 2009; Nurminen et al., 2013; White et al., 2013b). Aerial imagery acquisitions are often updated on a regular basis by national or regional mapping entities (Straub et al., 2013; Waser et al., 2008), further underwriting the costs of using these data in forest inventories, and making aerial images a dependable data source with temporal depth (St-Onge et al., 2008). The utilization of these datasets, which are often widely available, could be a useful and cost-

effective means for identifying and monitoring forest change, as well as realizing unforeseen inventory value.

Parameters of importance that have been tested in the literature that require continued benchmarking are flight altitude and GSD, across-track overlap, the type of sensor being used, and light conditions (Figure 4). Standardization and benchmarking studies that focus on these key parameters are therefore crucial to detailing best practice approaches to image acquisition. Given that the updating of EFIs is generally conducted at a landscape level, herein we focus on the use of manned aircraft for image acquisitions and their capacity to cost-effectively acquire imagery over large spatial extents (Leberl et al., 2010). The potential for UAS to be used as platforms for stereo-imagery acquisitions at a local operational scale is elaborated upon in Chapter 3.

2.1.4.1 Altitude and ground sample distance

Bohlin et al. (2012) tested multiple configurations of altitude (1200 / 4800 m) and GSD (0.48 / 0.12 cm) (Figure 7). The authors found that variation in GSD from lower flight altitudes generated denser point clouds, but did not improve tree height, basal area, or stem volume estimates. Similarly to results found in Lim et al. (2008) using ALS, Bohlin et al. (2012) concluded that plot-level variable estimation with DAP is robust, and that an increase in point density will not affect outcomes unless changes in forest structure occur. Honkavaara et al. (2012, 2013) found that GSDs of 30–40 cm provided surface models that adequately characterized leading forest cohorts. This could provide justification for increasing flight altitude to improve cost-effectiveness (Nurminen et al., 2013), however Gobakken et al. (2015) also highlight that the relationship between flight altitude, camera lens angle, and increasing GSD, can reduce height estimation accuracy.

Gobakken et al. (2015) note that while wide angle lenses provide increased overlap, especially at higher altitudes, that if image capture proximity is dispersed, point clouds will suffer from occlusion issues and become less accurate in estimating tree heights, a point that was confirmed by Tanhuanpää et al. (2016), who evaluated high altitude DAP data for individual tree detection. Furthermore, increased amounts of atmospheric noise at higher flight altitudes could increase error in estimates (Gobakken et al., 2015). Considerations regarding the need for completeness and height accuracy should guide acquisition planning and imagery capture (Lemaire, 2005). Järnstedt et al. (2012) conclude that differing requirements for ALS and DAP with regards to flying altitudes and distances between flight lines is potential justification for using imagery as a single data source to considerably improve inventory efficiency.

2.1.4.2 Image overlap

The most commonly used methods for planning imagery acquisitions involve flying in strips with a pre-determined level of along- and across-track overlap. Along-track overlaps between 60% - 80% are common for photogrammetric projects (Appendix A; McGlone et al., 2004), with values of 80% and above being used for improved penetration between objects for more effective and accurate depth reconstruction (Pepe et al., 2018), as well as to reduce the impact of shadows on image-matching algorithms (Baltsavias et al., 2008). Given that mission planning has generally focused on the acquisition of orthoimagery products and not digital photogrammetric analyses, imagery overlap has generally been lower than what is needed for complete point cloud derivation, potentially influencing area-based estimation capabilities. With digital camera systems, an increase in along-track overlap comes at no cost (Leberl et al., 2010). Several studies have demonstrated that an increase in along-track overlap from 60% to 80% reduces the relative root mean squared error (RMSE) for area-based attribute projections (Bohlin

et al., 2012; Nurminen et al., 2013; Puliti et al., 2017). It must be reiterated that a trade-off exists between image overlap, flight time, and increases in acquisition costs (St-Onge et al., 2015). Pre-planning of the most effective and efficient overlap for the desired data quality is therefore of great importance for utility, efficiency, and budgetary reasons.

Straub et al. (2013) concluded that imagery with overlaps of 65% and 30% along- and across-track respectively, are sufficient to support stereo-image matching and area-based outcomes, noting that increased overlap would likely improve other applications, such as detection of canopy gaps. White et al. (2018) compared the use of DAP and ALS data for canopy gap detection and mapping, concluding that point clouds generated from imagery with 60% along-track and 20% across-track could not provide analogous results to those of ALS for detecting canopy gaps in coastal rainforests on Vancouver Island, Canada. Indeed, the majority of imagery used for generating DAP point clouds for forest inventory applications are acquired with along-track overlaps of 60% and across-track overlaps that range between 20% and 35% (Appendix A), reducing the potential for multi-image matching. Further research into multi-image matching for reducing the influence of occlusions such as shadows is warranted (Haala et al., 2010; Nurminen et al., 2013; Vastaranta et al., 2013b). It may be that the best avenue to benchmarking and optimising overlap in differing forest types be conducted using UAS, as their ability to acquire imagery is fast, cost-effective, and can be parameterized to mimic aerial acquisitions (Frey et al., 2018).

2.1.4.3 Imaging sensors

Studies that have assessed the utility of DAP data for implementing the ABA have predominantly used large-format digital frame sensors, although Pitt et al. (2014) used a linear array system. Nurminen et al. (2013) outlined that flight efficiencies and significant cost-savings,

likely related to higher detail and larger film surface, can be realized when using large-format photogrammetric sensors. Straub et al. (2013) found that the frame-array sensors can be used to model inventory attributes in more structurally complex forests. Iqbal et al. (2019) compared photogrammetric approaches using small- and medium-format digital sensors. Their findings indicated that both sensors provide analogous results to those of ALS, providing rationale for managers to use data acquisition solutions that best fit operational needs. Conclusions from these studies indicate that forest inventories supported by an accurate pre-existing ALS DTM can be updated using optical imagery from a variety of sensors.

2.1.4.4 Illumination

The acquisition of imagery over portions of large forest tenures may be advisable. Gobakken et al. (2015) indicated that large-area imagery acquisitions for the purposes of generating an area-based DAP inventory may be prone to varying illumination conditions such as sun angle, which have been shown to influence the geometric properties of the generated DAP canopy (Baltsavias et al., 2008). White et al. (2015) and Rahlf et al. (2017), however found that sun angle had minimal influence on ABA outcomes. Rahlf et al. (2017) found that including sun inclination as a predictor reduced the relative RMSE of area-based predictions by ~2%. Variation in lighting conditions during a single flight could also be considered rationale for not incorporating spectral metrics as explanatory variables within forest parameter models unless rigorous radiometric calibration is possible (Rahlf et al., 2017). Systematic testing of the potential utility and importance of spectral metrics for estimating species-specific forest variables could help to improve forest management and planning (Bohlin et al., 2012; Honkavaara et al., 2009; Kukkonen et al., 2017; Puliti et al., 2017).

2.1.5 Point cloud generation

Following acquisition and compilation, acquired imagery must be photogrammetrically processed. Images are first optimized and aligned using meta-data including internal sensor specific information such as the focal length and field of view, as well as image specific external data such as GPS location and inertial measurement unit orientation. Image key-points, pixels or areas of interest with high contrast or texture that are easily identifiable in stereo-image sets, are then isolated within each image. The number of key-points that are compiled for an imagery dataset is dependent on the size of the images as well as its visual content. A landscape largely covered in snow with little spectral variation will likely yield less key point matches than a spectrally variable landscape.

Key-points are then matched amongst the image dataset and are consequently processed to derive their three-dimensional location, which are labelled as automatic tie-points. Manual tie-points can also be added, which are user defined markers that are often used to assess and improve 3D reconstruction accuracy. The result of the initial tie-point generation produces a low density DAP point cloud.

In order to increase the density of the output point cloud, automatic tie-point generation continues until pixel matching has reached a pre-determined limit, or is exhausted. Software packages generally have differing levels of automatic tie-point thresholds (Iqbal et al., 2018), which depending on available computational power increase the density of the output point cloud. The product following completion of densification is what will be exported and used for consequent point cloud processing and analysis (Figure 5). Generally however, the densified point cloud is used to generate a 3D textured mesh, a structural surface with image inherited spectral data, which is often used for the creation of orthomosaics to remove perspective

distortion from images and reflectance maps. The 3D textured mesh can also be described as a surface model.

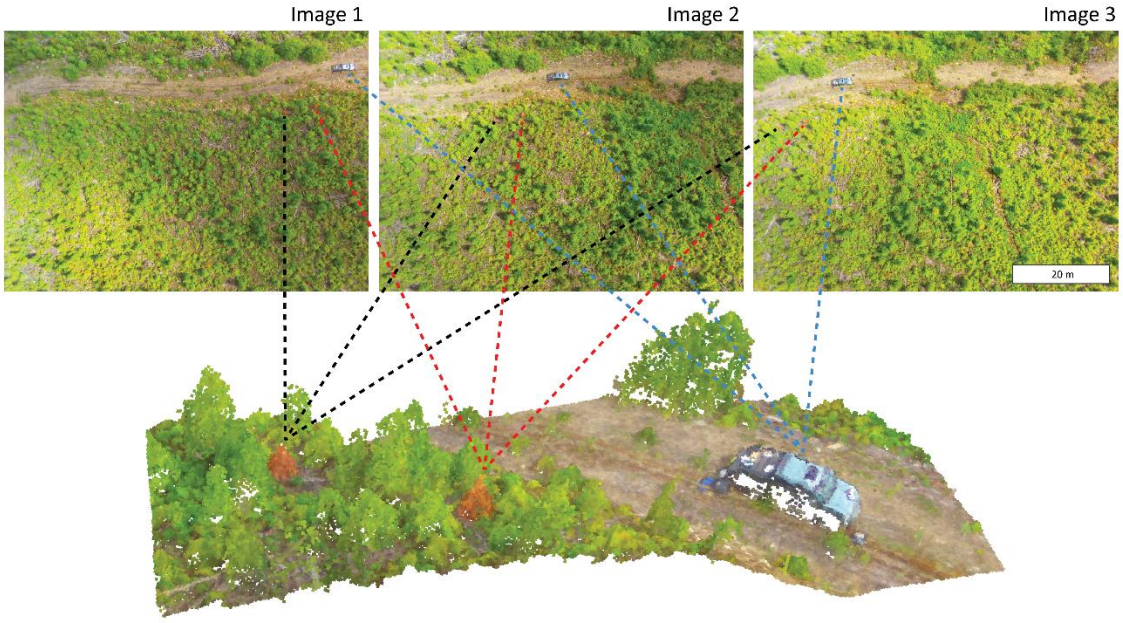

Figure 5: Simplified visualization example of how DAP point clouds are generated from stereo-imagery. Point cloud generated using Pix4D software. These data were acquired near Nakusp, BC, and are described in detail in Chapter 5.

2.1.6 Point cloud processing

Processing of densified DAP point clouds follow a similar stream to that of ALS. This is one of a number of reasons why the integration of DAP is logical for updating ALS EFIs. Major processing steps can be conducted as follows, however no common standards for point cloud processing have yet been established (Figure 4).

Exported densified point clouds, which are often stored as uncompressed *.las* format files (The American Society for Photogrammetry & Remote Sensing, 2011) are converted to compressed files (*.laz*) to improve processing speed and reduce digital storage requirements. This step is not mandatory, however is advisable as storage requirements can be reduced to 7 – 20% of original uncompressed file size (Isenburg, 2013). Converted files are then subdivided into tiles

with a pre-determined amount of overlap and processed individually to increase processing efficiency. Given that anomalies can occur in point cloud generation, tiles are filtered for noise that could introduce bias into future processing stages. Points within tiles are then classified into one of the ASPRS defined LAS classes (The American Society for Photogrammetry & Remote Sensing, 2011), which distinguish between ground, vegetation strata, and water amongst others. Points classified as ground are isolated and can be used to generate DTMs (Westoby et al., 2012).

A major limitation of DAP data is its inability to produce accurate DTMs over areas of moderate to high canopy cover (Goodbody et al., 2018; Tomaštík et al., 2017). DAP derived DTMs from forested areas are often inaccurate and are inadvisable as products for normalizing DAP point clouds to heights above ground level. Their use can potentially lead to inaccurate area-based estimates (Figure 6). Lack of the ability to provide accurate DTMs considerably limits the scenarios where DAP could be used to establish baseline EFIs. DTMs from other sources such as shuttle radar topography mission DTM products can be used (Goodbody et al., 2018), however will not provide results with the same reliability and spatial accuracy than ALS DTMs, which have the requisite spatial resolution and accuracy under canopy.

To remedy the issue of poor DAP derived DTM quality, co-located ALS derived DTMs can be integrated into the DAP processing stream for point cloud normalization (Bohlin et al., 2012; Goodbody et al., 2018; Granholm et al., 2015; Nurminen et al., 2013; Vastaranta et al., 2013; White et al., 2013b). Moreover, structural metrics derived from DAP point clouds that use the same terrain information for normalization to heights above ground readily facilitate multi-temporal comparisons, while improving the long-term value of ALS acquisitions. (Bohlin et al., 2012; Gobakken et al., 2015; Järnstedt et al., 2012; White et al., 2015).

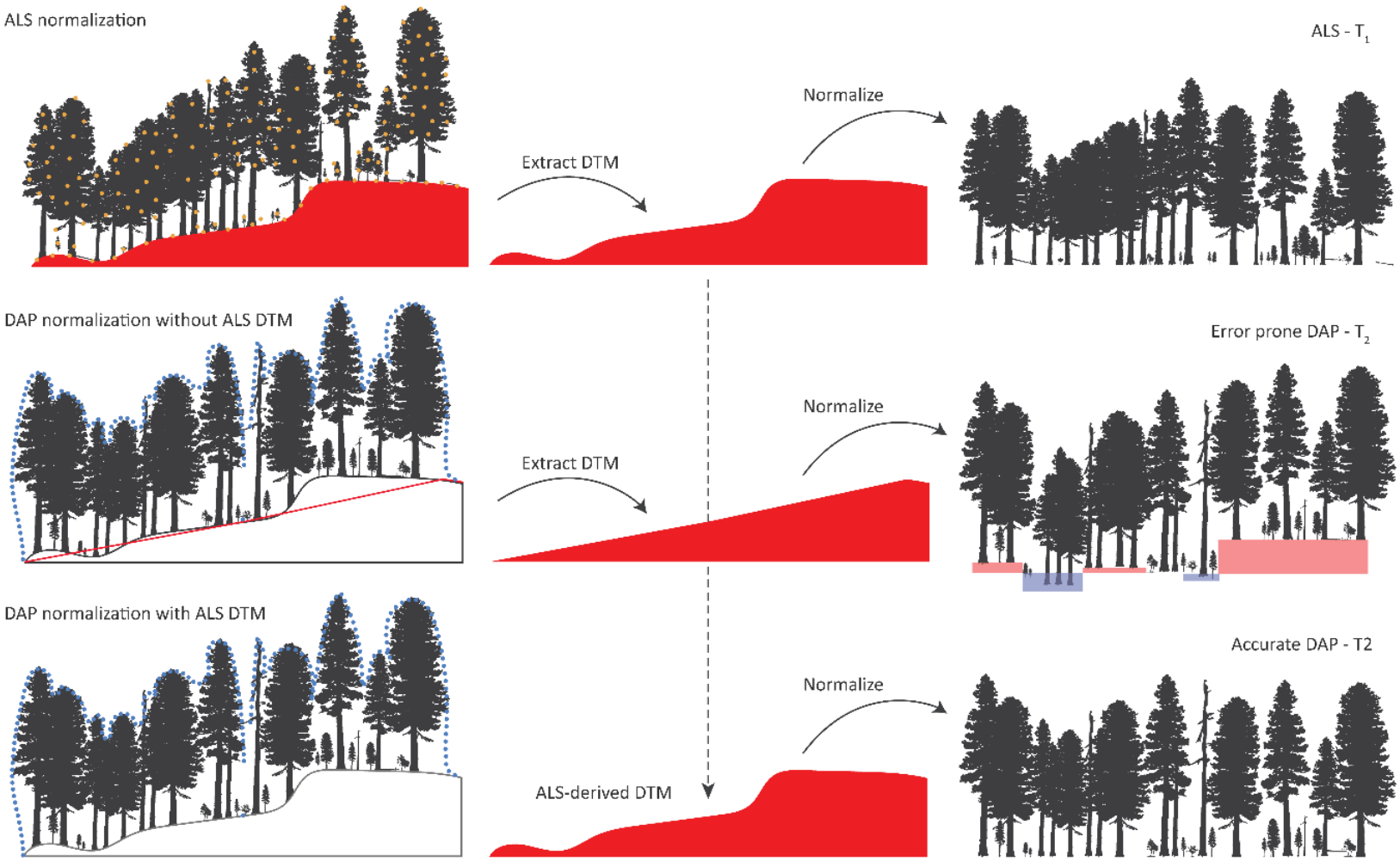

Figure 6: Schematic visualizing how normalization of T_1 ALS and T_2 DAP point clouds is conducted. ALS data is normalized using points classified as ground (top) to remove terrain influence. When the same concept is applied to DAP data (middle), however using DAP points classified as ground, data are prone to errors due to lack of accurate ground characterization by DAP. To solve this issue, ground points from T_1 ALS data are merged with T_2 DAP (bottom) and are used for normalization.

2.2 Area-based EFI update using DAP data

A DAP EFI updating framework would begin with assessing the effectiveness of baseline ALS strata to reflect stand growth as well as management and disturbance activity. Assessing the robustness of DAP data to generate similar strata to ALS should also be assessed. Specifically, calibration of canopy closure estimates is important for reliable change detection (Melin et al., 2017; Vastaranta et al., 2013b).

Following stratification and sample location, field measurement campaigns should be designed to ensure the acquisition of data to support area-based forest attribute modelling (White et al., 2013a, 2017). Attributes of primary interest have commonly included volume, basal area, height, stem density, and quadratic mean diameter (Bohlin et al., 2012; Puliti et al., 2017; Tompalski et al., 2018; White et al., 2015). Plot level point cloud metrics such as height and density are matched with corresponding field measurement data and used as predictors for parametric or non-parametric predictive models. The use of DAP spectral metrics as predictors, as used in Bohlin et al. (2012) and Puliti et al. (2017) could also be incorporated, however must be conducted with care due to the potential variation among flight imagery, and between successive imagery acquisitions (Rahlf et al., 2017; St-Onge et al., 2015). Following generation, models are applied wall-to-wall to enable landscape level mapping of attributes of interest with known error (Appendix A).

2.3 DAP data for forest inventory: A summary of quantitative findings

Preliminary studies looking to determine DAPs effectiveness for area-based attribute estimation used scanned analog photos with GSDs between 0.19 and 0.24 m. Næsset et al. (2002b) found that mean stand height underestimated true stand height by 5.42 m, and that

results were not superior to manual photogrammetric mensuration accuracies. Estimation bias was found to be influenced by image-matching parameters, stand age, and site quality. Similarly, St-Onge et al. (2008) also found that the accuracy of height estimates were influenced by image-matching parameters, as well as sun illumination, viewing geometry, and the complexity of the forest canopy. Correlations between ALS and DAP in St-Onge et al. (2008) were found to be highest in young forests. Results from these pioneering studies helped to establish a foundation for further photogrammetric forest inventory research, and highlight how DAP technology has changed since their publication.

The accuracy of attribute predictions using DAP are of comparable or higher quality than traditionally acquired inventories, while providing greater detail about their spatial distribution (Bohlin et al., 2012; Goodbody et al., 2016; Granholm et al., 2015; Nurminen et al., 2013; Rahlf et al., 2017; White et al., 2013b). Although studies vary dramatically in their parameterization, they form a solid basis for the decision to use DAP data for updating EFIs, as well as for continued research into effective acquisition and processing standards. A summary of studies comparing ALS and DAP attribute estimates are presented in Appendix A.

Studies comparing ALS and DAP estimation accuracies have predominantly taken place in Scandinavian boreal forest environments (Bohlin et al., 2012; Gobakken et al., 2015; Nurminen et al., 2013; Rahlf et al., 2015). Examples of large scale studies include Bohlin et al. (2017), which compared DAP and ALS attribute modelling over four 10,000 km^2 areas in Sweden, Rahlf et al. (2017), which examined a range of topographic and positional variables over a 25,000 km^2 area in Norway, and Tuominen et al. (2017), which assessed the potential contribution of structural DAP metrics to the Finnish Multi-Source National Forest Inventory over 5800 km^2. Authors outline the importance of understanding how well results translate to

differing forested ecosystems (Järnstedt et al., 2012). For example, Vastaranta et al. (2013b) achieved high estimation accuracies using DAP in southern Finland, however were hesitant to provide recommendations regarding DAP use in mixed-aged, multi-layered stands such as those used in White et al. (2015). Their reasoning was that small variations in landscape level stand structure resulted in low sample variance, and corresponding strong relationships with ALS and DAP metrics.

2.3.1 Height

Estimations of variables such as Lorey's mean height (Bohlin et al., 2012; Gobakken et al., 2015; White et al., 2015; Yu et al., 2015), mean height (Järnstedt et al., 2012; Nurminen et al., 2013; Vastaranta et al., 2013b), and top height (Pitt et al., 2014) using DAP were consistent across studies (Figure 7). Pitt et al. (2014), which was conducted in central Canadian boreal site, and White et al. (2015) in a coastal temperate rainforest found estimation accuracies similar to those in less complex forests in Scandinavia and Germany, indicating that DAP based estimates show some robustness to height measurements across forest types. Navarro et al. (2018) found that ALS %RMSE was slightly higher than that of DAP, the only height comparison where DAP was found to be more accurate than ALS.

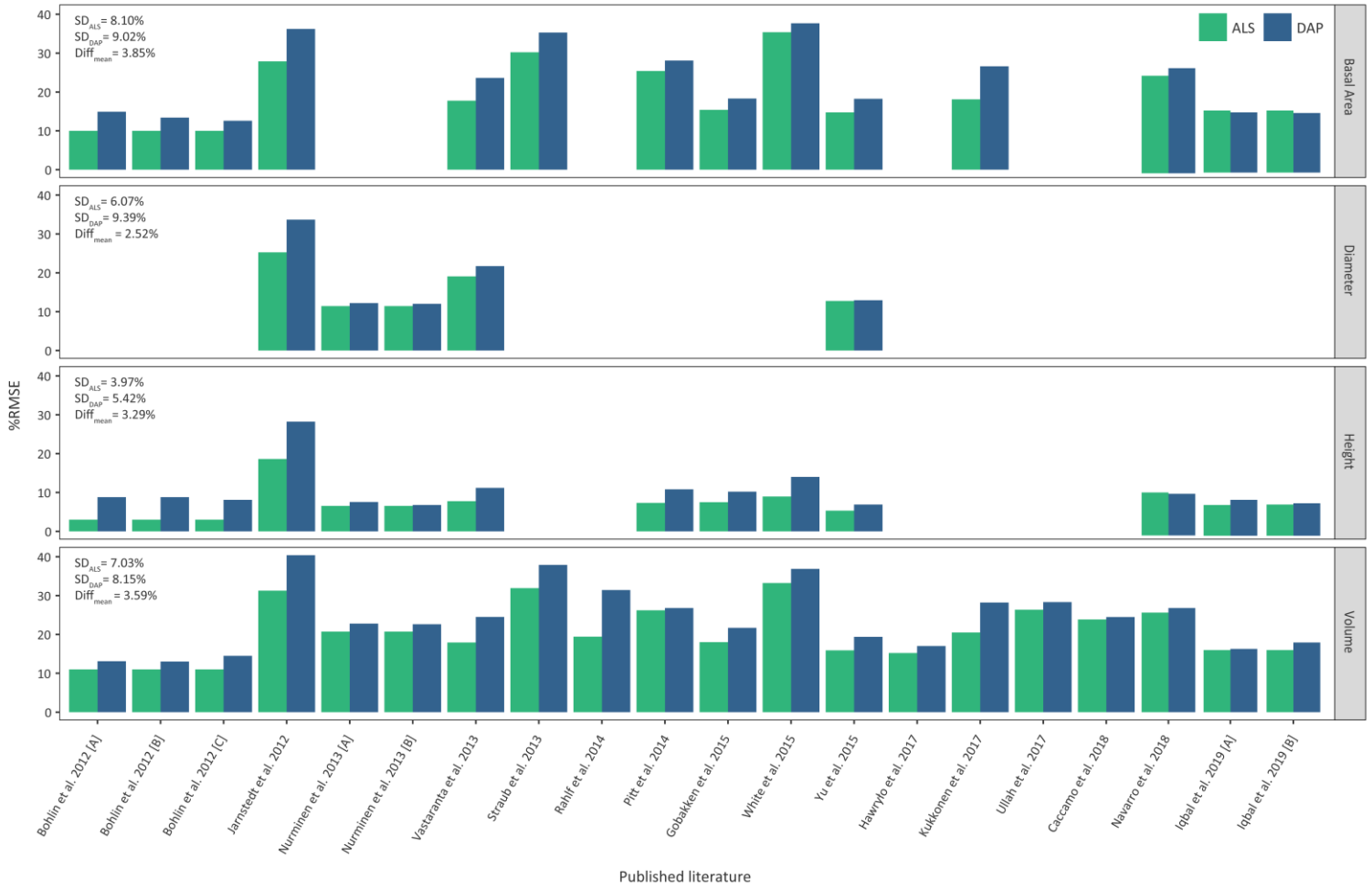

Figure 7: Result of literature review comparing %RMSE for ALS and DAP for the estimation of Volume, Height, Basal Area, and Diameter. Standard deviation (SD) % of ALS and DAP are presented for each attribute. Mean differences ($Diff_{mean}$) between ALS and DAP all indicate the average %RMSE difference for the attribute of estimation. %RMSE for DAP was higher for all comparisons except for dominant height in Navarro et al. (2018), and basal area in Iqbal et al. (2019). Blank spaces indicate that a comparison of ALS and DAP for estimating that particular attribute did not take place for that study. Bohlin et al. 2012 [A], [B], [C] as well as Nurminen et al. (2013) [A], [B] are separate analyses conducted within the same study with varying acquisition parameters. Iqbal et al. (2019) compared small- [A], and medium-format [B] digital sensors.

2.3.2 Density and stem diameter

The estimation of basal area (Järnstedt et al., 2012; Kukkonen et al., 2017; Pitt et al., 2014; Straub et al., 2013; Vastaranta et al., 2013b; White et al., 2015; Yu et al., 2015) and mean basal area (Bohlin et al., 2012), although larger in %RMSE than height estimates, were consistent across studies and comparable to their ALS counterparts. Iqbal et al. (2019) found that both small- and medium format sensors were comparable in accuracy to each other, as well as ALS (Figure 7). Their study found that basal area estimations using DAP had lower %RMSE values than ALS. Higher %RMSE values are expected for attributes such as basal area, which are dependent on variables such as stem diameter that cannot yet be directly measured by ALS or DAP. Studies using DAP to model mean diameter (Järnstedt et al., 2012; Nurminen et al., 2013; Vastaranta et al., 2013b), quadratic mean diameter (Yu et al., 2015), and diameter distributions (Penner et al., 2015) found very similar results between ALS and DAP estimates.

2.3.3 Volume

Comparisons for volume have been most common in the literature (Figure 7). Estimates of volume for ALS and DAP provide promising and consistent results, and although DAP is shown to have higher %RMSE, differences are generally small (Figure 7). Accurate and consistent volume estimates provide the ability to directly evaluate the economic worth of standing timber resources. This information can improve long-term

forest planning through maximizing revenue from harvesting operations, and delineating where and when operations should be conducted (Goodbody et al., 2017b).

2.3.4 Vertical complexity and cover

ALS and DAP characterize forest structure differently. Studies analyzing these differences have outlined that DAP height metrics often provide redundant information resulting from their high correlation. White et al. (2013b) found that the 10^{th} and 90^{th} percentile of height for ALS were not correlated, but that the same metrics were highly correlated for DAP. Lower height percentiles are generally found to be higher in the canopy for DAP, while higher percentiles are found to be comparable to their ALS counterparts. Nurminen et al. (2013) found that canopy cover metrics between ALS and DAP were all significantly different from one another, and that the density of DAP point clouds were predominantly higher than those of ALS, although this does not translate to higher accuracies.

Just as DAP's characterization of the outer envelope of the tree canopy limits its ability to provide reliable data on ground surfaces, it also limits its ability to provide statistical information on the internal structural complexity of forests (Figure 3). This could raise challenges where conventional ALS point cloud metrics do not provide analogous values using DAP, implying that existing ALS-based models may not be transferable with the same predictor set (White et al., 2015). This raises the need to utilize structural metrics

in model development that are similar between ALS and DAP to maximize potential for area-based model transferability (Stepper et al., 2017).

2.3.5 Cost considerations

It is well established that the cost of DAP acquisition is considerably lower than that of ALS, with estimation accuracies being similar (Bohlin et al., 2012; Hawryło et al., 2017; White et al., 2015). Results in Kangas et al. (2018) support this statement, concluding that the differences in accuracy can be considered negligible from a managerial perspective, especially if data will be used for 10 years or less, the approximate shelf-life of ALS data according to McRoberts et al. (2018). Kangas et al. (2018) assessed the value of ALS and DAP to support harvest scheduling. Both were found to be equally valuable although ALS was more precise. Given that economic losses and accuracy for both technologies were similar, it was recommended that DAP and ALS be considered analogous, and that the decision to acquire either data type should be dependent on availability, experience, project constraints / requirements, and cost rather than geometric properties of point density and accuracy (Kangas et al., 2018; Remondino et al., 2014). Notably, this study did not include the cost of the ALS DTM used to normalize the DAP data. Given that the provision of the ALS DTM is of major importance and motivation for data acquisitions, as well as being critical for DAP normalization, future studies should include its value within economic comparisons. Nurminen et al. (2013) suggested that airborne laser scanning could be replaced by DAP, with the presence of an ALS derived DTM.

2.4 Summary

DAP data have been proven accurate and cost-effective for estimating forest attributes using the ABA where high accuracy ALS DTMs exist. Analyses comparing area-based estimates for DAP and ALS have found that accuracies can be considered similar (although ALS data is generally more accurate), with DAP acquisitions being considerably less expensive relative to ALS. These findings highlight the potential role DAP can play in operational, tactical, and strategic forest inventory frameworks in a variety of forested environments. Although successful, I outline that further research and development into DAP acquisition parameters, image-matching algorithms, and point cloud processing streams are needed. Advances in these areas will help to further establish DAP as a logical data source for improving proactive forest management, and fill a gap for technologies capable of cost-effectively and accurately updating EFIs.

One such technology that has realized cost-effective, consistent, and accurate imagery data acquisitions that has witnessed a rapid increase in interest and investment in recent years are UAS, otherwise known as unmanned aerial vehicles, or drones (Figure 8). As briefly mentioned in this chapter, UAS have potential as a viable platform for acquiring high spatial and temporal resolution stereo-imagery datasets at local operational scales, as well as integration into DAP benchmarking experiments. The following chapter will review UAS technology in general, as well as detail its past use and future potential within an operational forestry context.

Chapter 3:

Unmanned aerial systems and their growing role in forest management[2]

3.1 Unmanned aerial systems

As DAP algorithms and sensor technologies continues to develop, acquisition platforms are seeing similar advances. With rapid technological innovation and an equally rapid adoption into commercial markets, UAS, and the wide range of compatible sensors, have become a viable tool for the acquisition of high quality imagery and forest inventory data (Goodbody et al., 2017b).

Primarily developed for military and espionage applications, UAS have become a popular multi-purpose tool for capturing high quality aerial data (Pajares, 2015) (Figure 8). UAS can operate at much lower altitudes and achieve finer spatial resolutions than conventional aerial and satellite surveying techniques (Zhang et al., 2016). Research and development of UAS have focused on the ability to miniaturize, automate and enhance navigation, improve payload potential, and maximize flight times. The emergence of a booming commercial UAS sector, fueled by increasing price competition and simplified flight technologies, projects to more than a quadrupling of sales in the next five years

[2] The content of this chapter has been adapted from:
Goodbody, T.R.H., Coops, N.C., Marshall, P., Tompalski, P., Crawford, P., (2017). Unmanned aerial systems for precision forest inventory purposes a review and case study. For. Chron. 93, 71–81.

(Peasgood and Valentin, 2015). Although problems and limitations exist currently, technological innovations in global navigation satellites and inertial navigation systems, digital camera and sensor technologies, geo-fencing and collision avoidance, and battery longevity, have allowed UAS to thrive, producing remote sensing information close to, or better than, conventional aerial methods (Colomina and Molina, 2014). These technologies have in a sense democratized remote sensing, allowing the public to acquire previously unattainable high quality data sets.

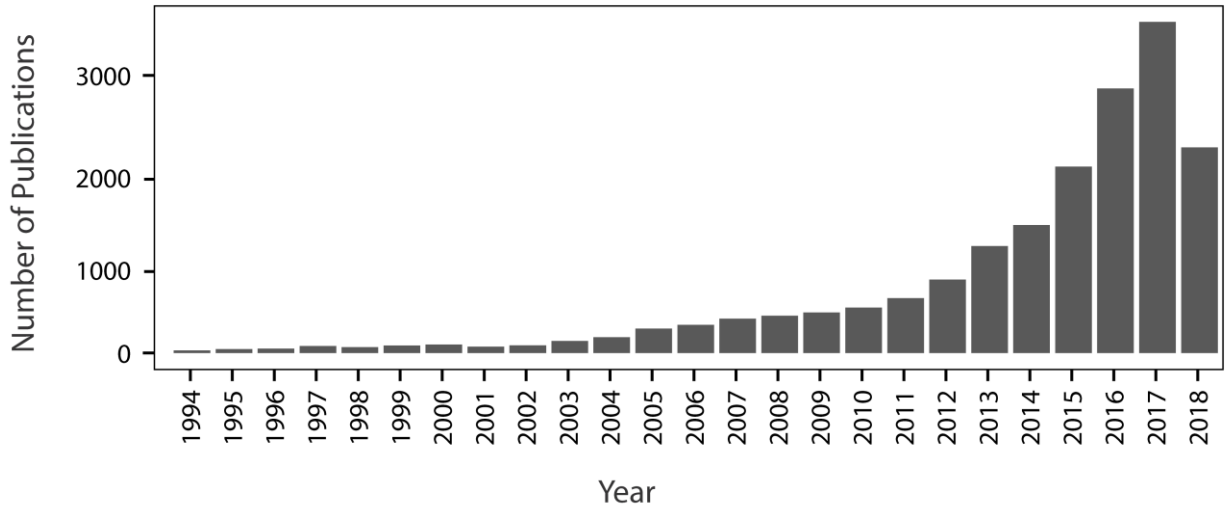

Figure 8: Number of publications annually in the ISI Web of Knowledge for a general search on ["Unmanned Aerial System", "Unmanned Aerial Vehicle"] conducted in November 2018.

Major factors promoting their adoption, as well as DAP point cloud use in operational forest management, have been ease of use, propensity for high spatial and temporal resolution data sets, and low long-term capital costs (Patias et al., 2017; Wallace et al., 2012a; Zhang et al., 2016). Global challenges currently surrounding the further adoption and implementation of UAS in resource management settings include propulsion longevity, limiting their ability to efficiently cover extensive areas, as well as line-of-sight

legislation (Clarke, 2014). The implementation of UAS is however well suited to improving managerial knowledge at a local operational scale, where they can be successful at updating previously acquired inventory data and establishing new inventory baselines (Goodbody et al., 2016, 2017a; Puliti et al., 2018a, 2018b).

Previous reviews of UAS technology, such as Pajares (2015), outline the significant potential of these systems for improving agricultural and forestry efficiency, earthquake and oil spill disaster response, and soil and aquatic systems monitoring. Similarly, Blyenburgh & Co (2014) provide a detailed review of optical remote sensing instrumentation, including active and passive visible, near-infrared (NIR), thermal infrared, and microwave sensors mountable on commercially available UAS.

In this chapter, I provide a condensed review as to why UAS platforms are increasingly being considered as platforms for the acquisition of high spatial resolution imagery and consequent provision of DAP point clouds. I then describe the past, current, and potential future roles of this technology within a forest inventory context. This chapter looks to provide a knowledge foundation for future analytical chapters (4, 5, 7, 8) within this dissertation that used UAS-acquired stereo-imagery datasets for DAP point cloud generation.

3.1.1 Airframes

The current UAS market is diverse in terms of airframe type, size, and performance (Blyenburgh & Co, 2014). In general, the capacity of UAS for aerial surveying or

geomatics purposes is determined by factors that are a function of size, including payload capacity, range, propulsion system, and cost (Stephens et al., 2000). Size classes, including micro, mini, standard, full size, and high altitude long endurance, largely define the potential for the UAS to perform desired tasks. In general, the majority of UAS used for resource management and geomatics purposes are in the micro and mini classes, also known as tactical UAS (Nex and Remondino, 2013).

Two major airframe types (fixed-wing and rotary) are available in these size classes and costs generally range between CAD $1,000-$150,000, depending on the sophistication of onboard instruments, propulsion system, payload capacity, airframe type, and flight autonomy. Lower end options are generally unable to perform autonomous flights, almost always require user assistance for take-off and landing, and are limited to specific sensor models (Nex and Remondino, 2013). As technology continues to develop, capabilities such as increased payload capacity to attach multiple sensors, improved range from battery or small engines, and completely autonomous pre-programmable flights are becoming more prevalent. Autonomous flight capabilities provide operators with a simple method of improving output data quality by maintaining flight elevation, speed, and trajectory (Siebert and Teizer, 2014).

3.1.2 Fixed wing platforms

Fixed-wing UAS consist of a single rigid wing with a predetermined aerofoil. Flight mechanics of fixed-wing UAS mimic conventional aeroplanes, where airspeed is generated

by a propeller powered by an electric motor or combustion engine. Maneuverability during flights occurs through manipulation of ailerons, an elevator, and a rudder to control the roll, pitch, and yaw. Advantages of these systems include simple maintenance, high flight speeds, and longer flight times, providing maximal area coverage at minimal costs. These characteristics make fixed-wing platforms ideal for larger scale mapping and surveying (Nex and Remondino, 2013). Limitations to these systems are that they generally require a launcher or runway, although more expensive vertical take-off and landing and short take-off and landing models can ameliorate these problems. Fixed-wing platforms are limited in that they must remain in a constant state of forward motion, nullifying their ability to collect imagery of objects that require stationary capture, such as hydro-electric or bridge inspection tasks (Montambault et al., 2010).

3.1.3 Rotary platforms

Rotary UAS have a high degree of mechanical complexity and customizability in terms of their hardware. Rotors attached to a fixed central mast allow the UAS to hover and fly in any direction. Rotor blades function in the same way as a fixed-wing aerofoil; however, their ability to produce their own movement facilitates lift and flight (Figure 9). Variation in thrust and torque of each rotor influences the overall movement of the UAS. The number of rotors on these platforms can range from one (helicopter), to three (tricopter), four (quadcopter), six (hexacopter), or even eight (octocopter) and above. Advantages of these systems are that they are capable of vertical take-off and landing,

allowing operators to launch in space limited environments and have responsive movement and hover capabilities making them very well suited to inspection-related tasks or where focus on specific objects is required (Montambault et al., 2010). The mechanically intricate designs of these systems can be disadvantageous as they require a higher degree of maintenance and larger draws on batteries or fuel to power. Comparatively high wind resistance, slower overall flight speeds, and increased power requirements mean these platforms have shorter ranges and consequently cover less area than fixed-wing platforms. These disadvantages generally mean that rotary UAS are more expensive and require more time to complete aerial surveying tasks.

Similarly to fixed-wing platforms, the price of rotary UAS is defined by software and hardware technologies. Higher complexity in flight maneuverability and control with rotary UAS increases the prices for models with autonomous flight capabilities. A large majority of rotary UAS are controlled using joystick controls, although autonomous models do exist.

Figure 9: Aeryon Skyranger quadcopter operated by FYBR inc. - https://www.fybrsolutions.com/

3.1.4 Sensor configurations

Typical sensors and integrated instrumentation attached to conventional aircraft can weigh upwards of 50 kg. Considering that UAS are highly limited in their payload capacity, drastic reductions in size and weight are needed for sensors to be compatible. An issue surrounding the attachment of sensors to UAS are that limitations to payload capacity and power draw requirements limit the compatibility of carrier and sensor. UAS compatible sensor development is occurring rapidly. The development of lightweight multi-spectral sensors to provide high spatial and spectral resolution data, is of particular interest to the forest management community. The potential for high fidelity radiometric data at ultra-high resolutions has become reality, which could have significant implications for precision

agriculture and environmental science. A in-depth review of sensors compatible with micro and mini UAS payload requirements can be found in Colomina and Molina (2014), who differentiated between visible-band, NIR, multispectral, hyperspectral, thermal, laser scanning, and synthetic aperture radar systems. Their review found that conventional high resolution cameras were the dominant sensor being used, although multiple models of each sensor type exist with UAS compatibility. Chapters 5, 7, & 8 of this dissertation use a low cost RGB sensor, while Chapter 4 data was acquired using a Sequoia multi-spectral sensor (Pix4D, 2018a).

Reductions in size and improvements in spatial resolution of visible-spectrum cameras has facilitated small, high-quality, low-cost sensor development such as those found on everyday smart-phone cameras (Colomina and Molina, 2014; Figure 10). The development of these sensors, along with 3D imaging software, has caused DAP usage to proliferate. The low cost of visible spectrum imagery collection and similarities of DAP point clouds to those produced from ALS sensors has prompted a dramatic increase in image-based point cloud research and commercial usage.

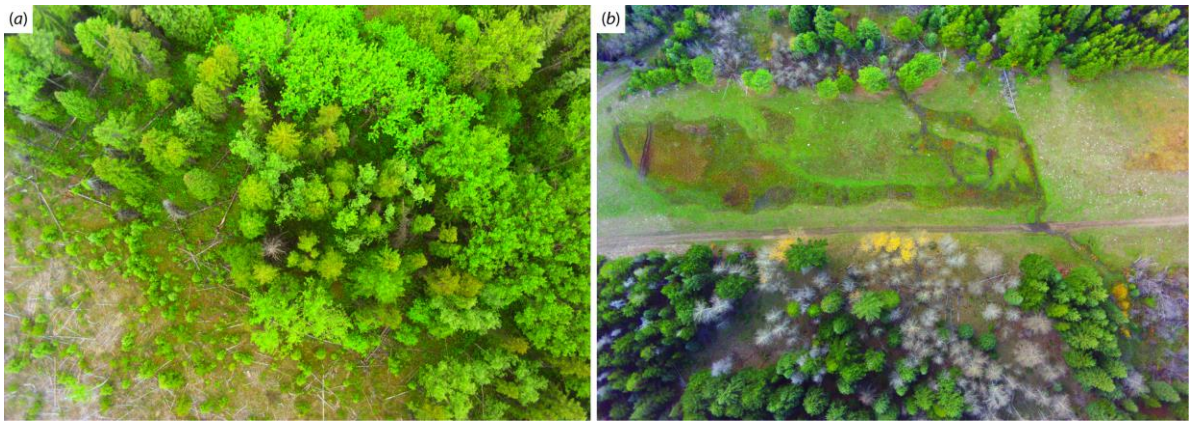

Figure 10: UAS-acquired imagery using SUNEX MT9F002 red-green-blue (RGB; true-colour) sensor at 100 m (a) and 200 m (b) above ground level

3.2 UAS applications for forestry

In order to improve the cost effectiveness and accuracy of operational forest inventories, forest managers require spatially and temporally accurate forest inventory data to make informed management decisions (Goodbody et al., 2016). Preliminary research has shown that images captured from UAS systems offer a definitive combination of very high resolution data capture at a consistently lower surveying cost (Wallace et al., 2012a). The capability for UAS to be deployed quickly and easily acquire imagery also facilitates updating inventories. Koh and Wich (2012) indicate that acquiring imagery and producing UAS acquired DAP point clouds could lead to significant reductions in capital and labour related costs, while also reducing the time needed for surveying.

The measurement of fundamental forest inventory parameters, such as tree height, has been a major focus for UAS research (Goodbody et al., 2017b). Knowledge of the physical location and distribution of timber resources prior to field reconnaissance can improve productivity and eventual delineation of operational areas. Studies such as Wallace

et al. (2014a), which used a UAS-ALS sensor, demonstrate the potential to measure tree heights at a similar precision to ground-based measurements. UAS-ALS have also demonstrated that measurements of tree height using these systems has the potential to be more accurate than those from conventional ALS data (Lin et al., 2011). Other research into UAS-ALS systems such as high resolution forest change detection (Wallace et al., 2012b), tree detection and crown segmentation (Wallace et al., 2014b), and fine scale forest mapping (Lin et al., 2011), indicate that UAS-ALS can extract information for forest inventory generation and monitoring at the stand and individual tree levels. The detailed and manipulatable nature of ALS point clouds shows strong potential to provide managers with information that increases the efficiency of forest reconnaissance at operational scales (Corona and Fattorini, 2008).

While UAS-ALS combinations show promise for measuring forest inventory information, concerns about cost have been a limiting factor for their deployment. UAS acquired imagery at an operational scale has been shown to be a relatively cheap and complimentary technology to conventional aerial photo surveying while providing point cloud outputs of similar quality and utility to ALS (Jaakkola et al., 2010; Osborn et al., 2017; White et al., 2015). Low cost, high spatial and temporal resolution data acquired using UAS-DAP point clouds has been shown to be accurate for observing phenological dynamics, spectral traits, monitoring changes, and measuring forested environments (Dandois & Ellis, 2013). Tang et al. (2015) and Siebert and Teizer (2014) indicate that the

acquisition of high resolution stereo-imagery using UAS should be encouraged for forestry purposes because it allows measurement of canopy and individual tree heights at lower costs than ALS systems. Depending on UAS flight parameters, orthomosaic imagery of forested areas can have spatial resolutions of 3 cm or less, providing managers with ultra-high definition images of operational areas and a 3D point cloud in a single flight plan (Zhang et al., 2016). Apart from studies such as Zarco-Tejada et al. (2014), which demonstrated that optical imagery can be used to measure canopy heights at operational scales, UAS-DAP point clouds have been used for many other forestry purposes including spatial quantification of riparian areas and determining vegetation composition (Dunford et al., 2009), mapping bark beetle damage at the individual tree level (Näsi et al., 2015), long-term forest monitoring (Zhang et al., 2016), and monitoring tropical forest recovery (Zahawi et al., 2015).

DAP is limited in that it cannot provide comprehensive structural information like ALS; however, the technique does produce a higher density surface model and includes spectral information (White et al., 2015). This balance between similarities in utility and differences in output products promotes their tandem utilization as a spatially and temporally accurate forest monitoring framework without burdening the manager with redundant information (Wallace et al., 2012a). Studies into the synthesis of ALS and UAS-DAP point clouds, such as Goodbody et al. (2016), which is elaborated upon in Chapter 7

of this dissertation, has shown the possibility of using UAS-DAP point clouds to outline the location and estimate residual timber volume following selection harvesting operations.

A combination of hardware limitations, such as the longevity of propulsion systems, and current federal transport regulations, such as the requirement to always have visual-line-of-sight with the UAS being flown, restrict the applicability of UAS for the mapping and/or imaging of large areas (Transport Canada, 2014). As technology, federal regulations, and knowledge of UAS mapping and inventory capabilities evolve, their use in large scale mapping procedures should become more prevalent. UAS-DAP does however have the potential to improve managerial knowledge of the land base at the local operational scale by updating areas where imagery was previously acquired or establishing new baseline inventory information.

3.3 Summary

This chapter reviewed UAS technology and presented research outcomes indicating their effectiveness as a platform for acquiring high resolution remote sensing data. Major benefits are that they are cost-effective alternatives to conventional acquisition platforms, are quickly operationalized, and offer solutions for data needs at an operational scale. The upcoming two chapters elaborate on these benefits, providing examples of how UAS-DAP can be used to provide operational scale inventory information on early successional forest structures. I outline in Chapters 4, 5, 7, and 8 that UAS-DAP is a viable method for the provision of high quality EFI data.

Given that UAS-DAP has proven effective for providing operational scale data, the following chapter looks to explore its potential to generate DTMs in forests in the early stages of secondary succession, specifically sparsely forested, deciduous dominated sites akin to those following harvesting.

Chapter 4:

Vegetation phenology driving error variation in digital aerial photogrammetrically derived terrain models[3]

4.1 Background and motivation

In the previous two chapters, I outlined how DAP data and UAS platforms have experienced rapid technological innovation. I have made the argument that improving forest inventories via the inclusion of structural data derived from 3D remote sensing technologies, such as DAP has shifted the paradigm of how forest mensuration and inventory management can be undertaken. The integration of DAP datasets and UAS platforms have facilitated a technological and data-driven revolution in forest inventory management and ecology, providing the ability to support multi-scale planning and decision-making.

The potential to acquire multi-temporal DAP data cost-effectively using UAS capitalizes on the potential for high spatial and temporal resolution data. The inherent potential of multi-temporal remote sensing data sets is well known (Hermosilla et al., 2015a, 2015b; Pasquarella et al., 2017; Pickell et al., 2016), and innovations associated

[3] The content of this chapter has been adapted from:
Goodbody, T.R.H., Coops, N.C., Hermosilla, T., Tompalski, P., Pelletier, G., (2018). Vegetation Phenology Driving Error Variation in Digital Aerial Photogrammetrically Derived Terrain Models. Remote Sens. 10, 1554.

with free open access big-data libraries have facilitated more frequent and meaningful time series analyses (Jin and Sader, 2005; Löw et al., 2018; Wulder et al., 2016). Trend analyses resulting from these data sets have been successful in outlining opportunities on how to improve upon traditional management strategies using results-based scientific foundations. Satellite based remote sensing programs such as Landsat, Sentinel, or MODIS have shown that repeated acquisitions and increasing temporal resolution of acquisition programs are invaluable for detailing economic and social development, and are critical for effective, evidence based environmental management and monitoring initiatives (Lu et al., 2017, 2016).

While UAS-derived imagery and DAP datasets have proven cost-effective and accurate for a variety of forest inventory information from single date acquisitions (Goodbody et al., 2017a; Puliti et al., 2018b; Rusnák et al., 2018), limited research has been conducted relating DAP derived forest structure descriptors and the timing or seasonality of their acquisitions.

As elaborated upon in Chapter 2, a fundamental requirement for DAP integration into an inventory is an accurate DTM. The ability to derive high resolution DTMs from ALS data sets is well known (Furze et al., 2017; Liu, 2008), and have been used to normalize co-occurring DAP datasets (Goodbody et al., 2016; White et al., 2015). This however requires previous ALS coverages, which are often not available, increasing overall inventory production costs. Studies analyzing the ability of DAP to provide accurate DTMs

from various aerial platforms have found that their derivation are highly dependent on canopy cover (Mohan et al., 2017; Tomaštík et al., 2017), limiting the ability for DAP to characterize sub-canopy features.

Recent research into the potential to utilize multiple DAP acquisitions (Eltner et al., 2015; Mirijovskỳ and Langhammer, 2015; Pádua et al., 2018; Rossini et al., 2018; Vega et al., 2015; Xiang et al., 2018) as well as variations in sensor orientations (Lin et al., 2015; Rusnák et al., 2018) have also been conducted. Findings predominantly indicate that flight repetition and sensor orientation variability can provide improved results compared to a single acquisition. For example, Mirijovskỳ et al. (2015) utilized UAS-DAP derived DTMs to analyze variations in the fluvial dynamics of a mid-mountain stream. Their findings were that DTMs were accurate and consistent at detailing stream bank shifts, as well as calculating changes and volumetric extent of bank erosion. Findings such as these promote further testing of multi-temporal DAP to generate DTMs for forest inventory analyses at an ultra-fine scale.

In this chapter, a sparsely forested, deciduous dominated site in the early stages of secondary succession was the focus of a multi-temporal UAS-DAP terrain analysis. These site conditions are common in managed forest landscapes, offering the first available opportunity to measure structure and provide opportunities for establishing DTM products capable of enabling multi-temporal forest change detection. DAP derived DTMs were generated for twenty time steps over two years and compared to a reference ALS DTM.

The focus of this chapter was to determine how timing of imagery acquisitions and seasonal changes in vegetation cover affected DAP derived DTM error, and consequently describe structural conditions where DAP is successful or limited for providing high quality forest inventory information.

4.2 Materials and methods

The methodology of this chapter can be broken down into three steps: photogrammetry processing, point cloud processing, and time series analysis. Figure 11 displays a conceptual workflow of the followed methodology. First, UAS imagery from twenty acquisitions were processed to generate photogrammetric point clouds. DAP point cloud outputs were then processed to generate DTM layers for each flight acquisition. Finally, a time series DTM analysis was conducted to determine error variability and its relationship with timing of imagery acquisitions. Summary error statistics were derived to outline error variability and illustrate the power of multi-temporal DAP data acquisitions, while a best available terrain pixel (BATP) compositing analysis, which helped to outline the importance of flight acquisition dates was conducted to produce a best possible multi-temporal terrain product.

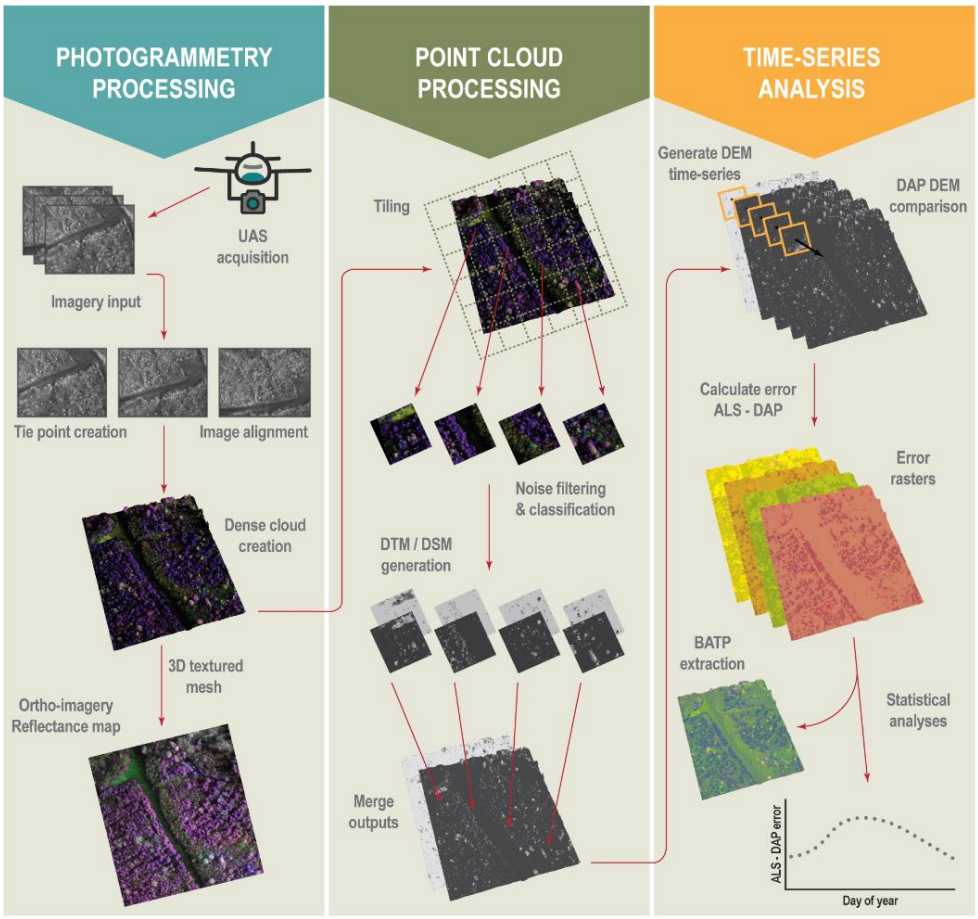

Figure 11: Methodological flow chart of photogrammetric processing, point cloud processing, and time series DTM analysis.

4.2.1 Study area

The study area is located on a 25 ha forest stand north of Edmundston, New Brunswick, Canada (Figure 12). The site is located in the central uplands ecoregion, specifically the Madawaska eco-district (47°27’04.29” N 68°06’09.65” W). This region is over 90% forested, being characterized by gently rolling terrain with a largely southern aspect. Mean elevation is 323 m above sea-level, receiving on average 475-525 mm of rain from May to September (Hébert, 2016). Forest cover in the region is predominantly hardwood dominated, comprised of sugar maple (*Acer saccharum*), yellow birch (*Betula*

alleghaniensis), and beech (*Fagus spp*.). Scattered and pure softwood stands also exist, being comprised of balsam-fir (*Abies balsamea*), as well as red (*Picea rubens*) and white spruce (*Picea glauca*) (Hébert, 2016). This area has a longstanding history of forest management from a variety of private, public, and research-based institutions (Central Uplands Ecoregion, 2013). The site itself is deciduous dominated with multi-age cohorts of balsam fir, red and white spruce, yellow birch and sugar maple. Stem density was spatially variable with a mean of approximately 50 juvenile (1-20 year old) stems per hectare.

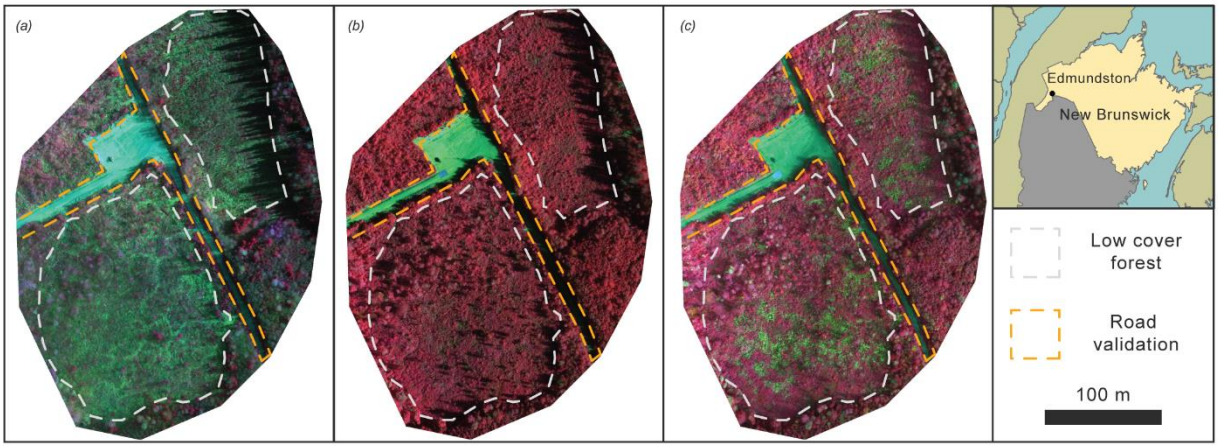

Figure 12: Study area on (a) 2017-05-25, (b) 2017-06-27, and (c) 2017-09-15, displaying the sparsely forested site used for DTM analysis and road validation area. The smaller, upper-most portion of the low cover forest area is comprised of short understory regeneration, while the larger section is sparsely forested with approximately 50 stems per hectare of juvenile mixed wood. Imagery used was acquired using a Sequoia multi-spectral camera and is displayed in a false colour composite of near infra-red, red, green.

4.2.2 Data

Twenty imagery acquisitions were performed using a senseFly eBee UAS with a Sequoia multi-spectral camera (Pix4D, 2018a). Average along- and across-track overlaps were 85% and 80% respectively. Imagery were acquired between September 2016 and December 2017 (Table 1). The Sequoia camera is comprised of 4 monochrome sensors

(green: 530-570 nm, red: 640-680 nm, red edge:730-740 nm, and near-infrared: 770-810 nm), a RGB composite sensor, and an external sunlight sensor placed on top of the UAS to capture sun angle from nadir and irradiance for each image during flights (Stroppiana et al., 2018). Acquisitions followed a standardized procedure, where images of radiometric targets were taken prior to aerial imaging missions, and a systematic gridded flight pattern was used for efficient imagery capture. Table 1 provides details related to individual flights as well as DAP point density following image post-processing. Kruskall-Wallis rank sum tests were performed on mean flight elevation and mean ground sample distance to determine whether there were significant differences amongst imagery acquisition parameters. Flight acquisitions took place when no snow coverage was present, except for 2017-12-04 (day of year 338), where snow coverage was negligible.

A reference ALS data set with an average density of 18.5 points m^{-2} was used. These data were acquired by the Government of New Brunswick as a part of their province wide 2017 ALS acquisition campaign. Acquisition of ALS data over the study area was conducted between 2017-06-12 and 2017-06-13.

Table 1: Imagery acquisition dates and corresponding mean flight altitude (above ground level), mean ground sample distance, mean sun angle from nadir, and mean DAP point density.

Acquisition date	Day of Year	Mean flight altitude (m)	Mean GSD (cm)	Mean sun angle (°)	Mean DAP density (pts/m^2)
2017-05-25	145	116.2	13.5	71.2	25.4
2017-05-28	148	102.2	12.1	68.3	31.0
2017-06-07	158	116.1	13.2	45.7	23.0
2017-06-27	178	114.7	13.4	54.0	26.6
2017-07-05	186	113.4	13.3	58.4	39.8
2016-08-03	216	102.5	12.2	68.7	23.8
2016-08-24	237	101.6	12.4	72.4	24.6
2017-08-29	241	99.9	12.1	67.0	33.4
2016-09-07	251	104.0	12.6	71.8	22.9
2017-09-08	251	102.1	12.2	64.9	33.3
2017-09-15	258	101.1	12.0	73.8	35.0
2016-09-21	265	110.0	12.9	68.9	25.8
2017-09-22	265	102.7	12.2	67.4	32.5
2016-09-29	273	116.5	13.9	75.8	20.8
2017-10-02	275	101.0	11.9	74.4	29.0
2016-10-20	294	102.6	12.6	82.7	22.7
2017-10-23	296	102.6	12.3	58.3	30.6
2016-10-27	301	105.8	13.1	72.9	26.0
2016-11-10	315	102.6	12.6	73.3	27.4
2017-12-04	338	100.3	12.4	74.5	27.4

4.2.3 Photogrammetric processing

UAS-acquired multi-spectral imagery were photogrammetrically processed to produce dense point cloud products using Agisoft Photoscan (Agisoft, 2018). Images were aligned, radiometrically calibrated using pre-flight target images, and optimized using inertial measurement unit and global navigation satellite system/GPS measurements. Following imagery alignment, conjugate tie-points between image pixels were then generated for locations with two or more overlapping images. Dense point cloud processing was then conducted at the original image scale to produce high quality and density point cloud outputs. Point cloud products were exported following densification for point cloud processing. Orthoimagery for each flight acquisition were generated and exported as auxiliary datasets (Figure 11).

4.2.4 Point cloud processing

In order to derive accurate DTM information from each point cloud, multi-temporal DAP and the ALS reference point cloud were processed using LAStools (Isenburg, 2018). Raw point clouds were first tiled using “lastile” (parameters: tile_size = 50, buffer = 25) and filtered to remove noise using “lasnoise” (parameters: step_z = 1, isolated = 10) (Figure 11). Points were then classified into ground or non-ground classes using the progressive triangulated irregular network (TIN) densification algorithm implemented in “lasground” (parameters: step = 10m, bulge = 0.05), which gradually removes non-ground points based on elevation differences and angles to the nearest TIN section to iteratively estimate ground

surface (Isenburg, 2018; Meng et al., 2010; Mohan et al., 2017). The ALS point cloud was used to co-register DAP point clouds using the iterative closest point algorithm (Besl and McKay, 1992). Iterative closest point alignment was used rather than ground control targets due to lack of target data for each flight acquisition. Classified and co-registered point clouds were then used to generate 0.5 m DTM layers using the "las2dem" (parameters: step = 0.5, kill = 2) algorithm (Isenburg, 2018). A 2 m interpolation distance was used for DAP derived DTMs to limit potential interpolation error. Errors between the reference ALS DTM and DAP derived DTMs for each flight acquisition were computed at the pixel level and then aggregated for the area of analysis.

A 15 cm height threshold was used to compute vegetation cover (proportion of points above threshold) at 2 m resolution for each DAP point cloud to capture seasonal variability and enable potential linkages between DTM error and above ground vegetation cover. The road within the study area (Figure 12) was used to validate the accuracy of the DAP derived DTMs without the influence of vegetation or obstruction. Statistical error summaries for the mean, standard deviation, and range of error were computed for each acquisition. Proportional coverages of the DAP derived DTMs compared to the ALS ground truth were calculated to outline whether image acquisition timing had an influence on overall DAP derived DTM coverage as well as error.

4.2.5 Time series analysis

4.2.5.1 Generalized additive mixed models

Mean vegetation cover, mean error, and proportional DAP derived DTM coverage were summarized and related to the acquisition day of year using generalized additive mixed models (GAMM) built in the 'MGCV' package (Shadish et al., 2014; Wood, 2011). The GAMM model was chosen due to its proven ability to detect and describe whether a trend exists between two variables, and if so, its linear or non-linear shape (Shadish et al., 2014; Zuur et al., 2009). These models are well suited for analyzing the functional relationship between variables within a single-case design such as the DTM error in a single location over time (Shadish et al., 2014). Single case designs, such as the study area used in this analysis serve as their own control, allowing for the effective evaluation of changes over time. The key advantage of these models over other conventionally applied parametric regression methods is that the researcher does not need to know the model's functional form *a-priori*, which is performed by the model internally. Given that the form is rarely known *a-priori* with confidence, GAMMs provide a means to solve this problem in a statistically sound manner. For further inquiry, Shadish et al. (2014) provide an in-depth overview of the application of GAMMs. GAMMs utilize cubic regression splines to estimate nonlinear associations between dependent and independent variables (Rickbeil et al., 2017; Zuur et al., 2009). To account for potential variation, the year of imagery acquisition was incorporated as a random factor. Individual models (Equation [1) were

constructed with a smoothing term between the day of year of imagery acquisition and the mean error, mean vegetation cover, and proportional DAP derived DTM coverage. Models were assessed by the significance of the smoothing term ($p > 0.05$), which were internally chosen using a restricted maximum likelihood approach (Shadish et al., 2014; Wood, 2011).

$$g(E(Y)) = \alpha + f_1(Day\ of\ year)_i \times f_2(x)_i + \varepsilon_i \quad [1]$$

Where $E(Y)$ denotes the expected value, $g(Y)$ denotes the link function, and x is either mean vegetation cover, mean error, or proportional DAP derived DTM coverage. α is the intercept, f_1 and f_2 are spline functions and ε represents the model error term.

4.2.5.2 Best available terrain pixel compositing

A BATP composite was generated using DTM error rasters. To do so, an iterative algorithm was created, which incorporated all available DTM error rasters to spatially select minimum error pixels. These pixels, with reference to the day of year of imagery acquisition, were labelled as the BATPs. This process produced a DAP derived terrain with the lowest possible overall error as well as reference to which acquisition donated each BATP.

4.3 Results

4.3.1 DTM summary and validation

Kruskal-Wallis rank sum tests on mean flight altitude and ground sample distance (Table 1) indicated that means were not significantly different from one another ($p > 0.05$).

Road DTM validation analysis indicated that DAP derived imagery acquisitions were capable of producing highly accurate DTMs in open areas regardless of acquisition timing (Table 2). Mean, standard deviation, and range of DTM error were found to fluctuate with acquisition timing (Figure 13, Figure 14, Table 2). Day of year 338, the only acquisition with snow cover, was found to have a comparatively high range of DTM error compared to other acquisitions.

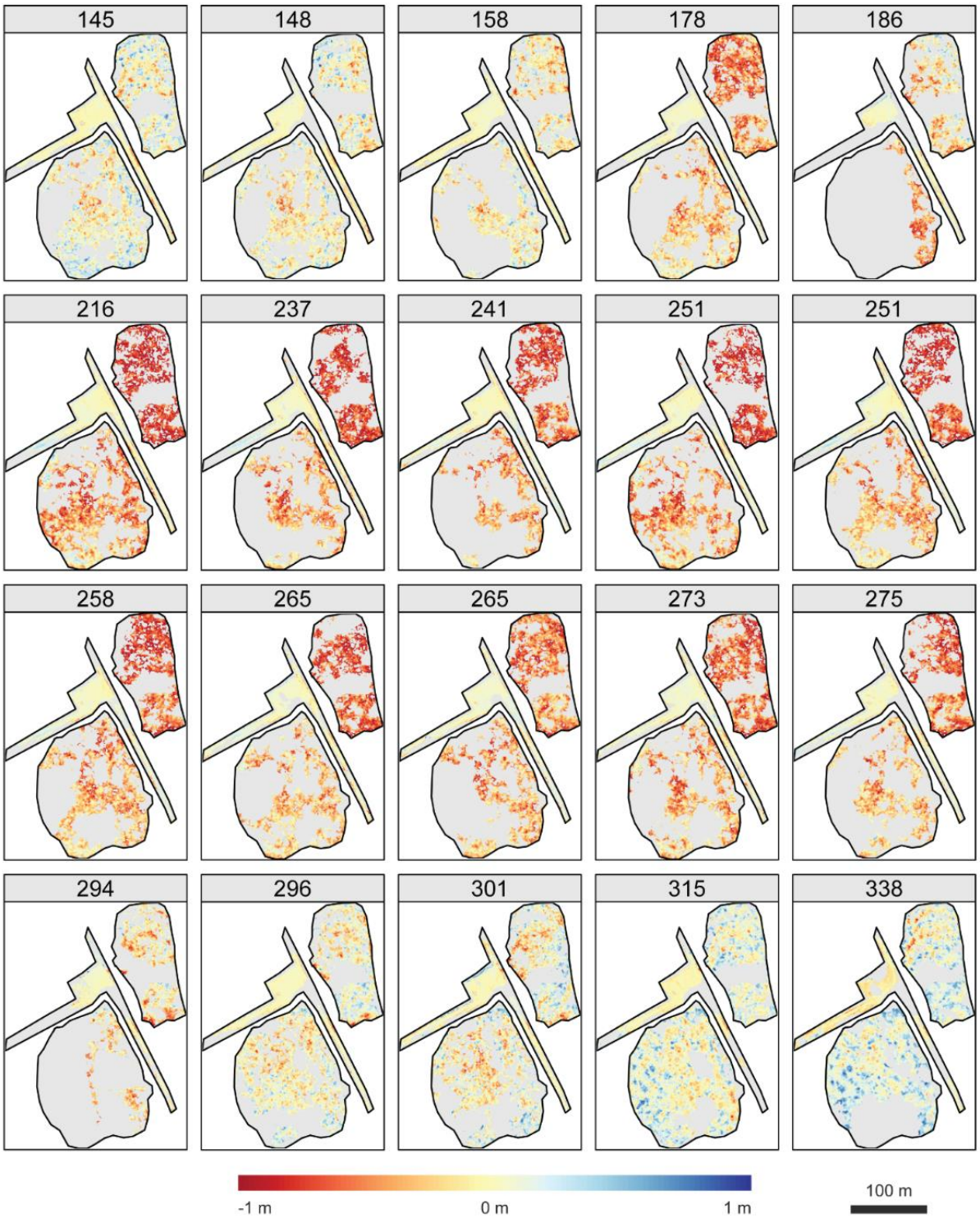

Figure 13: Visualized error (m) for each DAP derived DTM listed by day of year relative to the reference ALS DTM. Grey colour indicates the full extent of the reference DTM.

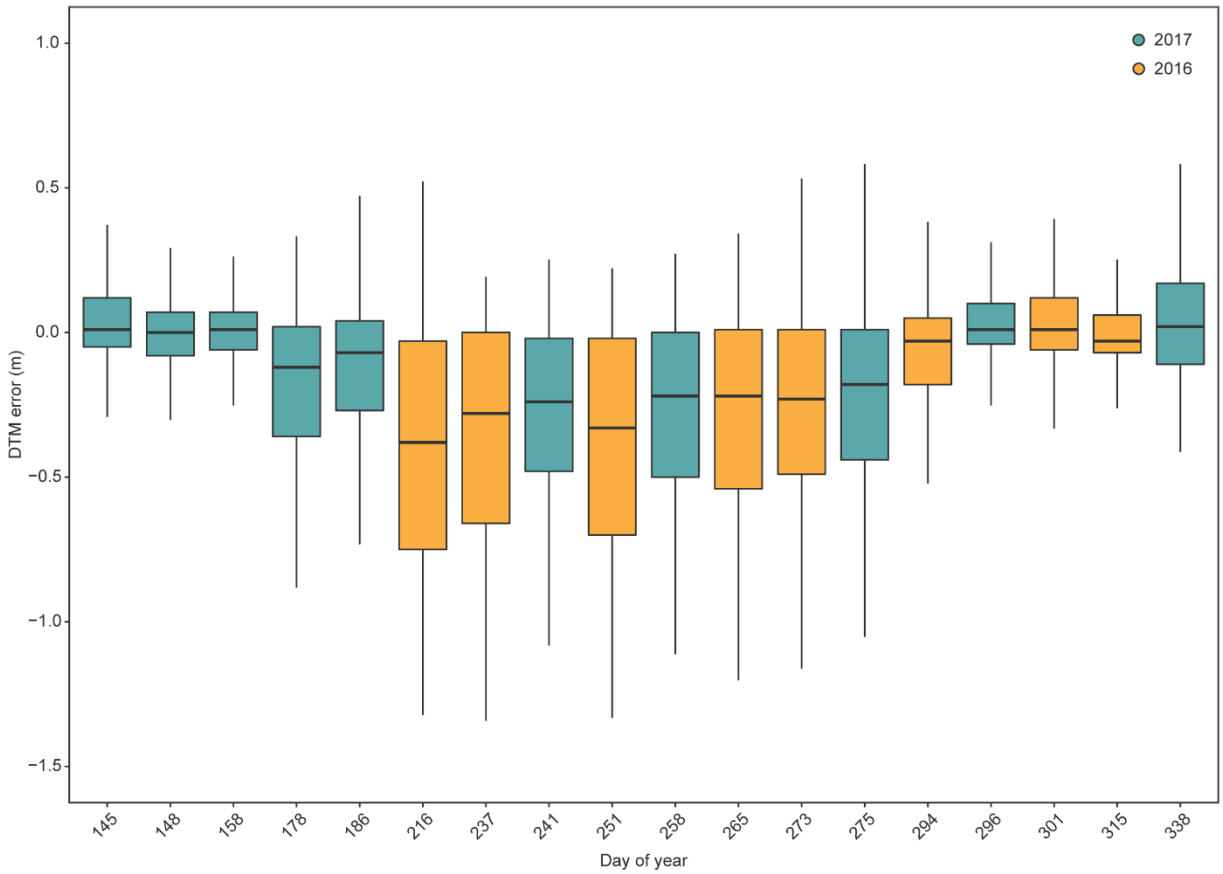

Figure 14: Boxplots of DTM error by day of year, coloured by acquisition year.

Table 2: Summary statistics of the differential error per flight for the entire study site as well as only the road validation section of the analysis.

		Study Area only					Road validation only	
Date	**Day of year**	**Mean error (m)**	**Standard deviation of error (m)**	**Range of error (m)**	**Mean vegetation cover (%)**	**DAP DTM coverage (%)**	**Mean validation error (m)**	**Standard deviation of validation error (m)**
2017-05-25	145	0.04	0.15	1.41	33.50	60.20	-0.02	0.06
2017-05-28	148	0.00	0.16	1.58	43.22	50.94	0.00	0.06
2017-06-07	158	0.01	0.15	2.28	48.26	41.75	0.01	0.06
2017-06-27	178	-0.17	0.23	1.28	47.85	45.29	0.03	0.07
2017-07-05	186	-0.12	0.22	2.55	66.67	23.47	0.02	0.11
2016-08-03	216	-0.41	0.38	1.96	45.29	52.54	-0.01	0.08
2016-08-24	237	-0.35	0.36	1.55	54.73	38.07	0.00	0.08
2017-08-29	241	-0.27	0.28	1.37	55.06	35.84	0.00	0.07
2016-09-07	251	-0.37	0.36	1.55	53.61	44.16	-0.01	0.08
2017-09-08	251	-0.33	0.32	1.59	52.06	44.19	0.00	0.08
2017-09-15	258	-0.27	0.29	1.39	49.29	44.43	0.01	0.07
2016-09-21	265	-0.28	0.31	1.54	52.03	40.91	0.01	0.08
2017-09-22	265	-0.18	0.23	1.37	48.59	42.03	0.04	0.07
2016-09-29	273	-0.25	0.29	1.87	48.33	44.20	0.03	0.09
2017-10-02	275	-0.24	0.28	1.63	55.85	37.07	0.00	0.09
2016-10-20	294	-0.08	0.21	1.65	55.48	24.92	0.01	0.08
2017-10-23	296	0.02	0.16	1.47	37.62	56.35	-0.01	0.05
2016-10-27	301	0.02	0.18	1.50	37.08	55.91	-0.02	0.07
2016-11-10	315	0.01	0.13	1.28	28.56	70.19	-0.06	0.05
2017-12-04	338	0.04	0.19	2.01	32.86	60.68	-0.11	0.10

4.3.2 Generalized additive mixed models

GAMMs with statistically significant smoothing terms were generated for mean vegetation cover (Figure 15 (a); *edf* = 3.074, *F* = 6.604, *p* = 0.003) and mean error (Figure 15 (b); *edf* = 5.483, *F* = 38.3, *p* = 0.001). The maximum mean vegetation cover was predicted to be 54% on day 216, while a minimum of 30% was predicted on day 340 (Table 2). The maximum mean error was predicted to be -0.35 m on day 227, while the minimum was predicted as 0.00 m on day 148. Acquisitions between days 178 to 281 were predicted to have mean DTM errors greater than 0.15 m, which corresponded to mean vegetation cover greater than 47%. Mean vegetation cover (Figure 15 (a)) was found to mimic the temporal trend of mean DTM error (Figure 15 (b)). A significant ($p > 0.05$) positive relationship between vegetation cover and DTM error found that DTM error increased by approximately 0.03 m for every 10% increase in vegetation cover. The GAMM model for proportional DAP coverage (Figure 15 (c); *edf* = 2.463, *F* = 3.105, *p* = 0.059) was not significant however, did indicate a potential relationship with mean vegetation cover. Two outliers (Figure 15 (c)), days 186 and 294, were found to strongly influence the significance of this model.

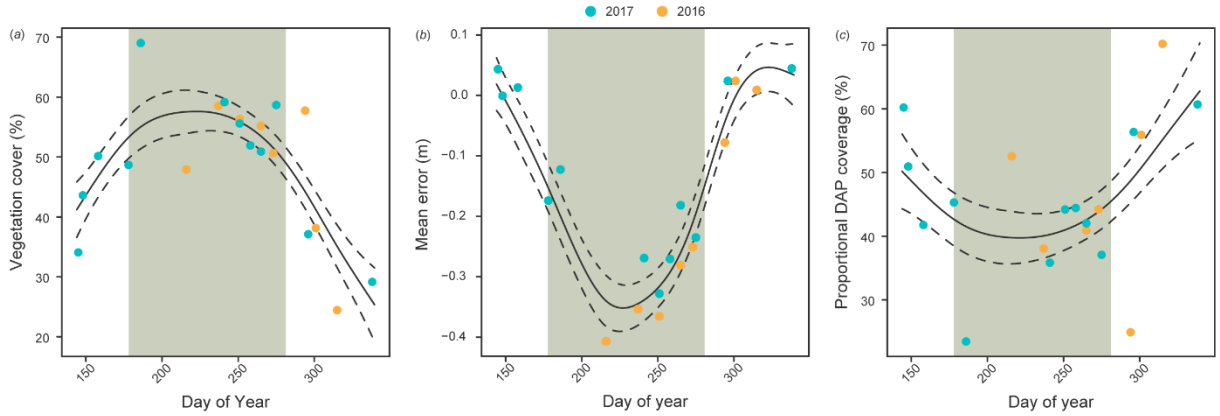

Figure 15: Generalized additive mixed models for (a) vegetation cover, (b) mean error, and (c) proportional DAP coverage. Solid smoothed lines indicate the fitted GAMM models and dashed lines indicate standard error bounds. Green backdrop from day 178 to 281 indicate locations where mean DTM error exceeded 0.15 m.

4.3.3 Best available terrain pixel compositing

A DAP derived BATP DTM (Figure 16 (a)) had a mean error of 0.01 m, a standard deviation of 0.14 m (Figure 16 (b)), and a relative spatial coverage of 86.3% compared to the reference ALS DTM. Locations with no data were found to have 100% vegetation cover for all acquisitions. Figure 16 (c, d) indicate that all flight acquisitions provided pixels to the BATP DTM. Data acquired in early spring, late-fall, and early-winter (145, 148, 158, 178, 296, 301, 315, 338) were the most represented donors for compositing. The day 315 acquisition provided the highest proportion (19.3%) of total donor pixels to the BATP analysis, while day 241 provided the least (0.80%).

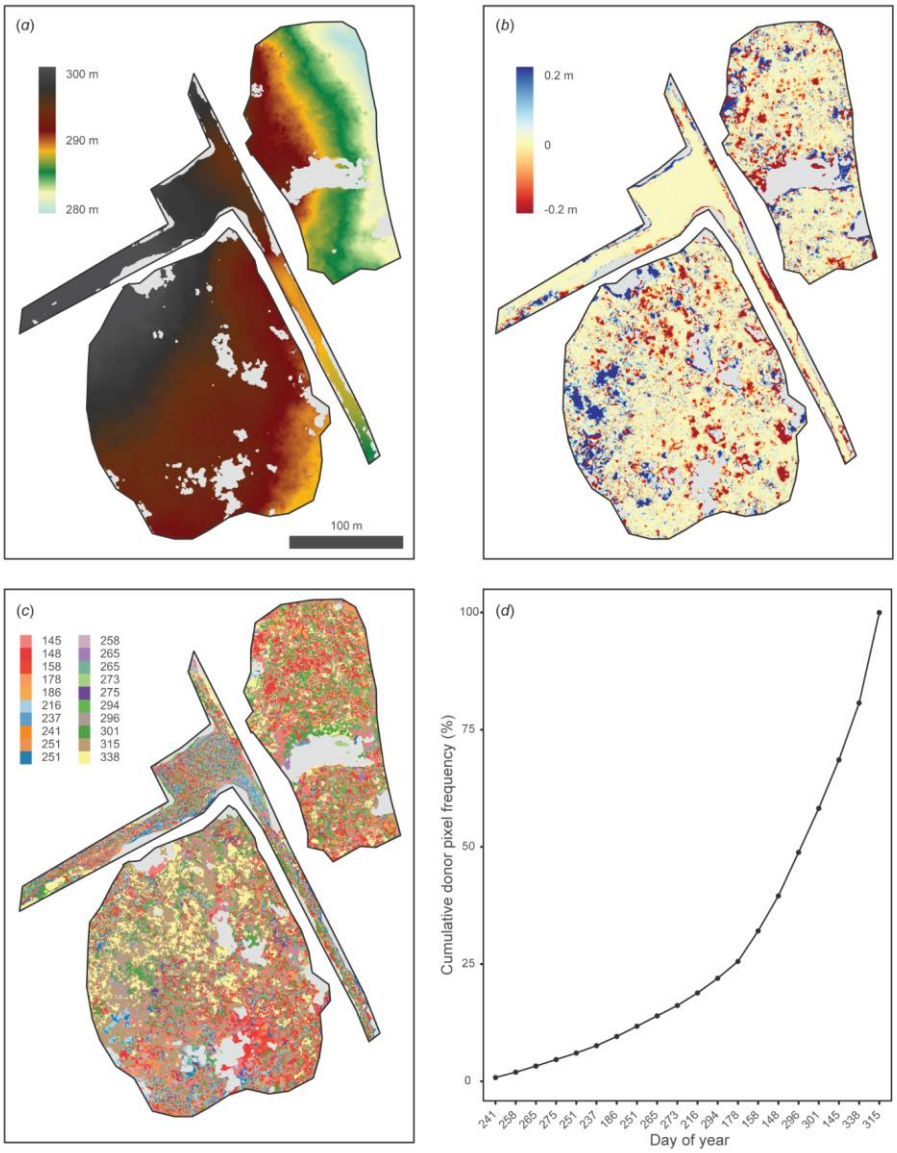

Figure 16: Results of the best available terrain pixel analysis including (a) the optimal DTM, (b) composite error map, (c) donor pixel map, and (d) cumulative donor pixel frequency indicating the days of year with the least to highest frequency of donated pixels. Light grey colour indicates the full extent of the reference DTM, delineating areas with consistent 100% vegetation coverage.

4.4 Discussion

This study utilized a multi-temporal UAS imagery dataset to create DAP point clouds and assess their accuracy for generating DTMs in a low cover, deciduous dominated forested site. Timing of acquisition was found to significantly influence mean DTM error. Error was shown to increase in summer months following a concurrent increase in mean vegetation cover. Although

the GAMM model for proportional DAP DTM coverage was not significant, linkages between increases in mean vegetation cover and consequent decreases in DTM coverage are logical, and should be investigated further. Acquisitions in early-spring, prior to leaf-on and seasonal shrub layer growth, or in late-fall and early-winter following senescence, were found to have lower error, and increased coverages of DTMs. This finding provides insight into the influence of phenological cycles on the ability for DAP to characterize the ground surface in open forested settings, providing managers with optimal windows to acquire imagery for the purposes of minimizing DAP derived DTM error. Results indicate that the use of UAS-DAP derived DTMs in low cover areas is entirely possible, but that as vegetation coverage increases it is expected that DTM error will also increase.

Our results found that an increase in 10% vegetation cover (up to the maximum of 54% witnessed in this study) was on average found to increase DTM error by 0.03 m. Increasing levels of vegetation coverage therefore correspond to increases in DAP derived DTM error. These results detail that the acquisition of DAP derived DTMs should ideally be planned for early-spring, late-fall, and early-winter periods. Portions of the BATP composite with missing data outline that DAP can be limited in characterizing terrain even in leaf-off conditions. This finding challenges the managerial assumption that the characterization of terrain occluded by deciduous vegetation using DAP can be improved when acquired in leaf-off conditions. Coniferous coverage continues to pose challenges to deriving DTMs using DAP. For this reason, it may be advisable for managers to target stands during early stages of succession to reduce ground occlusion from coniferous vegetation (Goodbody et al., 2017a).

Results from this chapter confirm that UAS-DAP has potential to produce accurate DTMs in low cover deciduous stands that are comparable to conventional ALS acquisitions. As

opposed to traditional methods of acquiring imagery from manned aircraft, a forest manager using UAS has precision control of where and when imagery is acquired on their land base, as well as tune acquisition parameters such as spatial resolution to best meet management needs (Colomina and Molina, 2014; Šedina et al., 2017; Singh and Frazier, 2018). Until the relatively recent emergence of commercially available high-performance UAS, the ability to acquire user defined datasets at ultra-fine scales was economically and logistically challenging, limiting multi-date acquisitions. This chapter provides evidence that multi-date acquisitions offer information about how DAP point clouds are able to characterize terrain through seasons and how multiple acquisitions can be consolidated produce a more comprehensive terrain data set.

The use of DAP points clouds for local operational scale forest inventories has several advantages over conventional ALS approaches. Firstly, DAP is able to provide both spectral and structural information from a single imagery acquisition that enhance forest inventory data sets (Goodbody et al., 2018a). Secondly, despite a rapid growth in the adoption of ALS technology, ALS data is not broadly available for all forested lands globally, often due to cost restrictions. While jurisdictions such as the Province of New Brunswick, Canada aim for full coverage by the year 2019, re-acquisition cycles are not yet determined and will likely not occur for at least 10 years following completion. While these landscape level data sets are an invaluable interdisciplinary resource, single acquisitions do not provide temporal depth needed for short-term change detection, monitoring, and inventory updating.

In contrast, DAP acquisition campaigns, especially when acquired using UAS, can be quickly planned and deployed for small areas, providing means to spatially, spectrally, and structurally update inventories as a result of natural forest dynamics such as growth over time (Goodbody et al., 2017b, 2017a; Guerra-Hernández et al., 2017), wind-throw (Mokroš et al.,

2017), fire events (McKenna et al., 2017), or anthropogenic treatments such as harvesting (Goodbody et al., 2016). A synergistic framework where landscape level ALS data (where available) is used as a baseline, followed by incremental updates using UAS-DAP acquisitions could provide the best possible, near real-time EFI data available for operational forest management. The continual acquisition of these data at user defined scales will facilitate opportunities for ecosystem-based-management approaches where policy and decision making can be systematically evaluated, and improved along-side data acquisition.

Research into the potential to utilize methodologies from this chapter for the purposes of creating DTMs in recently harvested areas could provide a means to establish frameworks for baseline structural inventories in areas without ALS coverages. The creation of DAP inventory baselines would help to promote the utility of acquiring multi-temporal UAS imagery of forests through succession, providing useful information related to regeneration success (Goodbody et al., 2017a), improved knowledge of tree growth rates in under-represented age and structural classes, and improve structural, spectral, and spatial knowledge of forest development through time at a wall-to-wall level. This would be especially useful in fast growing highly productive regions, or in plantations where accurate quantitative inventory data related to growth and structural change are desired.

An assumption in this terrain analysis was that the reference ALS DTM was static in time. This meant that incremental changes to the road surface and vegetation, which are expected to occur over the duration of the analysis, were not factored into the analytical process. This was largely due to the cost and infeasibility of acquiring repeat reference ALS datasets, and to provide analytical consistency. A single reference DTM also facilitated the use of the iterative closest point algorithm for point cloud alignment, rather than rely on ground control targets,

which were not consistently available during data acquisition. Future analyses should attempt to include consistent ground control targets, and potentially introduce multiple reference DTMs to account for incremental changes to features such as road surfaces.

4.5 Conclusions

This chapter indicated that DAP point clouds acquired over low vegetation cover, deciduous dominated stands were capable and accurate at creating DTMs comparable with a reference ALS DTM. These results were validated by comparing DTMs over an unobstructed road within the study area. Generalized additive modeling indicated that imagery acquisition timing was shown to significantly influence derived DTM error, and that acquisitions in spring, late-fall, and early-winter were most accurate. A best available terrain analysis, which utilized all imagery time-steps to generate a best-possible DAP derived DTM, reinforced this finding, indicating that best available pixel donations were proportionally highest within these seasonal periods. This confirmed that seasonal vegetation differences affected the performance of DAP for producing DTMs, providing managerial insight into the applicability of acquiring structural data for the purposes of producing DTMs in open areas. These results are form a promising foundation for the analysis presented in the following chapter that looks to determine the effectiveness of DAP data for structurally and spectrally characterizing post-harvest regeneration.

Chapter 5:

Assessing the status of forest regeneration using digital aerial photogrammetry and unmanned aerial systems[4]

5.1 Background and motivation

As I outlined in the previous chapter, opportunity exists for the integration of DAP to characterize young forests and integrate these data into EFI frameworks. When managing post-harvest stands, data content, quality, and surveying cost-effectiveness are of particular interest. Although natural regeneration is the most economical means of re-establishing forests following harvest or disturbance in Canada, artificial regeneration through seeding, dragging, and planting remains an integral part of forest management (Natural Resources Canada, 2016). Natural regeneration approaches require little to no human involvement, follow ecosystem-based management approaches, and offer substantial short-term reductions in silvicultural costs (Duryea, 2000). Although natural regeneration is effective, estimating certain parameters, such as species composition is difficult, while silvicultural treatments such as fill planting or thinning may be needed to meet mandated density and stocking regulations (Pitt et al., 1997). In order to reduce unanticipated long-term silvicultural costs incurred from natural regeneration approaches, artificial regeneration efforts are often conducted (Duryea, 2000; Minore and Laacke, 1992).

To monitor the efficacy of artificial regeneration efforts, silvicultural surveys are conducted on crown land in British Columbia (BC), Canada each year. Silviculture surveys are

[4] The content of this chapter has been adapted from:
Goodbody, T.R.H., Coops, N.C., Hermosilla, T., Tompalski, P., Crawford, P., (2017). Assessing the status of forest regeneration using digital aerial photogrammetry and unmanned aerial systems. Int. J. Remote Sens. 39, 5246–5264.

generally focused on three stages of regeneration: initial regeneration success, intermediary stocking status, and free-growing status (MFLNRO, 2016). Each of these surveys is conducted to spatially sample regeneration at a local scale in order to assess the success and status of regeneration stock, determine density and species composition, and outline whether these parameters are in accordance with management and silvicultural reporting obligations (Fiorella and Ripple, 1993). These surveys serve multiple purposes acting to compile information needed to develop, apply, and monitor silvicultural management scenarios, conduct resource stocking analyses, act as auditing tools, monitor compliance with silviculture prescriptions, and provide input data for growth projection models. Silviculture surveys are the most common type of sampling survey conducted on crown land annually. Survey results are used to plan treatments, conduct inventory analyses, perform audits, and monitor silviculture prescription compliance. These sampling surveys, which vary in intensity, plot size, and sampling methodology exceed coverage of over one million hectares in BC alone (MFLNRO, 2016). Although inexpensive when compared to other ground-based sampling such as timber cruising, the vast scale and coverage of surveys being conducted indicates a high annual expenditure for silviculture inventories.

Although survey-based inventories provide a relatively accurate estimation of regeneration, managers still lack, and would greatly benefit from, information related to the spatial coverage, physical location, and structural characteristics of regenerating stock (Franklin, 2001). One way to fill this information gap would be to use high resolution spatial and temporal imagery (King, 2000; Pitt et al., 1997). Previous success in using UAS to provide rapid, low-cost, and accurate high spatial resolution imagery in other forest management and inventory areas promotes their incorporation into the regeneration inventory process (Goodbody et al.,

2017). Very high spatial resolution UAS acquired imagery could provide forest managers with detailed information related to the spatial distribution of regeneration across their land base, while also providing spectral information that could improve classification of land cover and qualitative and quantitative inventory knowledge. To compliment orthoimagery, the relatively recent proliferation of DAP techniques have proven effective in providing managers with stand structure information, while establishing a baseline for multi-temporal regeneration monitoring.

In this chapter, I examine the utility of high spatial resolution UAS acquired imagery and DAP point clouds for spatially, structurally, and spectrally detailing forest regeneration on two contrasting sites. To do so, I develop a methodology which includes a supervised classification framework similar to those utilized for broad scale land-cover classification in Canada (Powers et al., 2015), to facilitate differentiation of coniferous, deciduous, and bare ground cover in regenerating stands of differing ages. A second processing stream utilizes the overlap between high spatial resolution images to apply DAP approaches to build 3D data for describing regeneration structure. The overall goals of this study are to provide a framework for forest regeneration monitoring that can be applied at temporal and spatial scales that best inform precision forest management and inventory knowledge.

5.2 Study sites

Two sites in BC near Nakusp and Quesnel were selected for field regeneration measurements (Figure 17; MFLNRO, 2016). Three previously clear-cut stands approximately 5, 10, and 15 years since planting (YSP) were chosen at each site. Stands similar in size, planted species, and terrain characteristics were prioritized. All stands had yet to be declared free-to-grow (MFLNRO, 2016) and had not reached crown closure.

The first study site was 80 km south of Nakusp, BC. The three selected stands were planted to achieve a minimum of 1200 stems per hectare and had a total area of 52.4 ha. Stands in this site were located in the Interior Cedar – Hemlock biogeoclimatic ecosystem classification zone. The Interior Cedar – Hemlock is the most productive zone for fibre production in the interior of BC (Ketcheson et al., 1991). Forests are comprised of a mix of conifers including Douglas-fir (*Pseudostuga menzieszii var. glauca*), western larch (*Larix occidentalis*), western white pine (*Pinus monticola*), lodgepole pine (*Pinus contorta*), Engelmann spruce (*Picea engelmannii*), and white spruce (*Picea glauca*). Drivers of composition in particular sites are longitude, aspect, elevation, and precipitation. Given its location within BC's interior mountain ranges, forested sites are often found on steeply sloping terrain. Mean annual temperatures range from 2.0°C to 8.7°C, and mean annual precipitation ranges from 500 to 1200 mm, with 25 – 50 % falling as snow (Ketcheson et al., 1991).

The second study site was 150 km east of Quesnel, BC. The three selected stands were planted to achieve a minimum of 1800 stems per hectare and had a total area of 66.4 ha. These stands were located in the Sub-Boreal Spruce biogeoclimatic ecosystem classification zone. Forests in this zone are dominated by lodgepole pine and hybrid spruce (*Picea engelmannii x glauca*). Generally occurring in valley bottoms, terrain is gently rolling with mountainous boundaries to the west, north, and east. The Sub-Boreal Spruce has a continental climate with a mean annual temperature below 0°C for 4-5 months of the year, and above 10°C for 2-5 months. Mean annual precipitation ranges from 440 to 900 mm with 25 – 50% falling as snow (Meidinger et al., 1991).

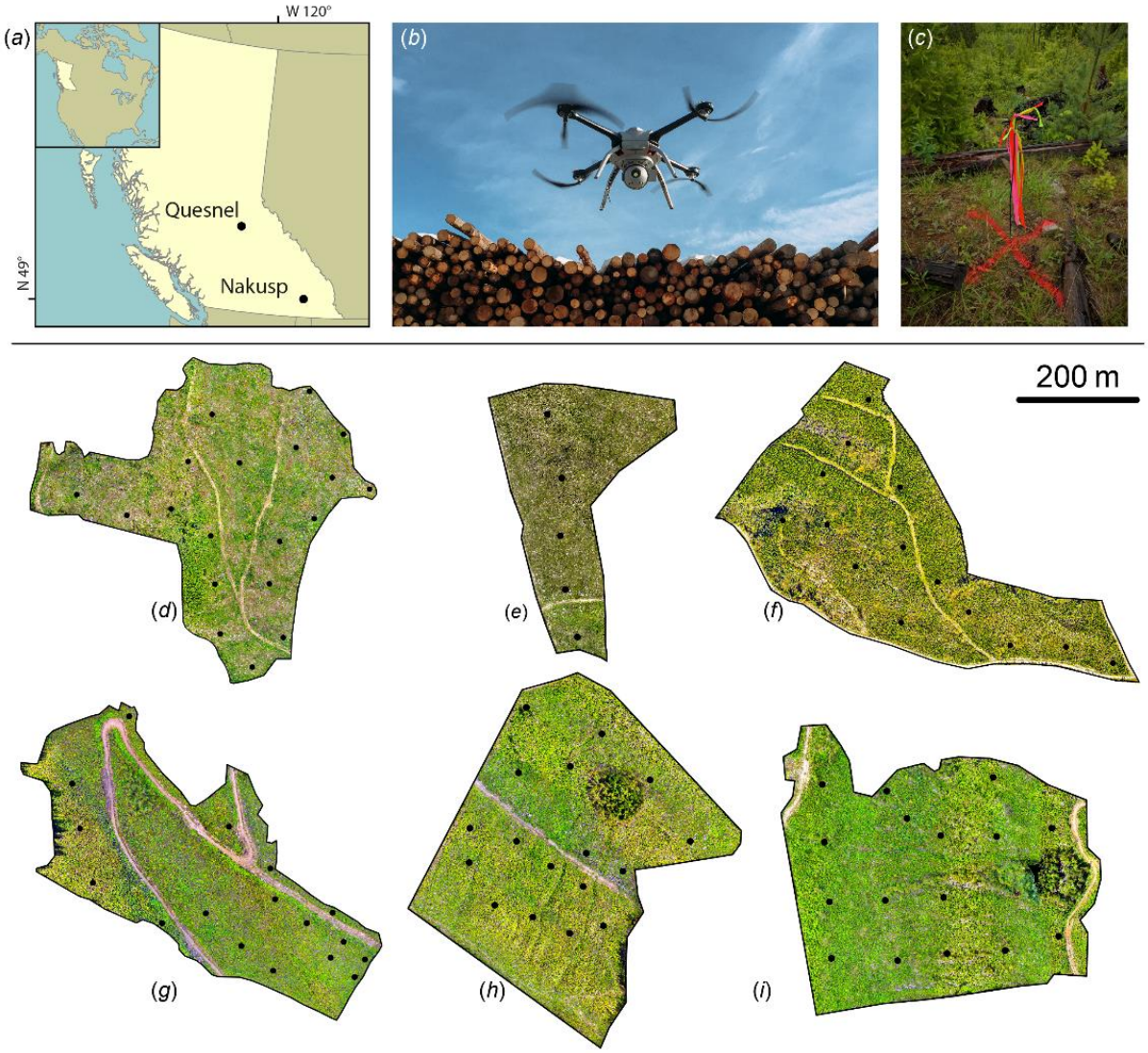

Figure 17: Upper section: study area map detailing locations of Nakusp and Quesnel within British Columbia, Canada (a); Aeryon SkyRanger UAS used for imagery acquisition (b); example plot centre delineated with red spray-paint (c). Lower section: Quesnel stands 5 years since planting (YSP) (d), 10 YSP (e), and 15 YSP (f) and Nakusp stands 5 YSP (g), 10 YSP (h), and 15 YSP (i). Plot locations within each stand are delineated by black points.

5.3 Methods

In order to accurately classify forest cover on both sites the following methodology was employed (Figure 18). Field plots were first located, demarcated, and measured (Figure 17 (c)). Wall-to-wall UAS imagery was then acquired, followed by orthoimagery and generation of a DAP point cloud. Image layer stacks including UAS RGB imagery, visible vegetation indices

(VVI), and DAP canopy height models (CHM) were computed. An object based image analysis (OBIA) was then performed (Blaschke, 2010). The OBIA methodology included image segmentation, descriptive attribute extraction, and supervised classification. Analysis was then performed on classified objects to illuminate structural, spectral, and temporal trends. Further description and definition of objects and the OBIA methodology can be found in Ruiz et al. (2011).

5.3.1 Field measurements

Regeneration data were collected in circular 50 m^2 (3.99 m radius) plots. Plots were divided into four quadrants delineated with hi-visibility red spray-paint (Figure 17 (c)). Locations of the plot centers were averaged using a handheld Garmin GPSMAP 64s. Starting from quadrant 1 in a counterclockwise direction, all coniferous trees were tallied noting quadrant number, species, visual health (Good, Moderate, Poor), and stem density (High, Moderate, Low). Stem density in this context refers to the number of stems per quadrant. Artificial regeneration in BC is generally planted to densities between 400-1600 stems per hectare (MFLNRO, 2016). Level of deciduous competition inhibiting coniferous growth was visually evaluated (High, Moderate, Low), and species was also noted for each quadrant. Tree height and average crown diameter were recorded for a representative tree in each plot. Crown diameter was recorded by measuring the major axis of the tree at the base of the crown, then measuring the minor axis perpendicular to the initial measurement.

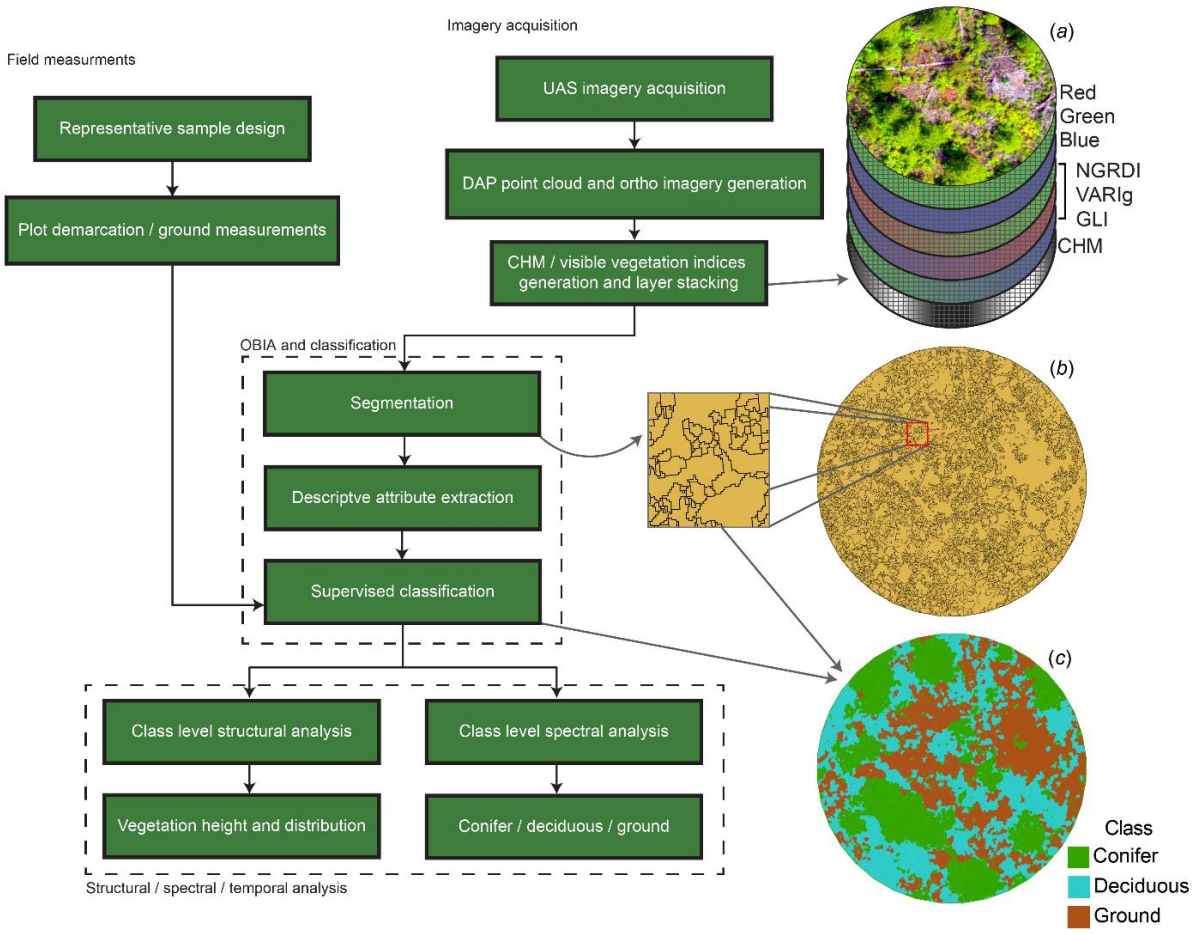

Figure 18: Flow diagram detailing the methodological process used for field sample and imagery data acquisition, OBIA and classification, and structural, spectral, and temporal analysis. Graphical representation of RGB, visible vegetation indices, and canopy height model layer stack with UAS acquired imagery of a 3.99m radius sample plot in the Nakusp site on 13 June 2016 with red X plot centre demarcation (a), segmented object product of same layer stack with zoom inset (b), and final classified objects (c).

5.3.2 UAS data acquisition

High spatial resolution imagery for each stand was acquired using a vertical take-off and landing Aeryon Sky Ranger UAS, weighing approximately 2 kg (Figure 17 (b)). All flights were completed within a week of field data collection (Nakusp: June 13-17, 2016; Quesnel: June 26-30, 2016) between 9am to 4pm local time under clear sky conditions. Acquired imagery was taken using a 16-megapixel SUNEX MT9F002 RGB sensor fitted to a 3-axis stabilized gimbal to maintain nadir image capture. Flights were pre-programmed in a grid pattern with reference to

terrain elevation to maintain flight elevations of approximately 100 m above ground, and to ensure along- and across-track overlap of approximately 85% and 70% respectively. Robust gyroscopic stabilization software was used to ensure the highest quality image capture and data integrity. All imagery was georeferenced, and assigned inertial measurement unit corrections. Average GSD was approximately 2.4 cm. The number of images acquired and the total flight duration depended on stand area.

5.3.3 Point cloud processing

Acquired UAS imagery for each stand were compiled for DAP point cloud and orthoimagery production using Pix4D software (Pix4D, 2018b). Images were aligned and optimized using in-flight inertial measurement unit and global navigation satellite system/GPS measurements, followed by conjugate tie-point pixels being matched in overlapping images. Orthoimagery generation for each stand were generated post-alignment. Dense DAP point clouds were then produced with an average density of 168.9 ± 57.1 points m^{-2}. Horizontal and vertical accuracies of the DAP point clouds were ± 6 cm and 9 cm respectively (Goodbody et al., 2017). Point clouds were classified into ground and non-ground points using LAStools point cloud processing software (Isenburg, 2018). Ground points were used for normalization and DTM creation, while surface models were produced from points with maximum heights. Pit-free CHMs with a 5 cm resolution were produced following methods presented in Khosravipour et al., (2014). Following structural metric extraction, maximum plot height from the DAP data was compared with the representative field measured height to determine the correlation between datasets.

5.3.4 Image processing

To reduce the influence of atmospheric effects on image segmentation and classification, normalized and atmospherically resistant VVI were produced. The VVI selected were those that utilize visible wavelengths, such as the normalized green red difference index (NGRDI; Equation 2), visible atmospherically resistant index ($VARI_g$; Equation 3), and green leaf indices (GLI_x; Equation 4; (Hunt et al., 2012). These VVI's were chosen as they have been shown to provide informative spectral products in the visible spectrum that help to limit the influence of atmospheric variation such as shadowing over the course of an imagery acquisition (Hunt et al., 2012). These indices have shown strong linear relationships with percent cover of vegetation. The indices were computed from the UAS imagery, after which OBIA was performed independently for each stand. The OBIA included segmentation, descriptive attribute extraction, and classification.

$$\mathrm{NGRDI} = \frac{R_\mathrm{g} - R_\mathrm{r}}{R_\mathrm{g} + R_\mathrm{r}} \quad [2]$$

$$\mathrm{VARI_g} = \frac{R_\mathrm{g} - R_\mathrm{r}}{R_\mathrm{g} + R_\mathrm{r} - R_\mathrm{b}} \quad [3]$$

$$\mathrm{GLI_x} = \frac{2\,R_\mathrm{g} - R_\mathrm{r} - R_\mathrm{b}}{2\,R_\mathrm{g} + R_\mathrm{r} + R_\mathrm{b}} \quad [4]$$

Where R_r, R_g, and R_b are the digital numbers for red, green, and blue channels respectively.

5.4 Object based image analysis

5.4.1 Segmentation

Image segmentation is conducted to create objects with homogenous and independent data properties. Segmentation was performed using the NGRDI, $VARI_g$, and GLI_x spectral

indices. Image objects were produced using the automated two-step 'watershed by immersion' segmentation algorithm (Powers et al., 2015; Vincent et al., 1991). This algorithm first outlines object edges by applying Sobel edge detection (Sobel and Feldman, 1968). Edges are delineated using a bi-directional convolution mask that produces a gradient magnitude image where the highest pixel values indicate areas with the highest pixel contrast. The watershed algorithm was then used to sort pixels by gradient value, and consequently 'flood' the image to produce pixel segments with similar intensities. To avoid issues with over-segmentation, the spectral composition of neighboring objects were analyzed and objects found to have similar spectral composition were merged using the full-schedule lambda methodology (Robinson et al., 2002). Objects were iteratively merged if their merge cost was less than a pre-established cost threshold, determined using spectral and spatial variables such as band intensity metrics and distance between segments. The segmentation and merging stages of the 'watershed by immersion' algorithm can be fine-tuned using scale-level and merge-level parameters. Variation of these inputs determines the overall shape and size of produced objects.

5.4.2 Descriptive attribute extraction

The purpose of attribute extraction is to derive meaningful object parameters that can be used to discriminate amongst classes and illuminate within class trends. Descriptive spectral and textural attributes were generated for each object. At this stage of the analysis, the CHM from each stand was incorporated as a structural image band. Statistics, including the minimum, maximum, range, mean, mode, and standard deviation, were computed for the original RGB bands, as well as the NGRDI, $VARI_g$, GLI_x, and CHM bands. Textural attributes such as the mean, range, variance, and entropy (arrangement of spectral data) were also computed (Ruiz et al., 2011). These attributes detail how intensity values were spatially distributed within each

object. Geometric attributes that describe the shape and dimension of objects such as length, compactness, and shape index were computed, but were not included in the classification process. Geometric attributes were discarded largely because segmentation objects were similar in size, shape, and elongation. Eighty-six descriptive metrics were produced during the attribute extraction process.

5.4.3 Classification

Within plot and quadrant composition from ground sampling facilitated the allocation of representative training objects via photo-interpretation. Knowledge of the vegetative composition within each plot quadrant improved the reliability of accurate supervised sample collection. An average of 1578 automatically segmented training sample objects were chosen from each stand (Table 3 and Table 4). Following representative training object delineation, a supervised classification utilizing objects of known cover types was performed to differentiate segmented objects into conifer, deciduous, or bare ground classes. To do this, the Random Forest classifier, which uses decision trees based on a random subset of training samples as well as a random samples of descriptive metrics, was used (Breiman, 2001). In Random Forest each individual tree allocates votes towards a particular class while evaluating variable importance in its class attribution. Objects being classified are then ascribed the class that has the highest proportion of votes from each tree (Powers et al., 2015). The number of votes received for each class is used as a means of evaluating the attribution confidence. Multi-collinearity of all metrics was assessed prior to classification to remove potential negative effects on the distribution and results. One metric from groups of highly correlated variables (Pearson's $r > 0.7$) were used in the analysis (Hermosilla et al., 2015a).

Table 3: Total number of samples for each class within each classification along with mean and standard deviations within and among classifications for the Nakusp Site.

Years since planting (YSP)	Class				
	Conifer	Deciduous	Ground	Mean	Standard deviation
5	106	1368	279	584	684
10	615	369	185	390	216
15	1666	369	185	740	807
Mean	796	702	216		
Standard deviation	796	577	54		

Table 4: Total number of samples for each class within each classification along with mean and standard deviations within and among classifications for the Quesnel Site.

Years since planting (YSP)	Class				
	Conifer	Deciduous	Ground	Mean	Standard deviation
5	671	1599	486	919	596
10	533	330	103	322	215
15	1191	1338	494	1008	451
Mean	798	1089	361		
Standard deviation	347	670	223		

5.4.4 Classification assessment and attribute analysis

Confusion matrices detailing the overall, user, and producer accuracies were computed for all supervised classifications. Overall accuracy was computed using the out-of-bag error estimate (Breiman, 1996). Individual classifications were performed for each stand in order to reduce negative influences of solar irradiance and atmospheric shadowing variability within and among UAS flights. Objects were grouped by forest cover class and YSP of the stands within the sites facilitating independent wall-to-wall statistical analyses of structural and spectral attributes.

5.5 Results

5.5.1 Field measurement analysis

A Spearman's correlation was performed to assess the relationship between representative field measured height and the maximum height from DAP point cloud plots. A strong, statistically significant correlation was found, $r_s = 0.91$, $p < 0.01$ (Figure 19).

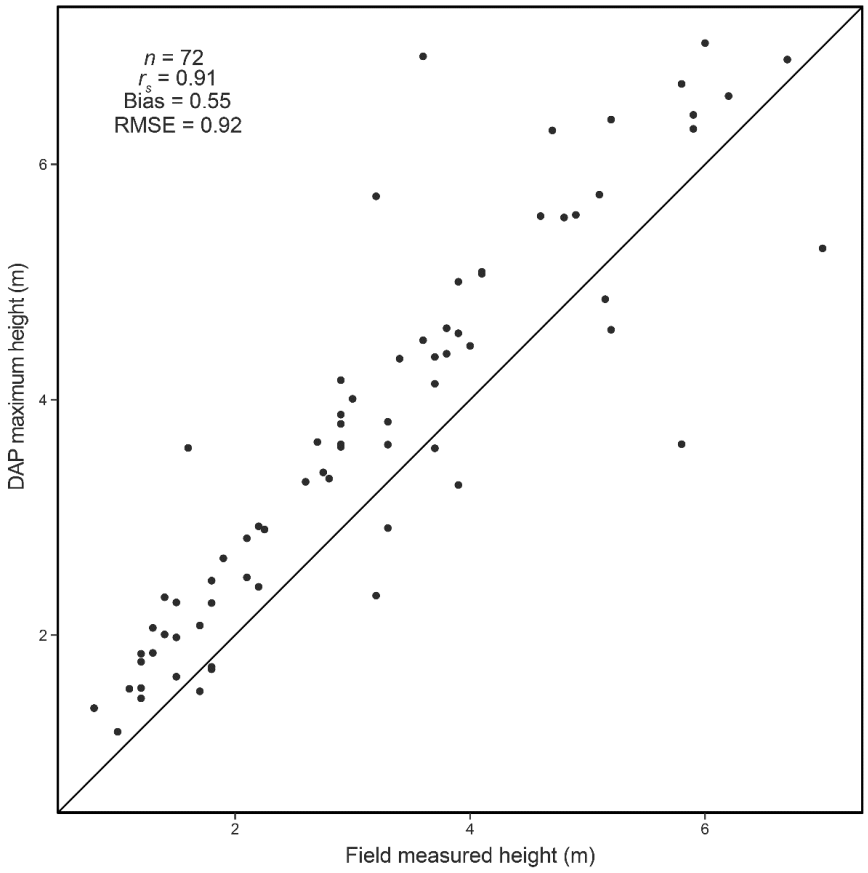

Figure 19: Scatter plot detailing the Spearman's correlation (r_s) between field measured representative height (m) and the maximum height from DAP plot point clouds. Solid diagonal represents the 1:1 line.

5.5.2 Forest cover classification

The highest overall forest cover classification (conifer, deciduous and ground) accuracy of 95.6% was achieved in the 5 YSP stand at the Quesnel site. Commission errors were highest in the 5 YSP stands at both the Nakusp (32.4%) and the Quesnel sites (10.5%). The lowest overall accuracy of 86.4% occurred in the 5 YSP stand at the Nakusp site (Table 5, Table 6). Proportional forest cover were derived from wall-to-wall objects for all stands (Figure 20). The 5 YSP stands at both sites had the lowest conifer and highest bare ground area coverage, while the 15 YSP stands showed the opposite trend. Deciduous coverage was found to be highest in the 10 YSP stand in the Nakusp site (Figure 21 (b)) and the 15 YSP stand in the Quesnel site (Figure

21, a).Variable importance for all Random Forest classifications showed that textural band metrics including entropy, mean, range, and average were found to be the important for describing the observed variance (Table 7). Textural, structural, and spectral metrics were all selected in each of the 6 classifications. The CHM standard deviation metric was the only structural metric selected in all 6 classifications. GLI_x textural metrics were frequently selected in all classifications.

Table 5: Confusion matrices comparing reference and classification data for the Nakusp site for (a) 5 YSP, (b) 10 YSP, and (c) 15 YSP.

(*a*)	Reference data				
Classification data	Conifer	Deciduous	Ground	User's accuracy (%)	Commission error (%)
Conifer	106	192	3	35.2	64.8
Deciduous	57	1368	2	95.9	4.1
Ground	8	13	279	93.0	7.0
Producer's accuracy (%)	62.0	87.0	98.2		
Omission error (%)	38.0	13.0	1.8		
				Overall accuracy (%)	86.4

(*b*)	Reference data				
Classification data	Conifer	Deciduous	Ground	User's accuracy (%)	Commission error (%)
Conifer	615	55	9	90.6	9.4
Deciduous	33	369	5	90.7	9.3
Ground	3	2	185	97.4	2.6
Producer's accuracy (%)	94.5	86.6	93.0		
Omission error (%)	5.5	13.4	7.0		
				Overall accuracy (%)	91.6

(*c*)	Reference data				
Classification data	Conifer	Deciduous	Ground	User's accuracy (%)	Commission error (%)
Conifer	1666	55	9	96.3	3.7
Deciduous	33	369	5	90.7	9.3
Ground	3	2	185	97.4	2.6
Producer's accuracy (%)	97.9	86.6	93.0		
Omission error (%)	2.1	13.4	7.0		
				Overall accuracy (%)	95.4

Table 6: Confusion matrices comparing reference and classification data for the Quesnel site for (a) 5 YSP, (b) 10 YSP, and (c) 15 YSP.

(*a*)

	Reference data				
Classification data	Conifer	Deciduous	Ground	User's accuracy (%)	Commission error (%)
Conifer	671	75	4	89.5	10.5
Deciduous	46	1599	1	97.1	2.9
Ground	1	1	486	99.6	0.4
Producer's accuracy (%)	93.5	95.5	99.0		
Omission error (%)	6.5	4.5	1.0		
				Overall accuracy (%)	95.6

(*b*)

	Reference data				
Classification data	Conifer	Deciduous	Ground	User's accuracy (%)	Commission error (%)
Conifer	533	22	4	95.3	4.7
Deciduous	17	330	1	94.8	5.2
Ground	1	4	103	95.4	4.6
Producer's accuracy (%)	96.7	92.7	95.4		
Omission error (%)	3.3	7.3	4.6		
				Overall accuracy (%)	95.2

(*c*)

	Reference data				
Classification data	Conifer	Deciduous	Ground	User's accuracy (%)	Commission error (%)
Conifer	1191	105	3	91.7	8.3
Deciduous	86	1338	6	93.6	6.4
Ground	5	14	494	96.3	3.7
Producer's accuracy (%)	92.9	91.8	98.2		
Omission error (%)	7.1	8.2	1.8		
				Overall accuracy (%)	93.2

5.5.2.1 Structure characterization

Mean conifer height increased as YSP increased for both sites, following the same trend as proportional conifer area coverage (Figure 21). Deciduous mean height followed a similar, but less pronounced, increasing height trend in the Nakusp site (Figure 21 (a)). At the Quesnel site, mean deciduous height was highest in the 5 YSP stand (Figure 21 (b)).

The majority of the conifer area coverage in the 5 YSP stand at the Nakusp site were less than 0.5 m in height (Figure 22). The 10 YSP and 15 YSP stands show progressive increases in conifer height, while area coverage becomes more evenly distributed among height classes. The 15 YSP stand was found to have the least conifer coverage below 1.5 m of the three stands. The 15 YSP stand indicated a more complex distribution indicating that conifer heights at this regeneration stage were predominantly taller, but that shorter conifer continue to be represented.

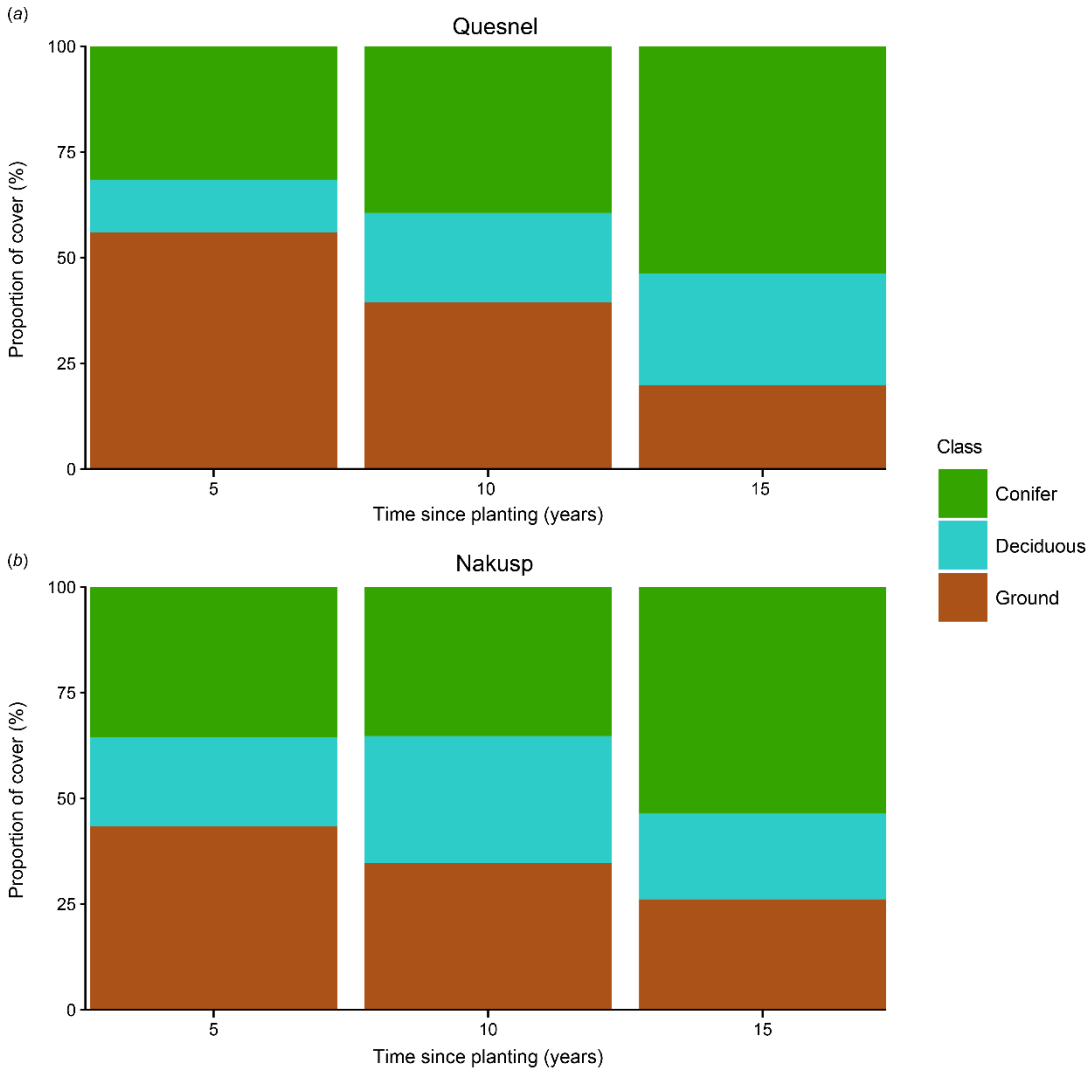

Figure 20: Aggregated plot level forest cover proportions in the Quesnel (a) and Nakusp (b) at 5, 10, and 15 YSP.

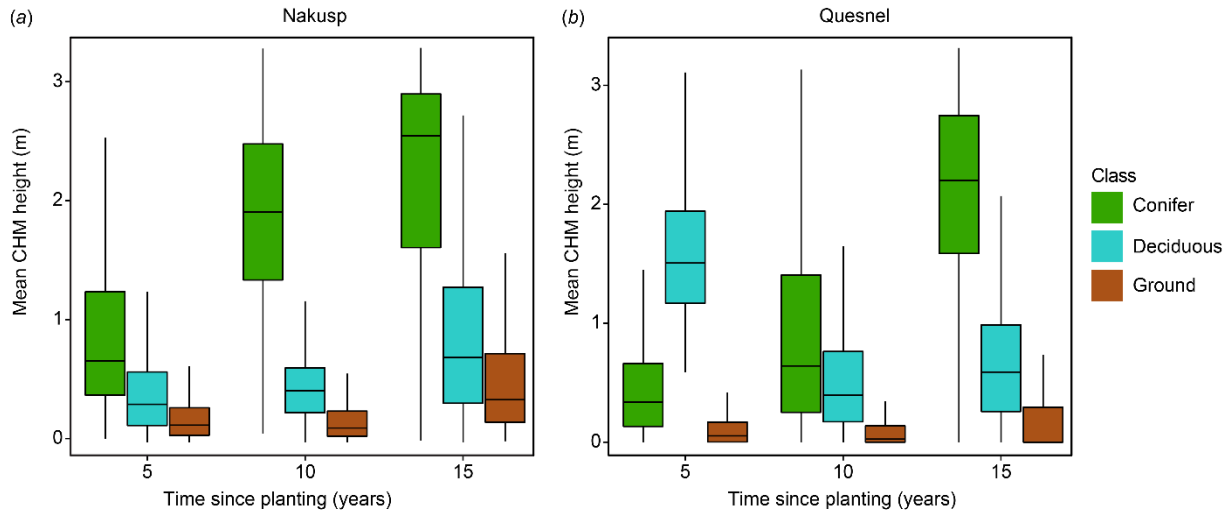

Figure 21: Mean height of conifer, deciduous, and ground features in Nakusp (a) and Quesnel (b) for 5, 10, and 15 YSP.

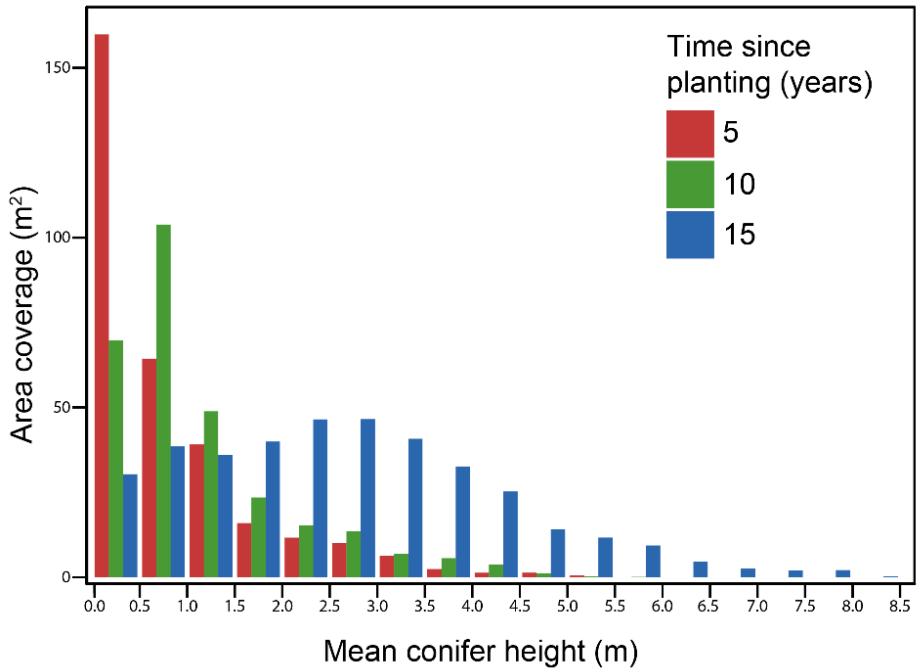

Figure 22: Distribution of object area coverage (m^2) and mean height (m) for 5, 10, and 15 YSP stands in the Nakusp site. The height of each bar represents the area of the canopy of trees with a mean height that fall within the range of the heights labelled on either side of the bars.

5.5.2.2 Spectral characterization

The raw RGB bands indicated similarities and inherent variability in brightness values across stands and sites (Figure 23). The NGRDI, VARIg, and GLI_x indices were successful in

differentiating vegetation (conifer and deciduous) objects from ground. Objects at the Nakusp site demonstrated similar statistical distributions for conifer and deciduous mean NGRDI, indicating that these VVI were successful, and consistent in differentiating between land cover at differing regeneration ages. Apart from the 10 YSP stand at the Quesnel site (Figure 23 (d)), mean deciduous NGRDI was found to be steady in its response. The Nakusp site showed consistency in conifer and deciduous mean NGRDI values for all stands (Figure 23 (c)). Differentiation between conifer and deciduous cover was found to be most successful using VVI in the 5 YSP stand, while the 10 YSP and 15 YSP stands at both sites indicated predominantly similar responses.

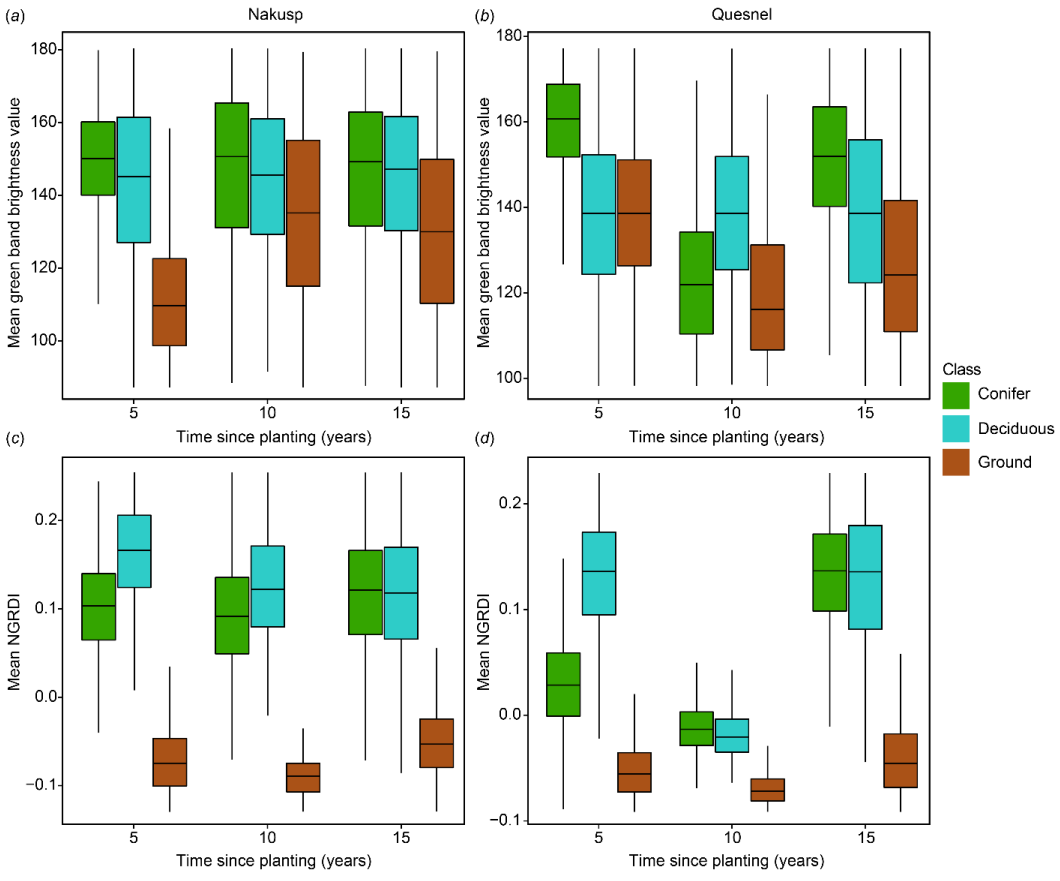

Figure 23: Mean brightness values for the green band (a, b) and the mean NGRDI (c, d) for 5, 10, and 15 YSP stands in the Nakusp and Quesnel sites.

Table 7: Most frequently selected metrics, their type, and the number of times they were selected in Random Forest classifications.

Metric	Descriptive Attribute	Times Selected
Entropy – Red, blue, GLI_r, GLI_g, GLI_b,	Textural	6
Standard deviation – CHM, green, GLI_b	Structural	6
Entropy - GLI_r	Textural	5
Mean - GLI_r	Textural	5
Standard deviation - Blue	Spectral	5
Entropy - $VARI_g$	Textural	4
Mean - Blue	Textural	4
Range – Green, GLI_b	Textural	4
Standard Deviation – Red, GLI_r, GLI_g	Spectral	4
Average – Green, GLI_g	Textural	4
Maximum - CHM	Structural	3
Maximum – Red, green	Spectral	3
Range – Red, blue, GLI_g	Textural	3
Variance - Blue	Textural	3

5.6 Discussion

Results show similarities with other studies where analogous classification methodologies were employed for large scale land-cover classifications in Canada (Powers et al., 2015). These results further illustrate the potential of incorporating UAS acquired imagery for forest management purposes. The methodology was successful at differentiating, classifying, and detailing forest cover for stands of different regeneration ages and geographical locations (Table 5, Table 6). Incorporating field plots of known vegetative composition for identifying sample

training objects likely limited forest cover miss-classification. There was methodological robustness within our sites and regeneration ages as we achieved high overall accuracies for all classifications.

The high accuracies facilitated wall-to-wall feature segmentation, attribute extraction, and classification for all stands providing highly detailed and reliable spatial, structural, and spectral information on forest cover. These data could have profound influence on management decision making, providing valuable information on the distribution (Figure 20), state (Figure 21, Figure 23), and extent (Figure 22, Figure 24) of differing forest stands and ages. Knowledge of the physical location, spatial distribution, and structural characteristics of forest cover facilitate precision forest management approaches (Goodbody et al., 2016; Holopainen et al., 2015). The use of UAS imagery and DAP point clouds in this study has shown their effectiveness in detailing all of these characteristics. The ability to detail location, distribution, as well as spectral and structural characteristics at the centimeter level from a single UAS flight plan demonstrates the effectiveness of DAP technology for providing enhanced forest inventory information in an efficient and cost-effective manner (Dvořák et al., 2015).

Compared to conventional ALS acquisitions (Wulder et al., 2008), high point densities used to produce the DAP CHMs in this study facilitated differentiation of vegetation at finer levels of spatial detail (Figure 21 and Figure 22). Results from the comparison between field measured representative tree heights and DAP maximum height showed a strong correlation, indicating that UAS acquired DAP is accurate in its ability to detail regeneration height (Figure 19). Future analysis should focus on regeneration measurements that can be directly related to DAP point clouds, such as maximum plot height, to assess absolute accuracy of height measures. The inclusion of the CHM standard deviation metric in all classifications provides insight into

the importance of including structural variables for discriminating amongst forest cover classes. These findings are promising for the incorporation of DAP technology for providing high spatial resolution structural information to forest managers that can be used to meet management and reporting goals. Both the DAP point cloud and orthoimagery also have potential to be incorporated to act as auditing tools, monitor compliance with silviculture prescriptions, and provide input data for growth projection models. The ability to routinely introduce height measurements into growth and yield projections would help to establish connections between EFI data sets, establishing linkages between inventory hierarchies.

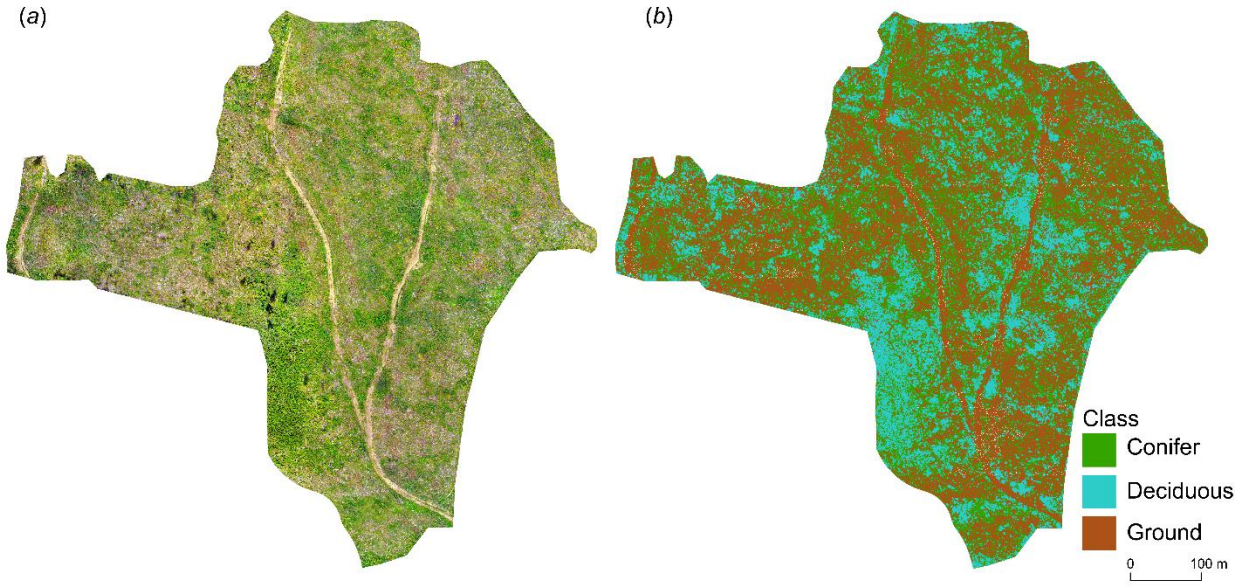

Figure 24: Comparison of (a) UAS-acquired ortho imagery and (b) wall-to-wall classification for 5 years since planting stand in the Quesnel site.

While DAP is effective at detailing forest surface structure, research into its ability to detect individual stems is ongoing (Nevalainen et al., 2017; Panagiotidis et al., 2017). Vauhkonen et al. (2012) noted that the performance of individual tree detection and segmentation algorithms in ALS typically depends on the tree density, point density parameters, and the spatial distribution and clustering patterns of trees. Results found in Tiede et al. (2006)

corroborate these findings, and further detail that physiological differences between deciduous and coniferous stems such as having more than one local maximum and inter-growth amongst deciduous individuals increase potential for detection, segmentation, and classification related errors. Other factors such as site level heterogeneity driven by topography, pre-disturbance composition, and post disturbance legacies promote highly heterogeneous forest regeneration, reducing potential to accurately differentiate amongst individuals (Oliver and Larson, 1996; Turner, 2010). It is for this reason that the potential to detect all stems using aerial remote sensing technologies is still limited. Given that stem density and species stocking criteria are needed for current reporting in regeneration surveys, further research into the improvement of individual tree detection algorithms is warranted.

The ability to detail the physical location, coverage, and structural attributes of vegetation in regenerating stands is of great importance to forest managers (Haddow et al., 2000; Pitt et al., 1997). Wall-to-wall orthoimagery and classification products, such as those provided using the methodology presented in this study, have great potential to improve managerial land base knowledge and operational efficiency (Figure 24). Conducting classifications on stands of interest prior to the application of treatments such as deciduous brushing or fill planting could not only provide enhanced knowledge of spatial and structural stand attributes, but also a means of increasing the cost effectiveness of treatment operations and improving knowledge related to the state of the land base being managed (Hall and Aldred, 1992). Easily interpretable digital mapping products facilitate effective pre-treatment planning and post-treatment evaluation. Linkages between treatment costs and associated forest cover changes can be quantified to evaluate the economic and operational success of management actions, while producing, and updating, high resolution, multi-temporal inventory systems (King, 2000). The adoption of

spatial and temporal forest regeneration monitoring at scales that reflect managerial and data reporting needs has potential to greatly benefit long term forest management approaches, potentially revolutionizing how forest monitoring and spatial ecology are conducted (Zhang et al., 2016). This is especially evident given that UAS surveys are able to acquire temporal and spatial resolutions that best suit environmental and economic management criteria (Goodbody et al., 2016; Goodbody et al., 2017b; Goodbody et al., 2018b).

As described in Chapter 4, an added benefit to using DAP for detailing the structural variation of open canopy stands is the ability to generate DTMs (Debella-Gilo, 2016). Increased stand density and vegetation coverage greatly limit the ability of DAP to produce reliable DTMs, which is a reason that ALS derived products are often preferred (Holopainen et al., 2015). The results of our study indicate that DAP was successful in generating DTMs due the relatively low vegetation cover compared to more mature forest stands, and that it has potential to do so in stands up to 15 YSP. Reliable and consistent generation of these products could be further improved by choosing optimal times of year to fly, specifically around those recommended in Chapter 4. Flights after snowmelt, and prior to the establishment of annual deciduous ingrowth, which is also a condition detailed in the appropriate times to sample forest regeneration in the field, should be prioritized (MFLNRO, 2016). The production of accurate stand-level DTMs will provide baseline elevation information that can be used for future multi-temporal inventory analyses. These data will help form a strong basis for ongoing, long-term ecosystem-based management and EFI approaches looking to assess and monitor the effectiveness of current management and inventory objectives.

Vegetation indices were shown to be effective in their ability to distinguish between vegetation and ground features, and potentially conifer and deciduous features in the case of the

5 YSP stands on both sites (Figure 23). Differentiation between conifer and deciduous features in the 5 YSP sites could be caused by differing spectral properties between younger and older foliage (Möckel et al., 2014), but further investigation is needed. Results indicate that the incorporation of VVI into the forest cover classification framework was effective and computationally simple. VVI textural metrics, especially from GLI_x bands were found to be among the most frequently selected variables in the Random Forest classifications (Table 7). Above threshold correlation ($r > 0.7$) values found between most VVIs reduced the number of these metrics included in Random Forest classifications, however also indicates that VVIs can be capable and effective as discriminatory classification variables across different sites (Figure 23). Frequent selection of textural and spectral metrics demonstrates that their inclusion in the OBIA classifications provided increased discriminatory depth regardless of site location. Entropy and standard deviation metrics were found to be the most frequently chosen, possibly due to their ability to recognize spatial patterns in contrast, uniformity, rigidity, and regularity of spectral data (Ruiz et al., 2011).

Given the success of forest cover differentiation using only a conventional RGB sensor, further success could be achieved using multi- or hyper-spectral UAS sensor configurations. Higher levels of spectral resolution could promote an increase in spatial forest knowledge, including individual tree detection, species differentiation, and health evaluation (Näsi et al., 2015). Given that species and forest health are fundamental in forest regeneration survey reporting, more research should be conducted to improve vegetation differentiation and classification. Classifications providing knowledge of the physical location, species, and health of vegetation at a wall-to-wall level could revolutionize silvicultural monitoring, enhance long-term forest inventories, and create useful products for auditing purposes.

The main challenges faced in this chapter revolve around the radiometric inconsistency of UAS imagery resulting from inherently variable atmospheric conditions, and the limited spectral resolution of consumer grade RGB sensors (Dvořák et al., 2015). Variability of solar irradiance and atmospheric shadowing within and among UAS flights introduced difficulty in generating spatially transferrable, robust classifications. The difficulty in controlling these parameters in our study required us to generate individual stand level classifications, which, depending on stand size and geographical location, may still be subject to within-stand variability of solar irradiance. These within-stand limitations become more cumbersome given current UAS flight longevity limitations and federal line-of-sight restrictions (Transport Canada, 2014). To limit the effect of atmospheric variability, future studies could follow the work of Hakala et al. (2013), which demonstrated the potential for radiometric correction of UAS imagery to produce high accuracy stereoscopic and spectrometric imagery in diverse atmospheric conditions. Generating radiometrically calibrated imagery could help to improve the ability to accurately differentiate between, and classify, conifer and deciduous forest cover, and potentially differentiate between species. The confusion between these two cover types were the most pronounced of all classifications in this study and would benefit from methodological improvement.

5.7 Conclusions

The dual benefit of structural data in the form of DAP point clouds and spectral data from acquired stereo-imagery has great potential within EFIs. Results from this chapter on characterizing post-harvest regeneration are promising for outlining that both data types have a role in generating a wide variety of data products. The following chapter continues along this theme, focusing on the utility and comparability of both data types for providing details on the severity and spatial distribution of biotic disturbance at a landscape level. Establishing that DAP

spectral and structural metrics each have inherent value to inventories improves rationale for its integration into EFI frameworks to generate traditional and non-traditional inventory data products.

Chapter 6:

Digital aerial photogrammetry for assessing cumulative spruce budworm defoliation and enhancing forest inventories at a landscape level[5]

6.1 Background and motivation

Forest health monitoring is integral to evaluating ecosystem biodiversity and the sustainability of forest management practices (Franklin, 1993). Monitoring activities that compile information related to current and future status, changes, and trends associated with forest health are ecologically, economically, and socially important (Noss, 1999; Lausch et al., 2017). From a Canadian boreal forest context, changes in phenology, distribution, and reproduction of forest insects such as eastern spruce budworm (*Choristoneura fumiferana* [Clem.], Lepidoptera: Tortricidae) could have major ecological, economic, and social implications (Candau and Fleming, 2005). Spruce budworm disturbances are estimated to account for 41 – 53% of Canada's volumetric timber losses resulting from biological disturbances (Power, 1991; Sterner and Davidson, 1982), and an average of 1.8 million hectares of forest in Ontario have been subject to moderate to severe levels of annual defoliation since 1990 (NFD, 2017). While defoliation events are natural in boreal disturbance regimes, improved understanding of their timing and trends, distribution, and severity will help long-term management under increasingly variable ecological and economic pressures.

[5] The content of this chapter has been adapted from:
Goodbody, T. R.H., Coops, N. C., Hermosilla, T., Tompalski, P., McCartney, G., & MacLean, D. A. (2018). Digital aerial photogrammetry for assessing cumulative spruce budworm defoliation and enhancing forest inventories at a landscape level. ISPRS Journal of Photogrammetry and Remote Sensing, 142, 1-11.

Historical spruce budworm defoliation events ranging in size, intensity, and duration have occurred roughly every 30-40 years with an approximate 10-15 year duration (Régnière and Nealis, 2007; Royama, 1984). Outbreaks of higher intensities lead to losses in previous year's foliage due to rapid consumption of the most recent year's growth. Following defoliation, beginning in late June to early July, a characteristic red colour becomes evident across affected forest stands. This discolouration results from dead, hanging foliage that has been caught in silk trails left behind during budworm movement, as well as from feeding tunnel formations. Factors such as outbreak intensity, temporal sequence, host species distribution (Candau et al., 1998), stand characteristics, as well as climate variables such as temperature and precipitation (Blais, 1961; Gray, 2008; Hardy et al., 1983) all have potential to influence defoliation severity (MacLean, 1984). Although singular instances of defoliation do not generally kill individual trees unless severity is extreme, repeated annual defoliation has been found to increase mortality risk due to reductions in photosynthetic capacity (Candau and Fleming, 2005). Stands affected by defoliation present forest management challenges associated with altered disturbance dynamics (James et al., 2017), reductions in stand vigour associated with height and diameter increment reductions (Baskerville and MacLean, 1979; Blais, 1958; Miller, 1977), loss of accrued volume (Power, 1991), as well as forest structural and compositional changes (MacLean et al., 2001). Research into accurate and cost-effective methods for enhancing landscape level forest inventories would help to improve knowledge on the relationship between spruce budworm defoliation and forest structure at a landscape level, while facilitating long-term monitoring frameworks.

Given the prevalence of spruce budworm induced defoliation and its associated influence on forest health related challenges, initiatives such as sketch mapping of red stage (current)

defoliation have been conducted. These surveys, primarily conducted by the Canadian Forest Service and provincial governments bodies such as the Ontario MNRF Northeast Biodiversity and Monitoring Section since 1941, are a simple, fast, and inexpensive method for helping to inform protection programs and delineate potential harvesting strategies (Candau and Fleming, 2005; Leckie and Ostaff, 1988). These surveys consist of the manual delineation and differentiation of current defoliation into three classes (light (0% – 25%), moderate (26% – 75%), and severe (76% – 100%)), providing data that detail spatial extent and estimated hazard level.

While these surveys provide useful approximations of the distribution and size of budworm populations related to current defoliation mapping (MacLean and MacKinnon, 1996), records of light defoliation are often ignored due to unreliability (Sippell, 1983), and surveys are unable to provide insight into the level of cumulative defoliation present within stands. The assessment of cumulative defoliation through time is important for improving knowledge of spruce budworm induced mortality risk as it details foliage losses in multiple age classes rather than just current defoliation manifested by the red stage (Leckie and Ostaff, 1988). Methods aimed at improving available cumulative defoliation data products at a landscape level would therefore help in guiding management and stewardship strategies and providing evidence for formulating effective forest health related policy.

While dendroecology and long-term ecological monitoring into the physiological and biological patterns of spruce budworm outbreaks has been extensively researched for over 60 years (MacLean et al. 2001), there is still a need for spatially explicit information on patterns and interactions at the landscape level (Senf et al., 2017). Forest managers require accurate, spatially explicit, and detailed information on the extent and severity of disturbances to inform options for

operational management. Remote sensing technologies have been used to facilitate fine spatial, spectral, and temporal scale analyses into forest insect disturbances (Senf et al., 2017; Trumbore et al., 2015). Numerous studies investigating the assessment of current spruce budworm defoliation have been conducted using aerial photography (Ashley et al., 1976; Leckie and Ostaff, 1988; Murtha, 1973), and Landsat multispectral scanner data (Harris et al., 1978; Madding and Hogan, 1978).

Results from these studies found that timing of acquisition, spectral resolution, and imagery scale were important factors for accurately mapping current defoliation with aerial imagery. More recent studies utilizing Landsat thematic mapper (Luther et al., 1997) and SPOT derived spectral indices (Franklin et al., 2008), found significant relationships for detecting spruce budworm defoliation. Multiple studies using satellite and aerial imagery with a focus on defoliation caused by western spruce budworm (*Choristoneura occidentalis*, Freeman) have successfully demonstrated the ability to detect defoliation (Franklin et al., 1995; Vogelmann et al., 2009). A growing body of literature focused on the detection of insect induced defoliation from varying optical remote sensing sources and at varying spatial, spectral, and temporal resolutions is promising for incorporation into operational management (Senf et al., 2017).

Potential tools that offer finer scale information beyond conventional aerial and satellite imagery to improve knowledge of cumulative defoliation are three dimensional remote sensing technologies such as DAP and ALS. These technologies have been proven to provide accurate estimates of forest inventory data such as timber volume and basal area at varying scales (White et al., 2013; Gobakken, Bollandsås and Næsset, 2015; Tompalski et al., 2018).

While analyses using DAP for forest health purposes have been limited to the detection of individual trees for subsequent classification during bark beetle outbreaks (Näsi et al., 2015),

ALS has shown potential for the accurate estimation and mapping of pine defoliation in Scandinavian boreal forest environments (Vastaranta et al., 2013a). Findings from their research indicated that plot-level defoliation sampling facilitated integration into operational level forest management and planning and offer additional value to ALS acquisitions. Given the similarities between ALS and DAP datasets, the successes of ALS for improving structural knowledge of defoliation, and recent advancements in photogrammetric processing streams, opportunities now exist to examine the utility of DAP for quantifying cumulative defoliation in a spruce budworm context.

The application of DAP techniques to aerial imagery acquisitions provide both spectral and structural metrics that, when combined or used independently, may improve knowledge of the spatial distribution and severity of cumulative defoliation. The provision of these metrics may also serve to improve upon landscape level estimates of standard forest inventory attributes such as basal area and volume (White et al., 2015), which have been used for the delineation of spruce budworm host species distribution (Wolter et al., 2008). Enhanced inventory products such as wall-to-wall DAP derived attributes also have potential to provide managers with accurate, up-to-date, and multi-use data that facilitate informed forest management decision making. The acquisition of aerial imagery for the purposes of DAP generation therefore present an opportunity to improve upon landscape level cumulative defoliation, susceptibility, impact damage, as well as forest attribute estimates through time from a single multi-use data set.

In this chapter, aerial imagery acquired over the Gordon Cosens Forest (GCF) south of Kapuskasing, Ontario, Canada, were used to produce DAP point clouds and multi-band vegetation metrics for the purposes of improving spatial, spectral, and structural knowledge of spruce budworm cumulative defoliation. The main objective was to determine whether spruce

budworm defoliation was detectable using DAP point clouds, and in doing so, assess the relative predictive power of structural vs. spectral metrics to model cumulative defoliation at a landscape level. Additionally, I assessed the effectiveness of DAP structural metrics for modelling field measured merchantable timber volume and basal area using the ABA presented in Section 2.2. The accurate estimation of these inventory attributes could be useful for assessing potential economic impacts of defoliation through time, as well as monitoring changes and trends in forest structure and health (Lausch et al., 2017). Results from this study could help to examine patterns in prevalent ecosystem processes, improve understanding of predominant disturbance regimes, provide a means of evaluating the sustainability of targeted forest ecosystems, and consequently, evaluate the socio-political and economic implications of forest health related changes (Dale et al., 2001).

6.2 Methods

6.2.1 Study area

The study site for this analysis was the GCF, located approximately 80 km south of Kapuskasing, Ontario, Canada (Figure 25). Situated in the heart of the clay belt of the eastern boreal forest, topography is very flat with an abundance of small lakes and muskegs. Forest stands are primarily comprised of black spruce (*Picea mariana*), balsam fir (*Abies balsamea*), white spruce (*Picea glauca*) and various deciduous species including birch (*Betula spp.*) and poplar (*Populus* spp.).

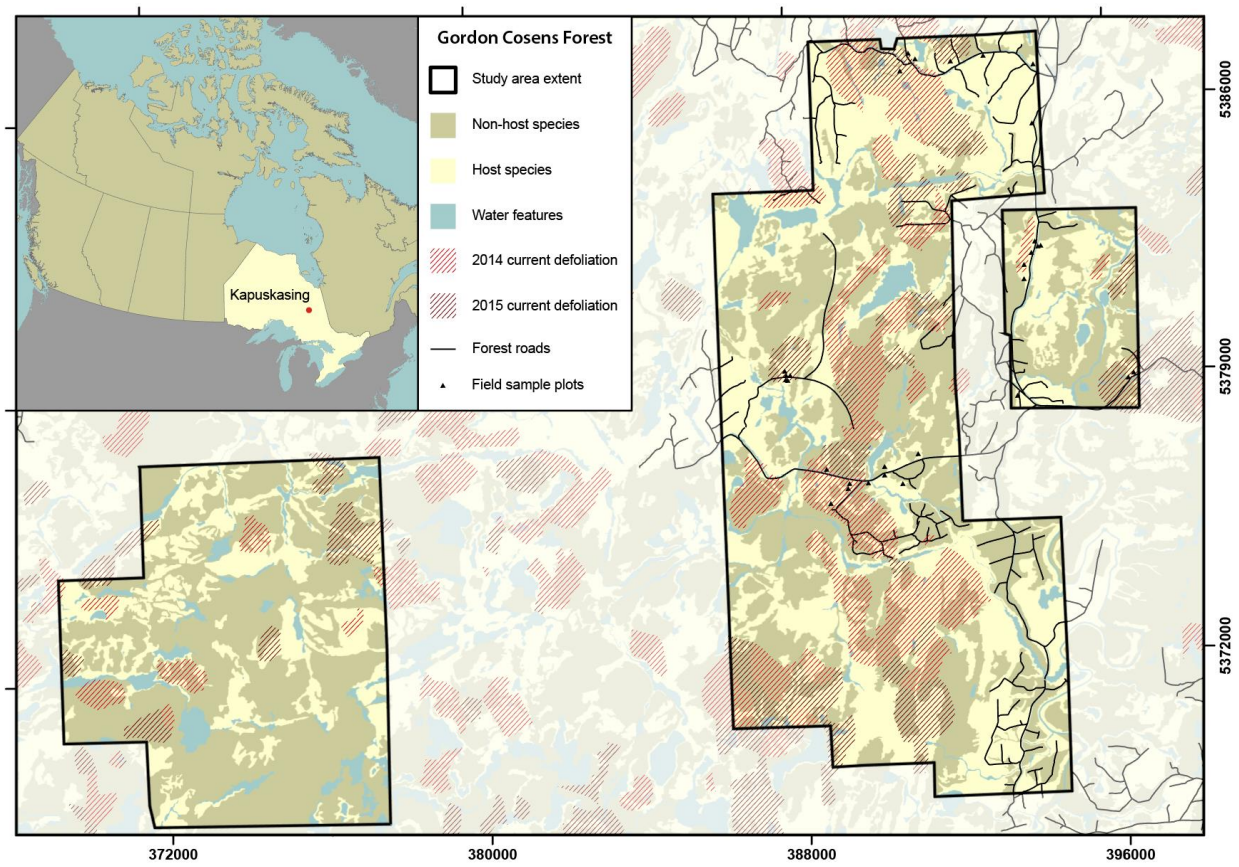

Figure 25: Study area map detailing location of Kapuskasing within Ontario, Canada and landscape level extents of the Gordon Cosens Forest study area. Land cover and species information taken from a 2008 enhanced forest resource inventory and road features were provided courtesy of RYAM Forest Management. Current defoliation features for 2014 and 2015 were derived from annual sketch mapping surveys conducted by the Ontario MNRF Northeast Biodiversity and Monitoring Section. Final sample plot locations (n=30) are marked with triangles.

6.2.2 Imagery acquisition and point cloud processing

High spatial resolution (25 cm) aerial imagery was acquired from a Piper Navajo PA 31 fixed-wing aircraft. Image acquisition was conducted in clear weather conditions on May 10th, 2016 over three sections of the GCF (Figure 25). Imagery acquisition was conducted prior to the red stage that is traditionally used to assess current spruce budworm defoliation. Timing for image acquisition is known to have occurred in the early stages of 2016 spruce budworm feeding period. Parameters for image acquisition are detailed in Table 8.

Table 8: Imagery acquisition parameters.

Acquisition parameters	
Sensor	UltraCamX
Spectral bands	RGB & NIR
Average flight altitude (m)	3375
Forward overlap (%)	65
Side overlap (%)	25
Ground sample distance (cm)	25
Image format	8-bit TIFF

Image processing was performed using Agisoft Photoscan Professional Edition (Agisoft, 2018). A total of 139 images were aligned into three separate forested areas (Figure 25). Tie-points were generated for overlapping stereo images using Agisoft image matching algorithms. Inertial measurement unit and GPS metadata were included in tie-point generation. Due to limited availability of terrain data, the Advanced Spaceborne Thermal Emission and Reflection Radiometer 30 m DTM was used to assign ground control point elevations to improve point cloud measurement accuracy and incorporate elevations to areas of higher canopy cover. Tie-point locations and camera positions were then used to construct dense point clouds with an average density of 4.3 points m^{-2}. Dense clouds were used to create surface mesh files for orthoimagery generation. Use of dense cloud derived mesh files ensured that structural and spectral data components were accurately co-registered for future analysis. Dense point clouds were exported and post processed using LAStools (Isenburg, 2018). Point cloud post processing followed the same procedure as described in Chapter 5, where data were filtered for noise, classified, and normalized prior to structural metric extraction.

6.2.3 Spectral metric extraction

Multi-band orthoimagery was used to compute a suite of vegetation indices (Figure 26) from which spectral and textural metrics were derived at a 400 m^2 (20 x 20 m) resolution grid (Hunt et al., 2012). This grid area was chosen to match the area of field measured plots, which is recommended as best practice for forest inventory modeling using the ABA (Næsset and Bjerknes, 2001; White et al., 2013, 2017). Next, descriptive spectral metrics were computed for all raw bands and vegetation indices following the methodology outlined in Section 5.3.4 and FETEX 2.0 feature extraction software developed by Ruiz et al. (2011). Spectral metrics were calculated using all orthoimagery pixels within each 400 m^2 grid cell (Table 9). Textural metrics were calculated using the grey-level co-occurrence matrix methodology (Clausi, 2002; Marceau et al., 1990), which characterizes image texture by calculating how frequently pixel pairs with specific spectral values occur in a specified spatial relationship. A semivariogram analysis (Balaguer et al., 2010; 2013), which detailed the spatial correlation of the spectral values in pixels, was performed on the NIR band (Table 10). For simplicity, use of the term spectral metrics within this analysis refers to the grouping of spectral, textural, and semivariogram derived metrics. For further in-depth description of FETEX 2.0 software and its processing routines see Ruiz et al. (2011).

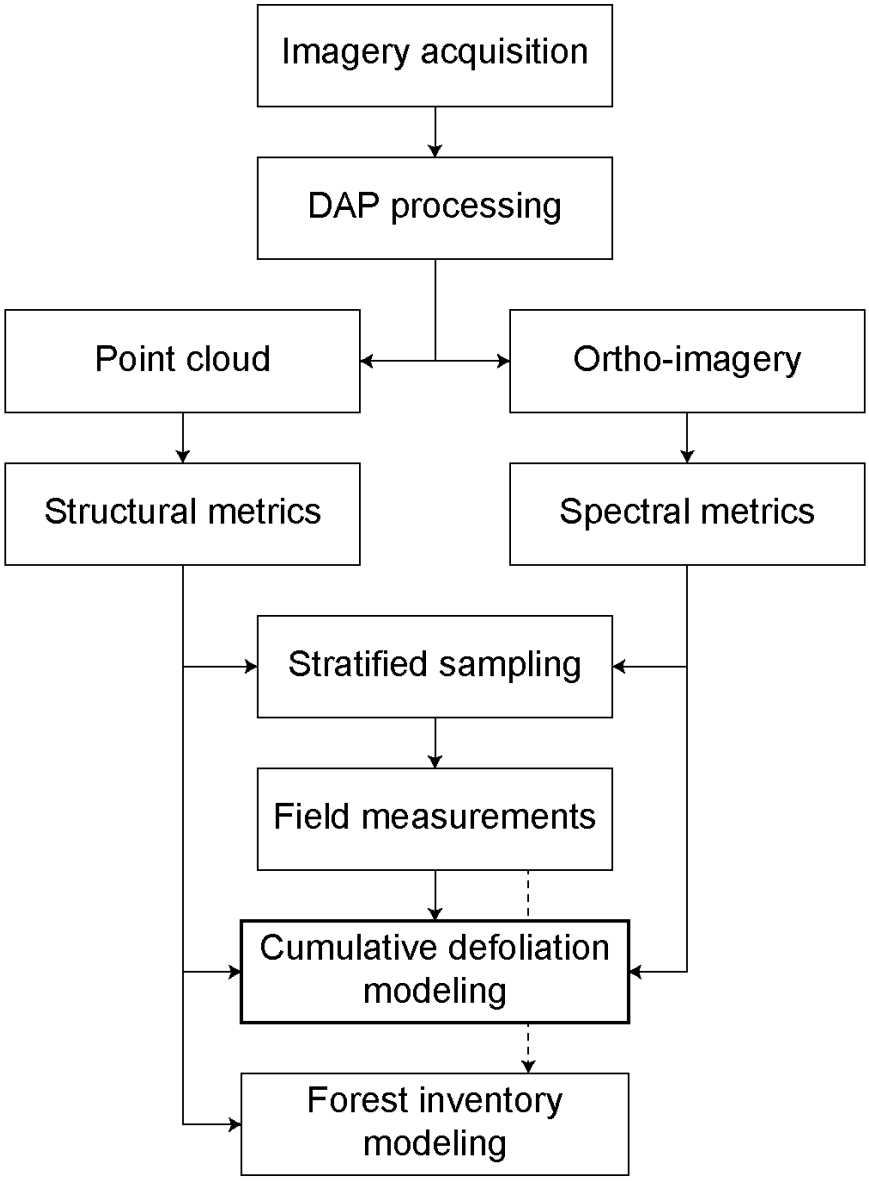

Figure 26: Analysis workflow starting with imagery acquisition, processing, implementation of stratified sampling, field measurement data collection, and forest modelling approaches and associated outcomes. Cumulative defoliation modeling, the primary objective of the study is outlined in bold.

Table 9: Spectral vegetation indices produced using raw imagery bands (B1 = Red, B2 = Green, B3 = Blue, B4 = NIR). Spectral type of index is listed as visible (Vis), near infrared (NIR), or a combination of the two (Vis-NIR).

Name	Type	Abbrev.	Equation
Green-red vegetation index	Vis	GRVI	$\frac{B2 - B1}{B2 + B1}$
Variable atmospherically resistant index	Vis	VARIg	$\frac{B2 - B1}{B2 + B1 - B3}$
Green leaf index – Red	Vis	GLI_R	$\frac{(B1 - B2) + (B1 - B3)}{2 \times B1 + B2 + B3}$
Green leaf index – Green	Vis	GLI_G	$\frac{(B2 - B1) + (B2 - B3)}{2 \times B2 + B1 + B3}$
Green leaf index – Blue	Vis	GLI_B	$\frac{(B3 - B1) + (B3 - B2)}{2 \times B3 + B1 + B2}$
Normalized difference vegetation index	NIR	NDVI	$\frac{B4 - B1}{B4 + B1}$
Green normalized difference vegetation index	NIR	$NDVI_G$	$\frac{B4 - B2}{B4 + B2}$
Chlorophyll index - Green	Vis-NIR	CIG	$\frac{B4}{B2} - 1$
Chlorophyll vegetation index	Vis-NIR	CVI	$B4 \times \frac{B1^2}{B2}$

Table 10: Description and codification of features extracted by FETEX 2.0 taken from Appendix A of Ruiz et al. (2011). GLCM refers to the grey level co-occurrence matrix produced within the FETEX 2.0 software. Listed spectral and textural metrics were computed for each of the raw bands and vegetation indices. Semivariogram metrics were computed using the raw NIR band. Further documentation on computational procedures can be found in Ruiz et al. (2011).

Spectral metrics		**Semivariogram metrics**	
MEAN	Mean value of band	RVF	Ratio between the values of the total variance and the semivariance at the first lag
STDEV	Standard deviation of band	RSF	Ratio between semivariance values at second and first lag
MIN	Minimum of band	FDO	First derivative near the origin
MAX	Maximum of band	FML	First maximum lag value
RANGE	Range of values of band	MFM	Mean of the semivariogram up to the first maximum
SUM	Sum of values of band	VFM	Variance of the semivariogram values up to the first maximum
MAJORITY	Majority of values of band	RMM	Ratio between the semivariance at first local maximum and the mean semivariance values up to this maximum
MEAN_EDG	Mean value of edgeness factor	DMM	Distance between the first maximum and the first minimum
STDEV_EDG	Standard deviation of edgeness factor		
Textural metrics			
UNIFOR	GLCM uniformity		
ENTROP	GLCM entropy		
CONTRAS	GLCM contrast		
IDM	GLCM inverse difference moment		
COVAR	GLCM covariance		
VARIAN	GLCM variance		
CORRELAT	GLCM correlation		
SKEWNESS	Skewness value of histogram		
KURTOSIS	Kurtosis value of histogram		

6.3 Sampling stratification

Thirty circular 11.28 m (400 m^2) radius plots were established. Prior to field measurements, a structurally and spectrally guided stratification was performed to ensure plot locations captured the range of structural and species variability in the region (White et al., 2017). To do so, an initial host species mask was generated using a publicly available 2008

enhanced forest resource inventory from the Ontario Ministry of Natural Resources and Forestry. Cluster analyses were then performed using two DAP point cloud derived structural metrics, the 90^{th} percentile of normalized point heights (P90) and proportion of points above 2 m (canopy cover; CC), and one imagery derived spectral metric, the sum of the normalized difference vegetation index ($NDVI_{sum}$) pixel values. P90 was used to stratify amongst landscape level vegetation heights and CC to describe variation in crown coverage. $NDVI_{sum}$ was chosen as a stratifier because it incorporated the spectral variation within each cell while providing information on the presence and absence as well as vigour of foliage.

In order to increase variability of cumulative defoliation amongst samples, spatial extents of annual current defoliation sketch surveys from 2014 and 2015 were also included in the stratification. To increase the efficiency of field surveying, 200 m road buffers were used to further subset resulting clusters. Finalized field measurement locations were randomly located within each metric cluster as well as being distributed within as many defoliation scenarios as possible (Figure 26).

6.4 Field measurements

Field measurements were collected by trained field technicians. Species and diameter at breast height (DBH) were recorded for all trees with DBH larger than 10 cm. The 10 cm DBH threshold was chosen according to local merchantability standards. A representative subset of trees within 5 cm DBH classes were measured for total height using a hypsometer. Species-specific DBH to tree height regression models were then derived and applied to all trees that were not measured for height (Mehtätalo et al., 2015). Following tree measurements, ocular and branch level defoliation assessments were conducted for host tree species following procedures detailed in MacLean and MacKinnon (1998) and MacLean et al. (2001). Ocular assessments

were conducted for all host trees using binoculars, while branch level defoliation samples were acquired from the mid crown of at least three host species trees per plot using pole pruning equipment. Cumulative branch level defoliation was adapted from the formula provided in MacLean et al. (2001), incorporating three years (2014, 2015, 2016) of defoliation data (Equation 5). Sampling accuracy for this methodology is detailed in MacLean and MacKinnon (1998) and Maclean and Lidstone (1982).

$$CD_t = 0.37C_t + 0.34C_{t-1} + 0.29C_{t-2} \quad [5]$$

where *t* is the year 2016, *CD* is cumulative defoliation (%) and *C* is current defoliation (%). More recent defoliation coefficients had higher weight on the final cumulative defoliation result (CD_t).

6.5 Cumulative defoliation analysis

Plot level structural and spectral metrics from the DAP point cloud and orthoimagery were incorporated as predictor variables to assess their capability to model cumulative branch level defoliation at the plot level. A partial least squares (PLS) regression modelling approach was used, which is appropriate for inter-correlated explanatory variables (Wold 1995; Wold et al., 2001; Möckel et al., 2014; Wolter 2008) and where predictor variables are more abundant than sample observations (Dormann et al., 2013; Schmidtlein et al., 2012). The intent of the PLS modelling approach was to determine the relative predictive power of spectral and DAP structural metrics for modeling cumulative defoliation in field samples. The assumption in PLS is that the variance observed in the dependent variable can be largely characterized by a low number of principal components (Palermo et al., 2009). Integration of potentially large quantities of inter-correlated variables to produce a limited number of components serves to reduce the

potential for model overfitting and to improve model accuracy (Carrascal et al., 2009). The PLS modeling framework identifies components by isolating predictors with the largest covariance to dependent variables. The first few components account for the majority of variance of the data being analyzed, while the remainder can be removed to reduce overfitting (Möckel et al., 2014; Palermo et al., 2009). The PLS characteristics listed offer a suitable approach to test the capability and importance of a suite of correlated metrics (52 structural, 111 spectral), as well as assess the relationships between dependent and independent variables and field measured samples through principle component analyses. The optimal number of components in each model was selected using the cross-validated coefficient of determination (R^2) and prediction error. Minimizing model error was prioritized first, followed by maximizing R^2.

Three separate PLS models with 10-fold cross-validation were computed. The first model incorporated only spectral metrics produced from DAP derived orthoimagery (PLS_{spec}), the second utilized DAP generated structural metrics (PLS_{struc}), while the third integrated both data types (PLS_{comb}) to determine if their combination would improve model performance. Prior to modelling, all variables were centered and scaled to have a mean of 0 and a standard deviation of 1 to improve the interpretability of the data for the modeling process (Bush and Nachbar, 1993; van den Berg, 2006). Following the creation of each model, a variable elimination process was conducted to limit the inclusion of variables not contributing to variance explained in cumulative defoliation. To do so, regression coefficients for each predictor variable in the initial PLS models were computed to determine the importance of each independent variable in the prediction of cumulative defoliation. In addition, the variable importance for projection (VIP) (Palermo et al., 2009; Wold, 1995; Wold et al., 2001), which represents the contribution each predictor had in fitting the PLS model for both predictors and response, was also calculated and used for variable

selection (Chong and Jun, 2005; Wold et al., 1993). Predictor variables with VIP and regression coefficients less than 0.8 in absolute values were removed from modeling inclusion (Wold, 1995). Following the modeling process, a discriminant analysis was conducted to visualize and inform the predictor variables with the highest importance for the prediction of cumulative defoliation.

6.6 Area-based approach for estimating forest inventory attributes

Wall-to-wall point cloud structural metrics were used to assess the capacity of landscape level DAP for predicting merchantable volume per hectare (m^3 ha^{-1}) and basal area per hectare (m^2 ha^{-1}). To do so, point cloud extents were first co-located with field plots. Tree level volume equations from Zakrzewski and Penner (2013) and basal area were calculated and summarized to the plot level. An ordinary least squares parametric modeling approach was used due to its proven record of point cloud based inventory metric modeling (Næsset et al., 2005; White et al., 2015; Ullah et al., 2017), as well as simplicity. This method also provides insight into the direct relationships that can be made between DAP structural metrics and field measured volume and basal area. Using the ABA and multiple linear regression, plot level volume and basal area values served as dependent variables, while DAP structural metrics were used as predictors (White et al., 2017). A forward stepwise modeling approach was conducted where all variables in the final selected models were significant ($p < 0.05$). Models were evaluated using leave-one-out cross validation.

6.7 Results

6.7.1 Cumulative defoliation modeling

The PLS_{spec} model with four components achieved an R^2 of 0.79 with an RMSE of 14.5 % (Figure 27 (a); Table 11). The PLS_{struc} model explained the least amount of cumulative defoliation variance (R^2 = 0.49, RMSE = 21.5 %) with four components (Figure 27 (b); Table 11). The PLS_{comb} model achieved similar explained variability (R^2 = 0.79) and accuracy (RMSE = 14.5 %) results to the PLS_{spec} model (Figure 27 (c); Table 11). PLS modelling demonstrated that spectral variables were more influential than DAP structural metrics in explaining the observed variance in field measured mean cumulative defoliation within our study area (Figure 27; Table 11).

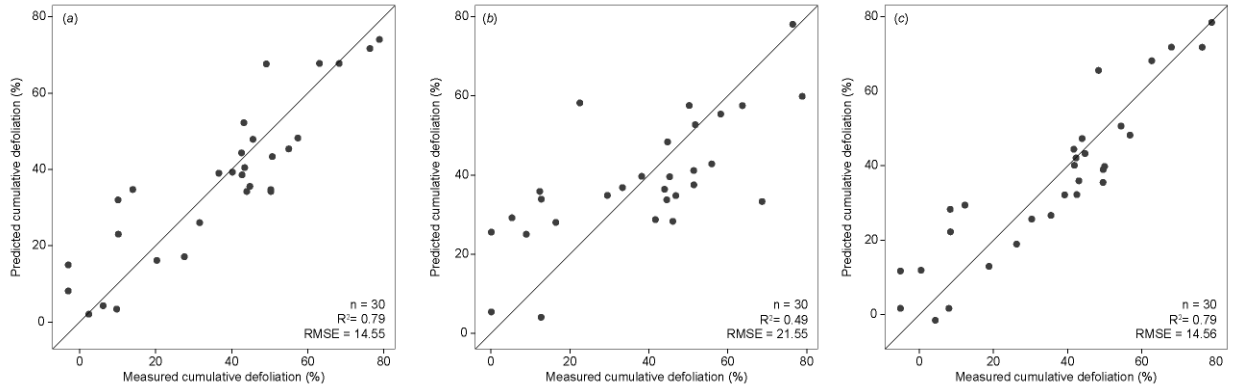

Figure 27: Scatterplots for the PLSspec (a), PLSstruc (b), and PLScomb (c) PLS regression models. Solid diagonal line represents the 1:1 line.

Table 11: Summary of PLS_{spec}, PLS_{struc}, and PLS_{comb} cumulative defoliation models. Coefficient of determination for each model were determined based on the inclusion of components. Best iterations of each model are displayed in bold with their associated explained variability (%), cumulative explained variability (%) with the addition of consecutive components, and cross-validated predicted root mean squared error (RMSE). Number of predictors is the number of spectral and/or structural metrics included in the final PLS models following variable elimination.

Model	Component	Explained variability (%)	Cumulative explained variability (%)	RMSE (%)
PLS_{struc} $R^2 = 0.49$ 11 predictors	1	24.4	24.4	20.4
	2	13.4	37.8	21.0
	3	7.7	45.5	21.9
	4	***3.6***	***49.1***	***21.5***
	5	0.4	49.6	21.2
PLS_{spec} $R^2 = 0.79$ 20 predictors	1	52.0	52.0	16.6
	2	15.3	67.4	15.3
	3	8.2	75.6	15.1
	4	***3.5***	***79.1***	***14.5***
	5	5.9	85.0	15.0
PLS_{comb} $R^2 = 0.79$ 22 predictors	1	52.5	52.5	16.9
	2	19.9	72.5	15.1
	3	***6.3***	***78.8***	***14.5***
	4	4.2	83.1	15.1
	5	2.2	85.3	16.0

Presence of metrics varied slightly between the PLS_{spec} and PLS_{comb} models, but metrics were predominantly the same (Figure 28). Spectral metrics from raw RGB bands (minimum brightness value of red, blue, green) as well as the standard deviation of $VARI_G$ were included in the PLS_{spec} and PLS_{comb} models. The PLS_{comb} model included two structural metrics, point

proportion between 5 – 10 m and the mean height between 5 – 10 m. These metrics were also included within the final PLS_{struc} model (Figure 28).

6.7.2 Partial least squares discriminant analysis

A discriminant analysis using the first two components of the PLS_{spec} and PLS_{comb} models, indicated that standard deviation, range, and NDVI derived semivariogram metrics were the most prominent and effective predictors for describing cumulative defoliation (Figure 28). These same metrics showed similar response profiles and indicated high multiple squared correlation with the dependent cumulative defoliation variable. The clustering of these metrics around field measured defoliation samples classified as severe (> 75%) indicates that they were all relatively similar in their ability to explain variance in this class. A less pronounced relationship can be seen where the min red, min chlorophyll vegetation index, min green, and to a lesser extent min blue were found to be important for modelling some plots in the moderate (26 – 75%) defoliation range in the sample set. The moderate severity class were more scattered within the principal components. Vectors nearing the figure edge for both of these defoliation classes indicate that the coefficients for these variables had heavier weights within their respective components. Tight clustering seen in the low (0 – 24%) severity class indicated that this class was most unique with regards to cumulative defoliation. Kurtosis and SDF were found to have the most highly weighted coefficients for describing the low severity class. The two structural metrics included in the PLS_{comb} model, proportion of points between 5 – 10 m and mean height between 2 – 5 m, were also found to be useful for the description of these classes. Sum and mean GLI_R metrics were highly weighted within each component for both models, however did not indicate strong relationships with defoliation samples.

The PLS_{struc} model included the fewest metrics resulting from variable selection using VIP and regression coefficients. Discriminant analysis on the first two components reinforced that structural metrics were not as effective as spectral metrics for discriminating amongst cumulative defoliation samples. Metrics associated with the upper tree canopy, P90, P95, maximum height, and mean between 10 – 20 m were all found to have high regression weights in the primary latent variable. Wide and overlapping distributions in the sample defoliation classes indicate that the metrics in the final structural PLS model were unable to differentiate levels of defoliation as well as spectral metrics (Figure 28). The class that was most effectively separated, the 0 – 24% class, was found to be most closely related to DAP skewness.

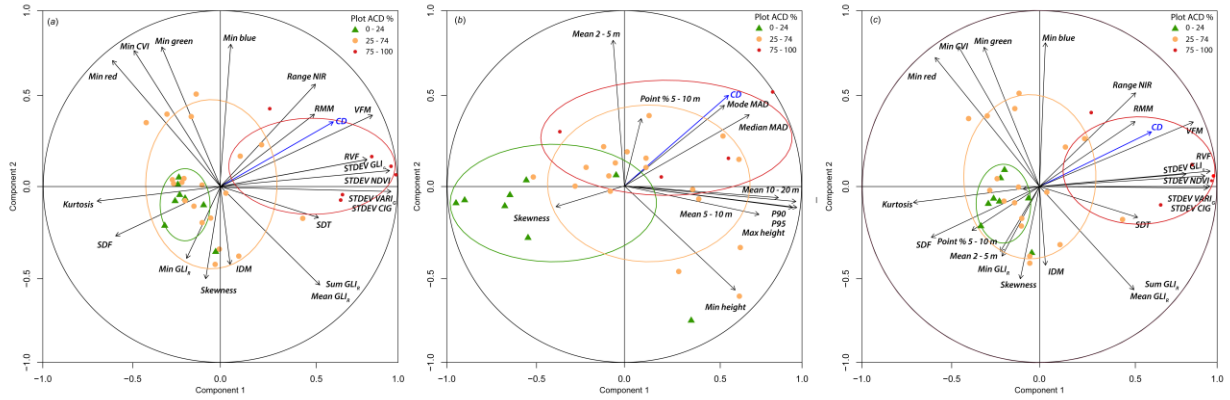

Figure 28: Circles of correlation comparing the first two components for the PLS_{spec} (a), PLS_{struc} (b), and PLS_{comb} cumulative defoliation PLS models. Metrics included in the model are written in bold with associated vectors indicating direction and magnitude of coefficient weights on the final model. Field measured cumulative defoliation samples are classified into three colour coded classes (low: 0 – 25%, moderate: 26 – 75 %, and severe: > 75%). The cumulative defoliation (CD) response variable with its associated correlation vector is depicted in blue, indicating direction and magnitude of correlation to the associated model predictor variables.

6.7.3 Forest inventory modelling

Linear regression using DAP structural metrics facilitated the accurate prediction of volume and basal area (Figure 29). The basal area model incorporated the 80th percentile of height and the proportion of points between 10 - 20 m and achieved an R^2 of 0.90 with a

corresponding RMSE of 4.11 m^2 ha^{-1}. The volume model incorporated only one metric, the 99th percentile of height, and achieved an R^2 of 0.80 with an RMSE of 49.7 m^3 ha^{-1}. The volume model generally indicated an over-estimation in the mid ranges of volume, while basal area showed relatively consistent estimation across the sampling range.

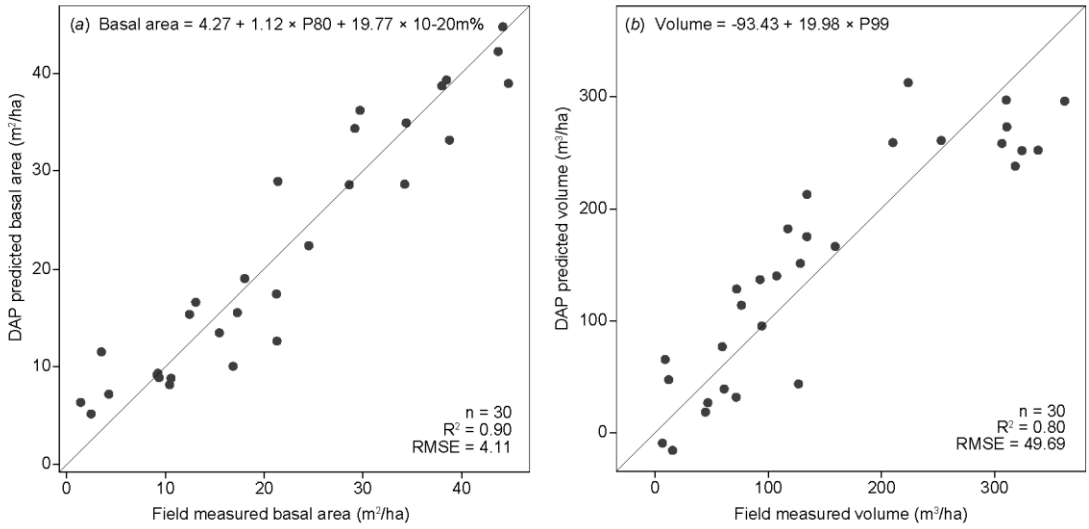

Figure 29: Scatterplots for the predictive linear regression models for basal area (a) and volume (b). Solid diagonal represents the 1:1 line.

6.8 Discussion

This chapter demonstrates the suitability of using DAP metrics and PLS modeling approaches for estimating cumulative defoliation in a Canadian boreal forest context. Findings indicated that spectral metrics had a greater ability to predict cumulative defoliation than structural metrics, and that metrics describing spectral variation were most important. Structural metrics were also incorporated to provide information on the basal area and volume of the stands affected by spruce budworm to determine the effectiveness of landscape level DAP for forest attribute estimation using multiple linear regression and the ABA. Models for both volume and basal area showed that DAP structural metrics were effective at producing accurate landscape

level inventory attribute estimates (Figure 30). The major outcome of this analysis shows that the data provided in landscape level DAP data sets is multi-use. The provision of both spectral and structural metrics facilitated an effective method for designing a cost-effective and efficient field measurement program, as well as provide solutions to forest health and inventory related challenges.

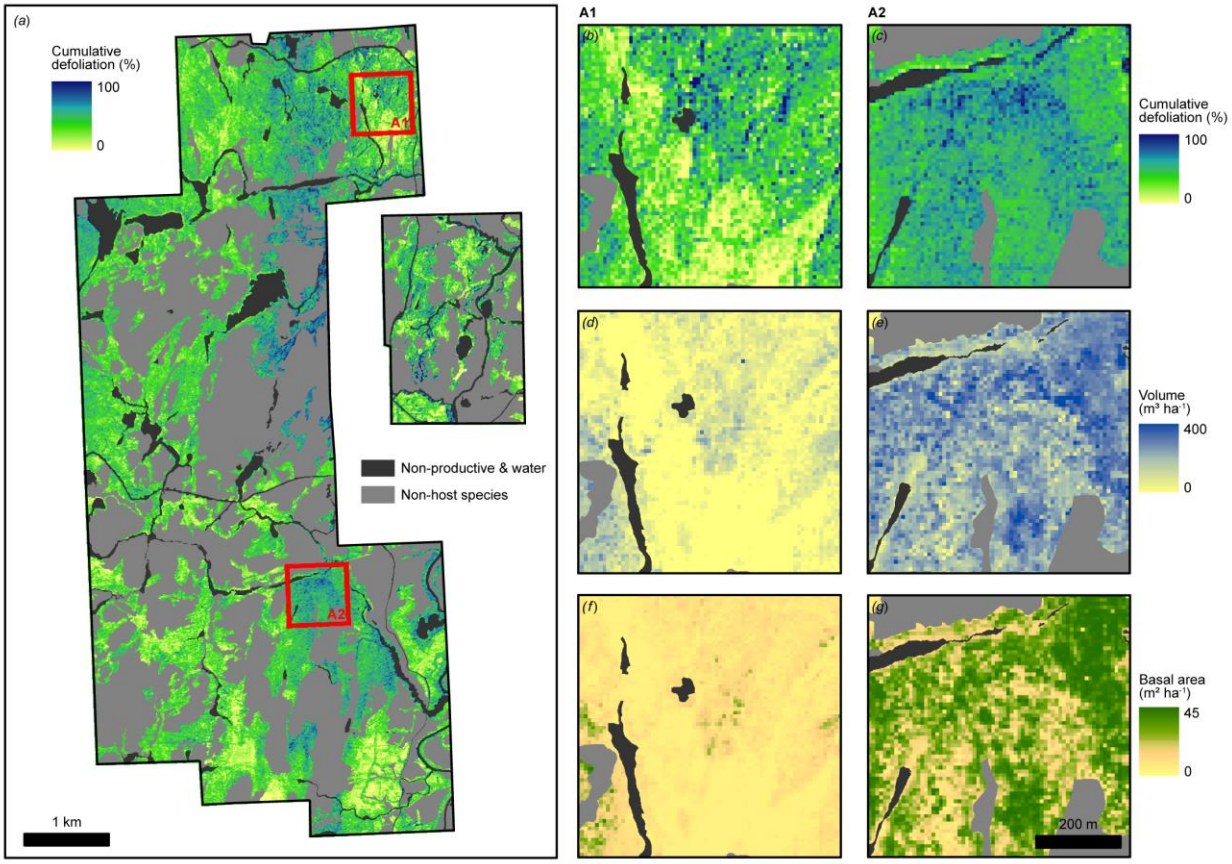

Figure 30: a) Landscape level prediction of cumulative defoliation (%) derived from the PLS_{spec} model. Zoom extents for areas A1 and A2 for cumulative defoliation (b,c), volume (m^3 ha^{-1}) (d,e), and basal area (m^2 ha^{-1}) (f,g).

Results within this chapter illustrate the inability of DAP derived structural metrics to be used to accurately predict cumulative spruce budworm defoliation. The PLS modeling analysis outlined that variation in cumulative defoliation could not be strongly linked to DAP structural metrics, reinforcing some of the limitations of DAP point cloud data sets. While DAP point

clouds are limited to characterizing the outer envelope of the dominant canopy, ALS pulses detect and record physical responses from the structural components throughout canopy layers. This may be the reason for the success in previous studies reporting ALS as an effective tool for detecting and quantifying conifer defoliation (Kantola et al., 2010; Vastaranta et al., 2013a).

Another probable underlying cause for poor structural metric performance is that DAP point clouds characterize the most recent or outer-most annual foliage on tree crowns, while spruce budworm defoliates the current year foliage in successive years, resulting in multiple age classes of foliage removed (cumulative defoliation). Annual branch level defoliation measurements illustrated this phenomenon, with DAP point clouds limited to characterizing only a portion of the potential defoliated foliage present within the stand. The influence of differences in sun-angle, viewing geometry, and image resolution also influence finalized DAP products (St-Onge et al., 2008). A further limitation to DAP point cloud analyses such as predicting defoliation is that various proprietary and open source processing algorithms are fundamental to their creation (Dall'Asta and Roncella, 2014). As described in Chapter 2, studies comparing the performance of image-matching algorithms showed parameterization and internal algorithm differences can lead to discrepancies in how DAP point clouds characterize forest structure, which can consequently affect the accuracy of high resolution structural analyses such as cumulative defoliation and inventory attribute modeling (Ullah et al., 2017).

Spectral metrics derived from multi-band orthoimagery showed an increased ability to predict cumulative defoliation over structural metrics. Semivariogram derived variance metrics (Balaguer et al, 2010; 2013) describing the spatial variation of spectral values were the most important in the PLS_{spec} and PLS_{comb} models. Discriminant analysis indicated that these variables were strongly linked to measured cumulative defoliation. Other metrics describing spectral

variability were also highly effective predictors. The importance of spectral variability metrics can be linked to the physical manifestation of defoliation, since budworm feeding introduces variation in the spatial distribution of foliage within conifer stands, thus influencing the variability of electro-magnetic reflectance. The ability to isolate important spectral variables that can be linked to cumulative defoliation is an important step to improving estimates at landscape scales. Further research into the regional robustness and sensitivity of these variables could help to facilitate automated classification routines for quantifying and reporting severity.

Acquisition timing of the imagery used in this study did not fall within the characteristic red-stage commonly used for the sketch mapping of current defoliation. Issues related to weather and logistics often cause problems for imagery acquisition during the red-stage. Results achieved using imagery not exhibiting the most prominent spectral variations associated with current defoliation are promising for future potential to improve defoliation modeling accuracy. Although current defoliation maps are often used to plan insecticide spray programs, cumulative defoliation is the best predictor of tree mortality (Erdle and MacLean, 1999). Future studies assessing both cumulative and current defoliation severity using spectral variables should focus imagery acquisition within this red-phase to determine whether prediction accuracy can be improved compared to images acquired following red-stage manifestation.

Future studies looking to improve upon linkages between cumulative spruce budworm defoliation and remote sensing should further investigate the potential relationships between aerial and satellite imagery. While studies such as Franklin et al. (2008) outlined that SPOT HRVIR satellite imagery elicited stronger relationships with cumulative defoliation than Landsat thematic mapper, their study also outlined that multi-temporal Landsat imagery was more effective than a single date. These results justify a more thorough investigation into multi-

temporal monitoring frameworks with high resolution data, such as the aerial imagery used in this analysis. Multiple aerial imagery acquisitions could help to provide a more detailed description of cumulative defoliation at a landscape level, potentially providing details about defoliation trends related to the spruce budworm life cycle. Methods to improve upon existing landscape level predictions for spruce budworm host species distributions (Wolter et al., 2008), and consequent defoliation susceptibility forecasting (Luther et al., 1997) are promising for monitoring trends in landscape level defoliation and host species changes, improving pro-active forest management strategies, and providing long-term data for the formulation of effective forest policy and stewardship.

With projected changes in climate posing an uncertain future for forest health, improved managerial insight will become increasingly necessary to balance the ecological, social, and economic values placed on forest resources (Dale et al., 2001). I view the acquisition of aerial imagery at regular intervals as an effective tool for managers to better understand, characterize, and quantify forest health and long-term management strategies. Results from the forest inventory modeling analysis reinforce that conventionally acquired aerial survey imagery can be used to create multi-use, accurate, and effective DAP point clouds for forest inventory modeling. These results corroborate with those discussed in Chapter 2.

Accuracies for predicting volume and basal area were competitive with results achieved from similar, and higher density DAP datasets, as well as ALS (Straub et al., 2013; P Tompalski et al., 2014; Tompalski et al., 2018; White et al., 2015). The ability to produce these data sets from conventional aerial acquisition programs greatly increase their value, and could help to improve upon well-informed forest management decisions. The prediction of forest inventory attributes at a landscape level through time could also provide a method of assessing the

influence of cumulative spruce budworm defoliation on the quantity and associated economic value of harvestable timber. This would allow relationships to be drawn to more accurately assess the impacts of defoliation through time, and how it may influence local economies.

Spectral and structural metrics facilitated an economically optimized field measurement campaign. Stratifying forest cover types prior to implementing sampling routines served to improve landscape level understanding of forest distribution and potentially add to statistical representation amongst target variables. Other studies utilizing a pre-sampling stratification can be found in Breidenbach et al. (2010) and Yu et al. (2011). The incorporation of spectral and structural metrics, spatial forest cover information, and current defoliation extents from 2014 and 2015 facilitated field plot positioning with minimal requirement to travel far distances to reach specific or under-represented forest types. Given limited road access across the GCF (Figure 25), a common scenario in Canadian forests, locating plots within 200 m of road access helped to increase the number of acquired samples while reducing sampling costs. This stratification strategy could be a useful starting point for forest managers requiring inventory datasets on large land-bases with limited access, or those looking to optimize sampling efficiency.

6.9 Conclusions

This chapter provides additional rationale that both structural and spectral metrics produced from DAP datasets can be used to improve estimations of forest inventory attributes, and enhance information related to forest health. Structural metrics were effective at predicting volume and basal area, while spectral metrics provided accurate cross-validated estimates of cumulative defoliation in host stands. PLS modeling outcomes reinforced that spectral metrics were the most effective for predicting cumulative defoliation, and that metrics providing information related to both the spatial variation in spectral responses, and variation in spectral

signals, were found to be most influential. The provision of both of these metric types from a single, conventionally flown, aerial imagery survey shows promise for enhancing forest health and inventory data in a cost-effective manner.

The ability to model standard forest inventory attributes such as volume is of great value to forest managers, and results from this chapter illustrate that landscape level DAP is capable and accurate at doing so. Chapters 7 and 8 look to reinforce these findings by further analyzing DAPs ability to model inventory attributes, and consequently establish a synergistic framework for updating baseline ALS EFIs. Both the ABA that was elaborated upon in this chapter, and updating attribute estimates at an individual tree level are presented.

Chapter 7:

Updating residual stem volume estimates using ALS and DAP point clouds[6]

7.1 Background and motivation

Generating forest inventories in Canada is complex due to a large forested land area that is generally difficult to access. The commercial forestry sector is a major contributor to national and subnational economies, a key source for employment, and a provider of a varied range of ecosystem goods and services. Sustainable forest management is therefore essential for balancing the economic values of timber production, social investment in forestry-related employment, and environmental stewardship. Inventories designed to inform harvest operation planning through the provision of information on volumetric estimates, species distribution, and general health status of standing timber have largely been conducted using aerial photographic interpretation, field plots, and manual timber cruising (White et al., 2013a). While effective and accurate at estimating standing timber composition and volume, these approaches are costly and time consuming. Although these methods may be informative in the short term, forest inventories should be updated periodically, increasing monitoring costs. The use of inaccurate and outdated inventories increases the potential margin of error for gross and net volume estimates, leading to potential economic losses. To ameliorate this problem, improvements are needed to increase the economic and temporal effectiveness of inventory collection, monitoring, and updating.

---

[6] The content of this chapter has been adapted from:
Goodbody, T.R.H., Coops, N.C., Tompalski, P., Crawford, P., Day, K.J.K., (2016). Updating residual stem volume estimates using ALS- and UAV-acquired stereo-photogrammetric point clouds. Int. J. Remote Sens. 1161.

Although ALS is now regarded as the preferred data source for detailing forest structure, discussions presented in Chapter 2 outline that the use of DAP to facilitate monitoring and increased frequency in inventory cycles has increased in popularity (Lim et al., 2003; Reutebuch et al., 2005). As mentioned in Chapter 1, DAP point clouds are regarded as being comparable under some situations to point clouds generated from ALS, facilitating a similar approach to structural analysis and metric extraction (Vastaranta et al., 2013b). Interest in DAP utilization can be attributed to factors including the provision of data packages complementary to forest inventory standards, comparatively low operational costs, and the ability to determine image-based forest attributes that are currently problematic for ALS data such as species composition and health status (Näsi et al., 2015; White et al., 2013b; Wulder et al., 2008). In addition, exploiting already acquired imagery to characterize and deliver structural information on forest stands could reduce operational costs and increase the efficiency of the forest planning process (Tao et al., 2011; White et al., 2013b).

In the following two Chapters, I implement and demonstrate a periodic semi-automated inventory cycling framework comprising an initial time 1 (T_1) ALS baseline inventory and corresponding time 2 (T_2) UAS-DAP update. Framework goals include increasing the temporal accuracy and cost effectiveness of the inventory, providing information on the spatial distribution of forest cover change from harvesting practices and natural disturbances, and accurately estimating and monitoring residual timber volumes post-harvest. To do so we assess the ability of UAS-DAP to update pre-harvest ALS inventories by modelling residual standing timber volume following selective harvest in the Cariboo region of British Columbia, Canada. ALS data and field measurements were acquired prior to harvest in 2013. Following a selective harvest in 2015, additional field measurements were collected and UAS stereo-imagery was

acquired for DAP point cloud generation. The ABA to forest attribute estimation, which was initially described in Section 2.2 and implemented in Chapter 6, was then used to develop models of stand volume at T_1 pre-harvest and T_2 post-harvest. Following the creation of T_1 and T_2 volume models, change in volume between periods was analyzed using indirect and direct modelling approaches. We then develop an inventory-cycling framework where the ABA incorporates T_1 ALS and T_2 DAP point cloud metrics to determine both the spatial location of harvesting operations and resulting volume differential.

7.2 Materials and methods

The ALS and DAP datasets used in this analysis are the same as those used for Chapter 8.

7.2.1 Study area

Inventory information was collected from compartments A (16.5 ha) and B (31.6 ha) within the Knife Creek block of the Alex Fraser Research Forest (AFRF) southeast of Williams Lake, BC, Canada (Figure 31).

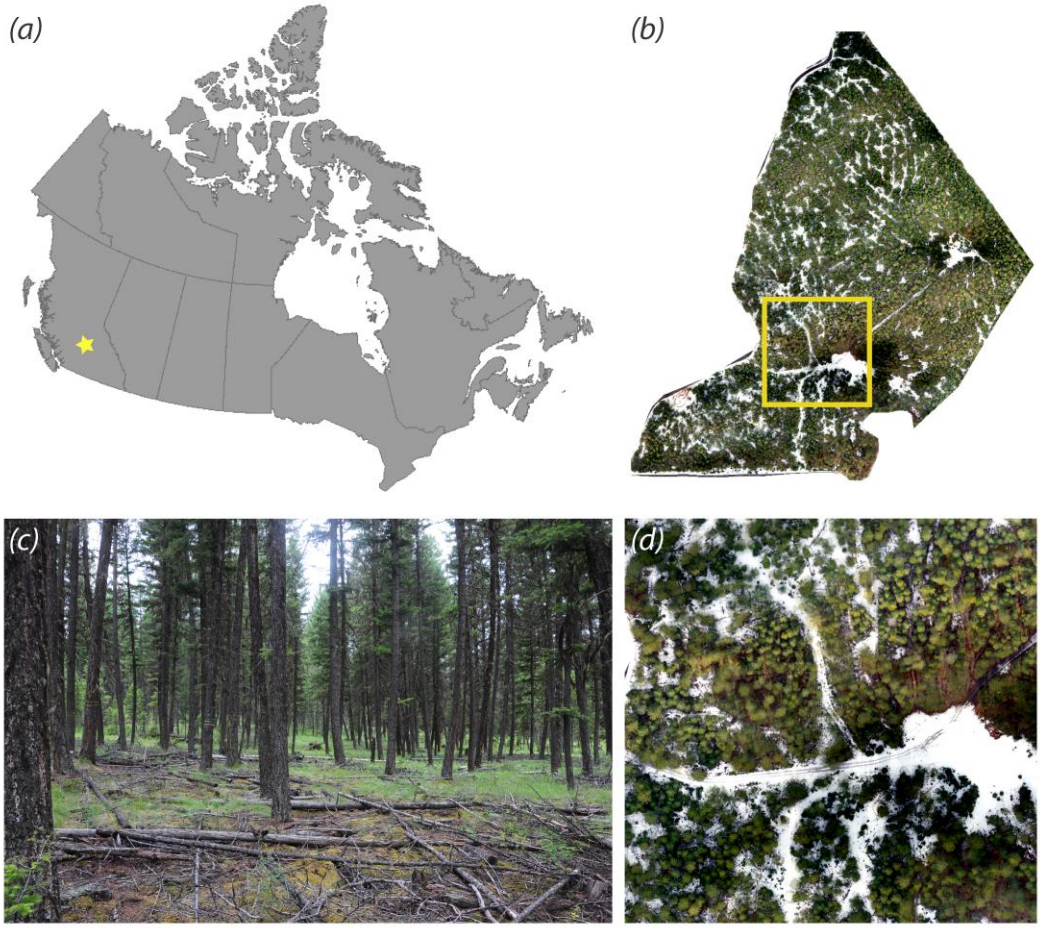

Figure 31: Study area southeast of Williams Lake, BC (a) with UAS-acquired orthomosaic of compartment B (b) with inlay (d), and sub canopy image (c).

Knife Creek falls within the Interior Douglas-Fir biogeoclimatic ecosystem classification zone with a small percentage in the transition to the Sub-boreal Pine Spruce zone (Day, 2007).

The forest is dominated by uneven-aged Douglas-fir (*Pseudostuga menzieszii* var. glauca) stands, with small proportions of lodgepole pine (*Pinus contorta* var. latifolia) mixed throughout. The topography is gently sloping and the climate is dry to very dry. The Knife Creek block location is within Cariboo mule deer wintering range habitat and is subject to stand-level harvesting direction that includes minimum basal area retention, a minimum cutting cycle of 30 years, and formation of small canopy openings with clumpy distributions of mature Douglas-fir (Dawson et al., 2007; Koot et al., 2015).

7.2.2 ALS data acquisition

ALS data was acquired for the Knife Creek block in August 2013 using a Riegl VQ-580 laser scanner operating at 200 kHz on a Cessna flown approximately 600 m above ground level. The scanner captured data ±30° from nadir with a dual frequency NovAtel Span-SE GPS receiver and IMAR inertial measurement unit.

Point density averaged between 7–9 points m^{-2} for all returns. ALS data accuracy was determined by comparing matching tie planes on overlapping scan lines. The overall ALS data had an estimated RMSE of 0.048 m, and absolute accuracy of ± 0.094 m stated at the 2σ level (1.96 × RMSE) (Aguilar and Mills, 2008).

7.2.3 UAS data acquisition

In March 2015, a Aeryon SkyRanger vertical take-off and landing quadcopter weighing approximately 2 kg captured 2400 16-megapixel RGB images. The sensor was fitted to a 3-axis stabilized gimbal to maintain nadir image capture. The UAS was flown in a pre-programmed rectangular grid pattern over the forest to ensure adequate horizontal and vertical image overlap. Altitude was maintained at approximately 100 m above ground level throughout the image

capture sequence. Images were captured over multiple hours on the same day with slightly varying sun and weather conditions. A high resolution DAP point cloud was produced using Pix4D software (Pix4D, 2018b). High resolution orthomosaic maps were produced for site reference (Figure 31). In order to obtain the highest quality imagery possible, robust stabilization software was used to maximize data integrity in adverse weather conditions such as high winds. In the event of communication or control failure, this software would also autonomously return and land the UAS at its point of commencement. The system used is a suitable analogue for low-cost off-the-shelf UAS solutions.

7.2.4 ALS point cloud processing

A DTM was created using ground returns from the point cloud followed by ground-level normalization. A surface model was produced from the maximum heights of all returns and a 0.50 m CHM was produced by differencing the surface model and DTM. Processing for T_2 DAP data followed the same procedure as described above, with the exception of the DAP point cloud being normalized to the ALS derived DTM (Figure 6). Following points presented in Chapter 2, the ALS derived DTM was used as they have been shown to provide accurate high resolution sub-canopy terrain data (White et al., 2013b)

7.2.5 Stand level measurements

Prior to harvest, 23 variable radius plots were located within the project blocks area to be harvested. Plot centres were located using handheld GPS. At each plot, species was determined for each ‘in’ tree, and DBH and height were measured. Individual tree locations were mapped. Given that a variable radius plot does not measure all trees within a fixed radius, the CHM was used to detect trees not included in the field sample. To do so, tree canopies were identified using

a local maxima search to determine seed regions similar to Zhang et al. (2013). Crown extents for each tree were determined by applying a 'seed growing' approach as in Maltamo et al. (2003). All detected treetops within plots bounds were included within the inventory. Stem maps and CHMs were overlaid for validation of CHM and field measured heights. Diameters for included trees were estimated using the model developed by Hall et al. (1989) using the point cloud based tree heights and crown area from individual tree detection polygons. Once all trees were identified, individual tree volumes (m^3) were computed as in Tompalski et al. (2014).

The 23 plots were revisited following a selective harvest in 2015. Seven plots had all of their timber removed. At the remaining plots, all residual, previously measured trees were re-measured. Stumps of harvested trees were recorded on the stem map. As with the ALS data, the DAP CHM was used to find trees not included in the variable radius sampling to allow their heights to be updated and DBH and volumes recalculated.

7.2.6 Area-based volume modelling

Conventional plot-based cloud metrics were calculated for the T_1 ALS and T_2 DAP data sets (Table 12) using a 2 m height threshold (Nilsson, 1996). Height of percentiles of non-ground returns, canopy return density metrics, and strata metrics were computed using normalized point clouds as in White et al., (2013a).

The direct and indirect approaches to modelling change in the point clouds were used to determine volume change between T_1 ALS and T_2 DAP data sets as in Cao et al. (2016) (Figure 32). Volume change using the indirect method ($V_{Indirect}$) was estimated by modelling volume for pre-harvest ALS (V_{T1}) and post-harvest DAP (V_{T2}) independently and estimating the change as their difference. The direct method (V_{Direct}) utilized differences between plot-level metrics and the volume calculated between T_1 ALS and T_2 DAP data sets to directly model changes in

volume. The T_1 ALS volume model included all 23 sample plots while the T_2 DAP model included 16 due to 7 of the original plots exhibiting null (totally harvested) volumes. Using multiple linear regression techniques, individual predictive volume models for T_1 ALS, T_2 DAP, and direct volume change were generated. Pearson product moment correlation coefficients (r) were computed to assess the relationship among point cloud metrics. Any metrics with an $r > 0.75$ were removed from the data set. A stepwise modelling procedure was used to determine the optimal parameters for model inclusion that were uncorrelated. Table 12 outlines which parameters were included in the modelling process. The RMSE and bias were calculated and wall-to-wall visual outputs were produced for each model outlining volume ($m^3\ ha^{-1}$) for T_1 ALS and T_2 DAP and volume change for the indirect and direct models.

Table 12: Descriptive statistics produced for ALS and DAP point clouds. Elevation and strata metrics are comprised using combinations of first and all returns.

Elevation metrics	Strata metrics
Minimum, Maximum, Median*, Mode of height	Percentage all returns above 2m*
Standard Deviation, Variance	Percentage of first returns above mean, mode height
Interquartile Difference, Skewness, Kurtosis	All returns > 2m*, mean , mode
Percentile Values (1^{st}, 5^{th}*, 10^{th}, 20^{th}, 25^{th}, 30^{th}, 40^{th}, 50^{th}, 60^{th}, 70^{th}, 75^{th}, 80^{th}, 90^{th}*, 95^{th}, 99^{th})	Min, max, mean, median, mode, standard deviation, median height between 10-20 meters*, mean height between 10-20 meters*

*Indicates metric inclusion in modelling

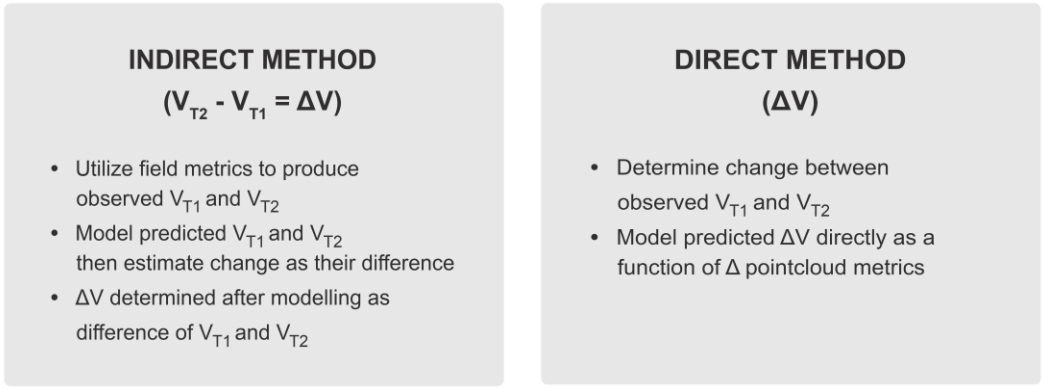

Figure 32: Framework for indirect and direct modelling approaches.

7.3 Results

7.3.1 Canopy height

CHMs were created for T_1 ALS and T_2 DAP data sets detailing the spatial distribution of standing timber before and after selection harvesting (Figure 33 (a, i) and (b, ii), respectively).

The result of their subtraction was CHM_{diff} (Figure 33 (c, iii)), which outlines the location and extent of growth and loss from harvest between 2013 and 2015.

7.3.2 Metric comparison

The ALS and DAP point clouds were compared using a number of conventional metrics including 5th and 95th percentile of height, mean height, and standard deviation of height (Figure 34). Canopy cover metrics such as proportion of points above 2 m were also compared. As anticipated due to the lack of penetration of the DAP point clouds into the forest canopy, similarities between ALS and DAP height metrics increased as the height percentile increased. Correlation between height percentiles ranged from $r = 0.06$ for the 5th percentile of height to $r = 0.84$ for the 95th percentile of height. The largest correlation change of $r = 0.61$ occurred between the 25th and 50th percentile of height. Correlation for mean height was $r = 0.64$, and $r = 0.42$ for standard deviation of height. The proportion of points > 2 m showed the lowest correlation of $r = 0.02$. Overall, mean height and proportion of points >2 m was greater for DAP than ALS. DAP height metrics were greater than ALS metrics up to the 75th percentile of height. The ALS standard deviation was larger than DAP.

7.3.3 Stem volume estimations

Individual predictive volume models were produced for T_1 ALS ($R^2 = 0.91$, $p < 0.01$, %RMSE = 17.34, and bias = -3.45) and T_2 DAP ($R^2 = 0.93$, $p < 0.01$, %RMSE = 18.50, and bias = -2.18) (Figure 35 (a) and (b), respectively). These models exhibited similar relationships for observed and predicted volume, both yielding significant values for all parameters. The indirect and direct approaches to modelling change in volume were used. The $\Delta V_{Indirect}$ model ($R^2 = 0.85$,

$p < 0.01$, %RMSE = 16.65, and bias = -0.29) and ΔV_{Direct} ($R^2 = 0.75$, $p < 0.05$, %RMSE = 86.56, and bias = 11.08) showed a 69.91 % difference in RMSE (Figure 36 (a) and (b), respectively).

Table 12 outlines the predictor variables used to generate each model and their corresponding significance while Table 13 summarizes the linear regression equations used for each model. For compartment A, the T_1 ALS model estimated volume as 170.78 m^3 ha^{-1} (SD = 65.75 m^3 ha^{-1}), while the T_2 DAP model estimated residual volume following harvest at 110.78 m^3 ha^{-1} (SD = 66.81 m^3 ha^{-1}). The indirect model estimated volume change as -60.00 m^3 ha^{-1} (SD = 64.39 m^3 ha^{-1}), while the direct model estimated -32.66 m^3 ha^{-1} (SD = 38.21 m^3 ha^{-1}) For compartment B, the T_1 ALS model estimated volume as 266.74 m^3 ha^{-1} (SD = 114.94 m^3 ha^{-1}), while the T_2 DAP model estimated residual volume following harvest at 210.85 m^3 ha^{-1} (SD = 115.48 m^3 ha^{-1}) (Figure 37 (a), (i) and (b), (ii), respectively). The indirect estimated volume change as -55.89 m^3 ha^{-1} (SD = 99.26 m^3 ha^{-1}), while the direct model estimated -23.00 m^3 ha^{-1} (SD = 38.99 m^3 ha^{-1}).

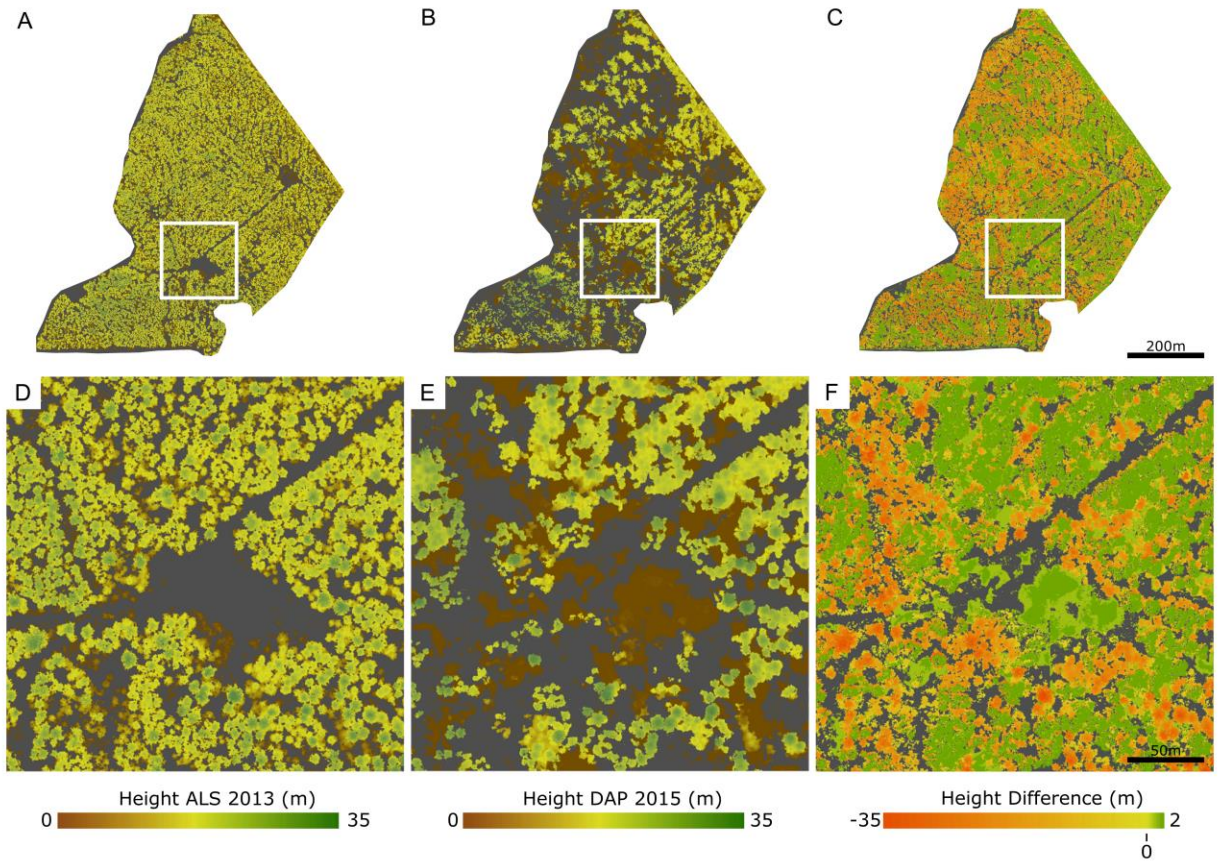

Figure 33: Cartographical representation of (a, i) ALS derived canopy height model in 2013 (CHM_{T1}), (b, ii) UAS stereo-photogrammetric canopy height model in 2015 (CHM_{T2}), and (c, iii) their difference (CHM_{diff}) for compartment B.

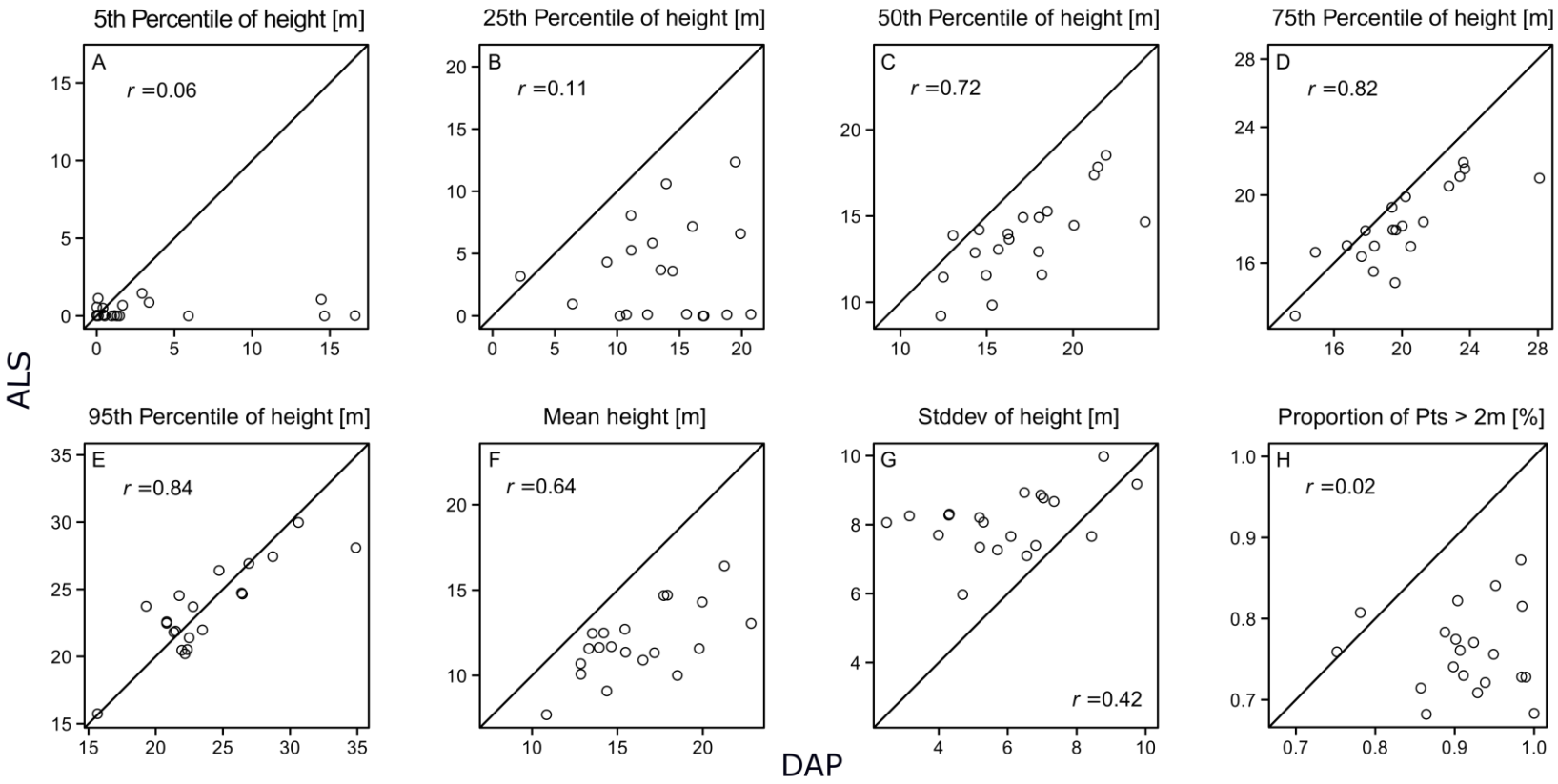

Figure 34: Comparison of ALS and DAP metrics for (a) 5th, (b) 25th, (c) 50th, (d) 75th, (e) 95th percentile of height (m), (f) mean height (m), (g) standard deviation of height (m), and (h) proportion of points above 2 m (%). 1:1 line is shown in each plot.

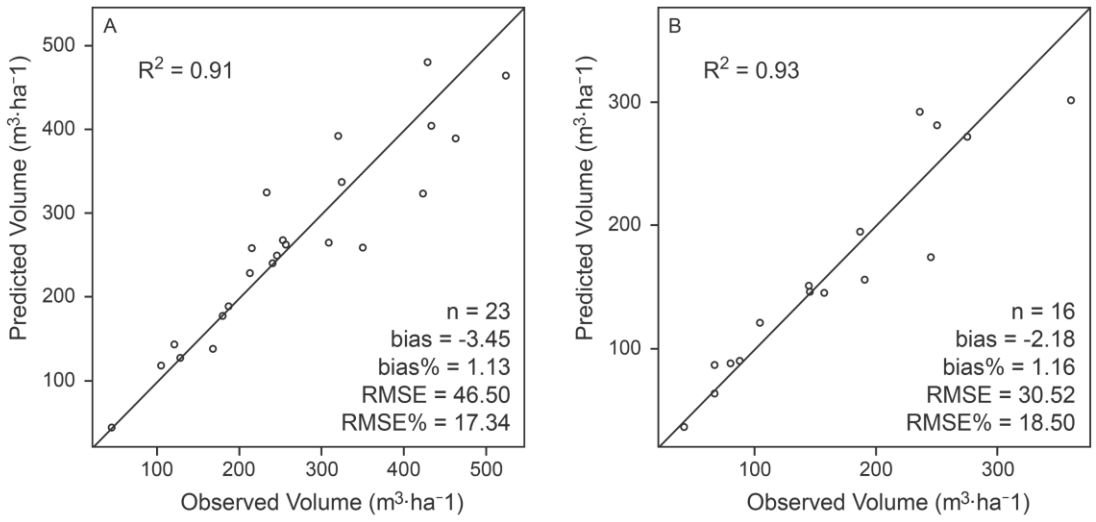

Figure 35: (a) T_1 ALS and (b) T_2 DAP predictive volume models. 1:1 line is shown in each plot.

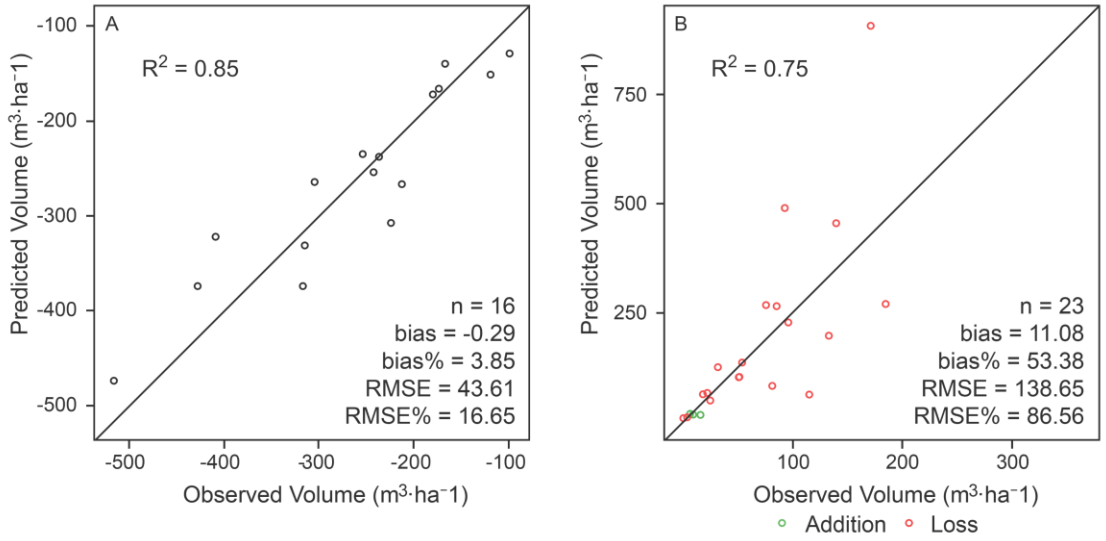

Figure 36: (a) Indirect and (b) direct predictive volume difference models. 1:1 line is shown in each plot.

Table 13: Linear parameters and metrics used for T_1 ALS and T_2 DAP predictive volume models and $\Delta V_{Indirect}$ and ΔV_{Direct} volume change models.

Model	Predictor variable	Response variables	Parameters	Intercept	R^2
T_1 ALS	Volume ALS (V_{T1})	Mean height log(All returns > 2 m) Median height between 10 to 20 m	0.128 ** 0.656 ** 0.111 **	-6.216	0.926
T_2 DAP	Volume DAP (V_{T2})	90^{th} percentile of height log(All returns > 2 m) Mean height between 10 to 20 m	1.971 ** 0.651 ** 0.114 **	-12.328	0.934
$\Delta V_{Indirect}$	$\Delta V_{T1} - \Delta V_{T2}$ (Observed)	$\Delta V_{T1} - \Delta V_{T2}$ (Predicted)	1.074 **	19.623	0.849
ΔV_{Direct}	$\log(V_{T2} - V_{T1})$	5^{th} percentile of height Percentage all returns > 2 m	0.198 * 0.223 **	0.232	0.748

* $p < 0.05$
** $p < 0.001$

7.4 Discussion

In this chapter, I compared pre-harvest ALS and post-harvest DAP data acquired over the same area with a two-year interval to determine the location and volume of residual timber following selection harvesting. Multiple linear regression and the ABA to attribute estimation were used to estimate volume from ALS in 2013 and DAP in 2015 using field measurements and point cloud metrics. Stand volume change was estimated using two modelling approaches: first, an indirect method that incorporated separate models for V_{T1} and V_{T2} data sets with their difference estimating volume change, and second, the direct method, which involved developing a single model that estimated volume change as a function of change in T_2 DAP – T_1 ALS point cloud metrics.

As anticipated, the ALS point cloud provided accurate structural stand and terrain information, which were critical for model development. The T_1 ALS model variables and accuracy were as significant as similar studies (Rahlf et al., 2014; Vastaranta et al., 2013b) confirming the potential of ALS to provide stand volume estimations and data for planning decisions. The incorporation of stand-level CHMs and corresponding inventory information into the planning and operational process could improve management decision-making including the timing, location, and scale of harvest operations.

To maintain the spatial accuracy of the operational inventory, systematic updating must be prioritized on a periodic basis. The combination of fast operationalization of UAS with the high precision of DAP technology has proven comparable in this study area to its

ALS counterpart (Vastaranta et al., 2013b). DAP showed promising results in its ability to update locations of harvest operations, locate residual timber assets, and estimate corresponding residual stand volumes (Figure 37). The comparable accuracy of the T_1 ALS (%RMSE = 17.34) and T_2 DAP (%RMSE = 18.50) models agrees with those presented in Figure 7, further justifying the incorporation of UAS-DAP to facilitate an inventory updating framework that provides spatial and temporal inventory information of comparable accuracy for a fraction of the ALS collection cost (Grenzdörffer et al., 2008; Näsi et al., 2015). These results suggest that the ongoing use of UAS to periodically collect DAP information after harvest could be useful in future efforts of gauging the success of applied harvesting regimes, monitoring residual stand behaviour post-harvest, updating allometric forest growth models, gauging the success of natural and planted regeneration, and updating inventories after abiotic disturbances such as wind or fire (Koh and Wich, 2012; Tang and Shao, 2015).

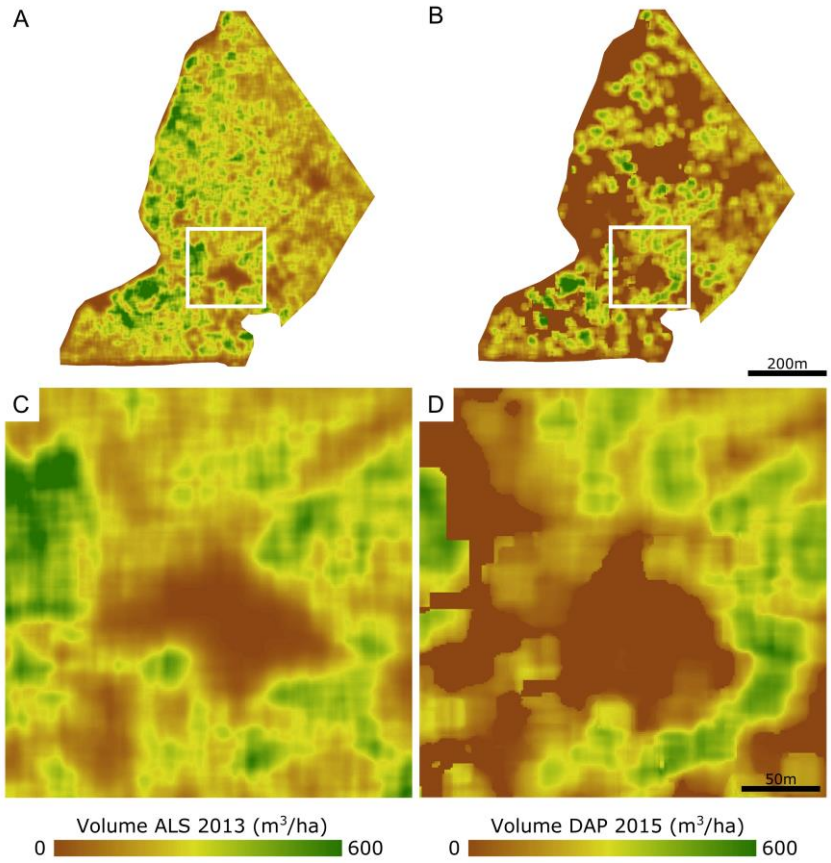

Figure 37: (a, i) T_1 ALS and (b, ii) T_2 DAP predictive volume wall-to-wall outputs for compartment B.

Although DAP has proven accurate in estimating residual timber volumes, a limitation of the technology is that it is highly influenced by ambient light conditions (Gobakken et al., 2015). The collection of DAP imagery in our study area was easily accomplished; however, the acquisition of larger areas could prove complicated due to the changes in illumination and weather conditions over time. Therefore, the acquisition of DAP point clouds using UAS should be limited to smaller areas to better manage for variability in illumination and weather conditions. This would also follow the framework of updating a much larger T_1 ALS data set with DAP post-harvest. This methodology

improves cost effectiveness of forest practices, while providing managers with accurate stand-level structure, terrain, and high resolution RGB photography information.

In spite of the above-mentioned limitations, it is evident that the numerous benefits to managers adopting UAS in place of conventional light aircrafts are abundant. In order for managers to maximize the utility of UAS, special attention should be given to determine which features are best suited to their data collection needs. Apart from reductions in short- and long-term costs, features such as intuitive flight planning and autonomous control capabilities make operating the UAS and capturing high resolution imagery simple and convenient. First-hand control during flights provide managers with the capability to tailor spatial resolution and coverage to best match their data needs, while quick set-up and launch features facilitate frequent data capture and improve overall utility. Managers should be aware that commercial UAS have a diverse array of physical and technological features that alter their ability to acquire aerial imagery including sensor compatibility, battery life, and software capabilities.

In this chapter, I compared indirect and direct approaches to modelling change in volume. The indirect model, which was determined by the difference between T_1 ALS and T_2 DAP volume estimates, showed a higher accuracy (RMSE% = 16.65) than the direct method (RMSE% = 86.56). The poor accuracy of the direct model can be attributed to the fundamental differences in how ALS and DAP point clouds characterize forest structure. ALS data, having the potential to penetrate through the crown canopy, has lower height

percentiles than DAP. This is generally due to the inability of DAP to penetrate the crown canopy restricting its metrics to the forest canopy. Previous studies such as White et al. (2015) have shown that ALS and DAP metric correlations increase as height percentiles increase. The results of those studies agree with the results of our analysis into the differences between DAP and ALS metrics at increasing percentiles of height. The indirect model used in our analysis indicates that estimates of volume change for this study area can be achieved regardless of differences in metric stratification. This result aligns the use of the indirect modelling method with our proposed framework of updating ALS inventories with DAP after harvesting.

Future analysis into indirect versus direct volume modelling approaches should follow the methodology of studies such as Bollandsås et al. (2013) and Økseter et al. (2015), where the same technologies are compared (T_1 ALS vs. T_2 ALS) to determine whether the direct or indirect approach is more accurate at estimating metric change over time in specific forested areas. Results of studies to date show mixed outcomes for which method is most accurate, often dependent on data type, forest type, location, and age (Cao et al., 2016). In the interest of preserving the low acquisition cost of DAP data, it would be beneficial to compare a post-harvest DAP data set immediately following harvest, and data acquisition a number of years afterwards. This analysis could also prove useful in elaborating on results achieved in Chapter 5 for estimating and monitoring stand regeneration.

7.5 Conclusion

Both ALS and DAP have the ability to model forest metrics utilizing the ABA. The ability for ALS to create accurate DTMs and provide structural information for forest managers provides a strong basis for its implementation in large-scale inventory generation over areas of future operations. DAP has been proven accurate in its ability to estimate residual volume in harvested stands, and thus serves as a technology capable of updating ALS generated inventories. The indirect method of modelling volume change proved the most accurate in our study area, likely because it does not incorporate the fundamental differences in ALS and DAP metrics. The cost effectiveness, ease of deployment, and collection of very high resolution imagery makes UAS-DAP a strong candidate for incorporation into forest management and inventory updating practices.

Chapter 8:

Updating individual tree heights and volumes using DAP[7]

8.1 Background and motivation

This chapter utilizes the same UAS-DAP and ALS datasets as Chapter 7 however analyzes the ability of DAP to detect individual trees consistently through time, and update inventory metrics within a previously established tree level EFI. I present a case study where UAS-DAP point clouds were used to update a previously established ALS EFI to demonstrate another potential use of this technology in an operational context. Point cloud outputs from ALS in 2013 and DAP in 2015 were used to determine UAS-DAP point clouds legitimacy as an EFI updating tool. To identify the validity of using multiple point cloud metrics for measuring height and volume increments, both the CHM and 95th percentile of height (P95) were analyzed. Motivations for this analysis included maximizing the temporal accuracy and cost effectiveness of the EFI, as well as monitoring tree height and volume growth over the inter-inventory period. This study is among the first to evaluate UAS-DAP as a data set to update existing ALS generated EFIs.

[7] The content of this chapter has been adapted from:
Goodbody, T.R.H., Coops, N.C., Marshall, P., Tompalski, P., Crawford, P., (2017). Unmanned aerial systems for precision forest inventory purposes a review and case study. For. Chron. 93, 71–81.

8.1.1 Tree identification and delineation

To compare the maximum tree heights from the DAP and ALS CHMs, 20 image plots, each 20 m^2, were established within the study area in parts of the stand that were undisturbed between 2013 and 2015. The CHM of each image plot with a 10 m buffer was extracted and individual trees were identified using a local maxima search followed by crown delineation routines (Tompalski et al., 2014). Image plot extents were overlaid on the CHM and all detected treetops within the bounds were included. Individual trees were assigned CHM-derived heights. Treetop locations and crown extents for both ALS and DAP datasets were processed to ensure the same trees were identified across both datasets. Identified trees were classified as being detected in both datasets or in one dataset only. Trees matched in both datasets were principally dominant individuals in the canopy with the most prominent crowns. For the purposes of this analysis, it was assumed that all matched trees were Douglas-fir.

8.1.2 Height and volume comparison

Individual matched tree height metrics produced from both the CHM and P95 in both the ALS and DAP datasets for all image plot locations were compared (White et al., 2015). CHM heights were validated using independent field measured sample plots in the same study area at the time of ALS and imagery collection. The ALS CHM was shown to under predict tree height by 4 %. This was likely due to laser pulses not intersecting tree apexes. As a result, a correction factor was applied (Yu et al, 2004). Validation indicated

that the DAP CHM did not experience the same problem due to the much denser point cloud. In order to generate gross volume estimates for all matched trees, DBH for all subject trees was required. To estimate these values, tree crown areas and their corresponding CHM and P95 heights from locally validated samples were fit using local data in equation [**6]** (Hall et al., 1989):

$$\boldsymbol{DBH = e^{2.590283+0.043808 \times H-0.001381 \times CA}} \quad [6]$$

where DBH is diameter at breast height in cm, H is tree height in m, and CA is crown area in m^2.

After DBH was estimated for each tree, DBH as well as CHM and P95 heights were used as inputs for equation [7], a Douglas-fir gross volume equation (BC Forest Service, 1976):

$$V = 10^{-4.383102+1.749240 \times log_{10}(DBH)+1.156410 \times log_{10}(H)} \quad [7]$$

where V is tree volume in m^3 and DBH and H are as defined previously.

Height and volume estimates for matched trees were compared with local independent field measured plots averaged over 21 years of measurements. Sampling methodologies for these plots can be found in Marshall (1996). At the time of writing, the most recent re-measurement period for these plots was completed at the end of the 2013 growing season.

8.2 Results

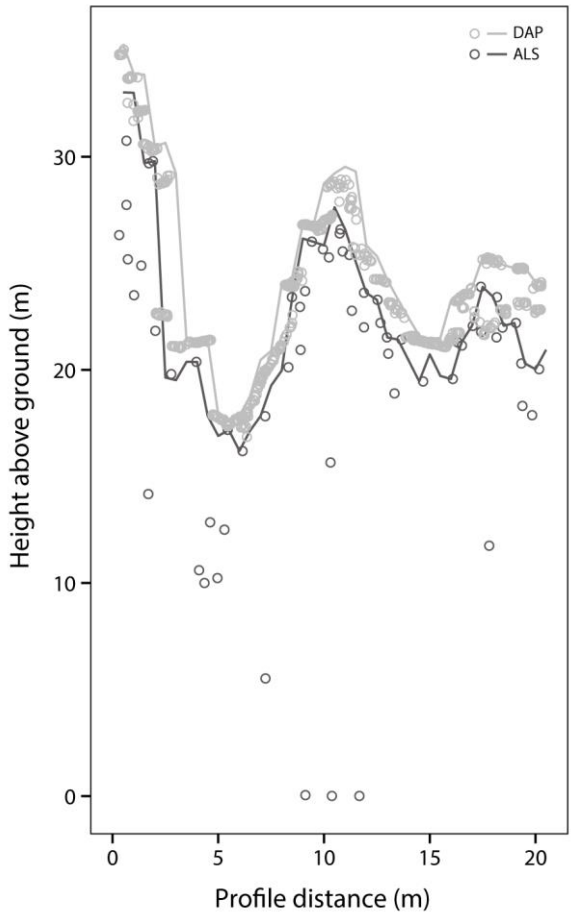

Figure 38: Canopy height model (CHM) height profile (m) of 2013 ALS (dark grey) and 2015 DAP (light grey) and associated point clouds denoted by circles. Treetops can clearly be identified in both data sets, outlining how the CHM local maxima were used to delineate crown extents and estimate heights.

A total of 246 trees were detected across all image plots with 171 (70 %) being detected in both data sets. The remaining trees were detected in only one of the data sets (30 in the ALS and 45 in the DAP). Both the CHM and P95 heights of matched trees from all image plots were compared (Figure 38 and Figure 40). Mean height growth for all trees over the inter-inventory period was 0.68 m, with a standard error of 0.05 m for the CHM, while P95 height increased by 0.50 m ± 0.05 m. Height growth was detected for 152 trees

while 19 trees showed a reduction in height. Measured growth of well-growing trees on independent field measured sample plots indicated average annual growth rates of 0.25 m to 0.30 m over 21 years of measurements. Gross volume estimates for each matched tree were produced using CHM and P95 derived heights and modelled diameter values. CHM gross volume increased by an average of 0.05 $m^3 \pm 0.005$ m^3 (Figure 39), while P95 gross volumes indicated slightly less growth of 0.03 $m^3 \pm 0.005 m^3$ over the inter-inventory period (Figure 41). These levels of tree volume growth slightly exceeded the growth found on the independent sample in area (average ~ 0.01 m^3 per year over the last 21 years).

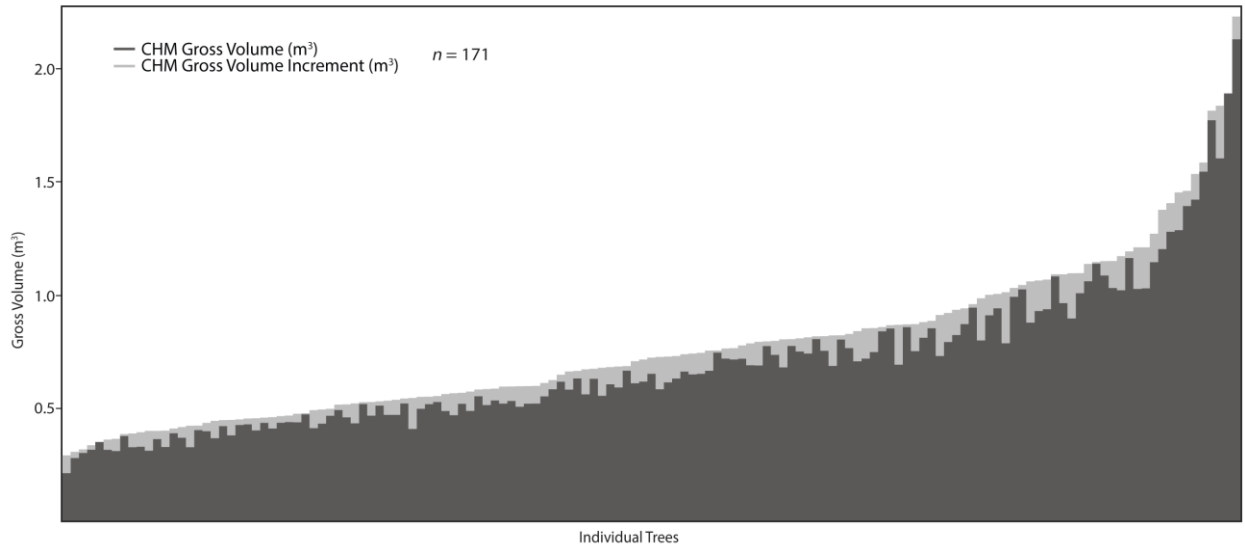

Figure 39: Histogram of all 171 individually matched trees with their 2013 CHM gross volume (m^3) estimates (dark grey) and corresponding gross volume (m^3) increment estimates (light grey). The sum of the gross volume and increment equates to the CHM gross volume estimate for 2015.

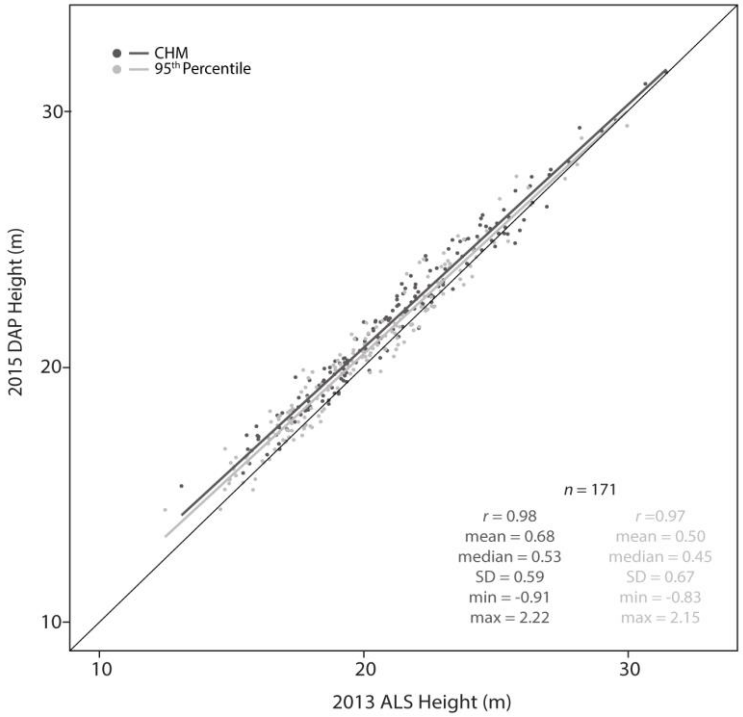

Figure 40: Comparison of tree heights (m) for all ALS and DAP trees from the CHM (dark grey) and 95th percentile of height (light grey) along with tree growth statistics. 1:1 line shown.

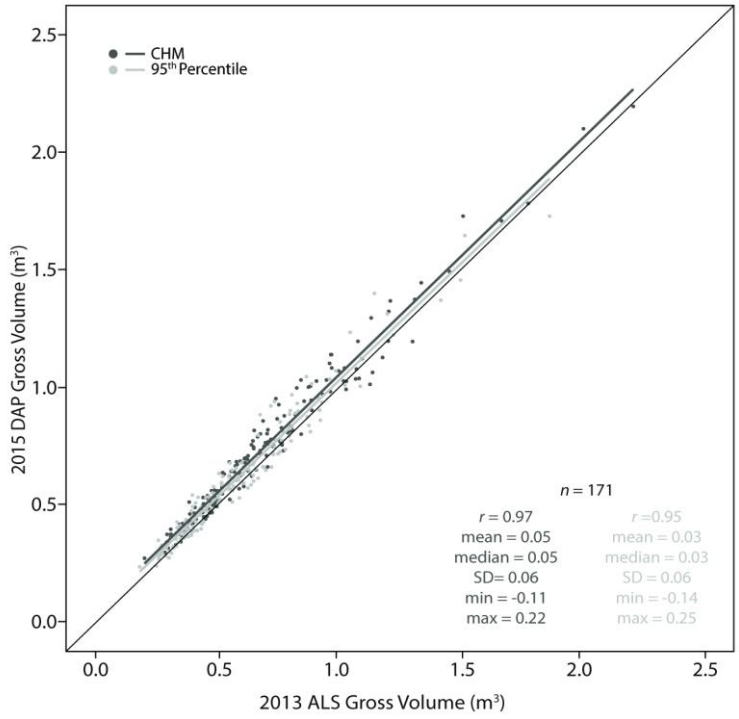

Figure 41: Comparison of gross volumes (m^3) for all ALS and DAP trees from the CHM (dark grey) and 95th percentile of height (light grey) along with volume increase statistics. 1:1 line shown

8.3 Discussion

The 2013 ALS data generated a baseline individual tree level inventory, providing height, structure, and location information for each detected tree. The comparison of ALS and UAS-DAP point cloud height data from both the CHM and P95 height in our analysis indicated that individual trees can be matched across data types to update height and volume for individual tree level inventories. Height and volume results indicate that UAS acquired DAP CHM and P95 heights can be used for measuring growth. The technique developed synthesis between the ALS and UAS-DAP point clouds in our study area to produce individual tree inventory data, following the movement towards precision forestry at local and regional scales (Holopainen et al., 2014).

UAS-DAP point clouds were effective in updating individual tree growth and volume between 2013 and 2015. Estimates were within the limits of regional growth models (Thrower and Goudie, 1992) and local independent field measured sample plot data. CHM and P95 data both indicated that height growth decreased as total tree height increased, potentially due to slowing of productivity associated with mature individuals. Individual tree volume showed the opposite trend, where the volume increment increased with larger trees. This finding agrees with assumptions that larger, taller trees may be exhibiting slower primary growth, but that increased basal areas result in larger annual volume increments. Past research into the relationship between ALS and DAP point cloud metrics has shown that correlations between the two data types increase as height

percentiles increase (Goodbody et al., 2016). Both the CHM and P95 heights were analysed in our study to outline the consistency in growth and volume estimations between the two metrics, but also to indicate that both are highly correlated and reliable for measuring forest inventory metrics (White et al., 2013a).

Neither point cloud was error free. Due to the relatively lower point density of ALS compared to the DAP point cloud, it is unlikely that the absolute apex of each crown was detected (Ontiveros et al., 2005). It was for this reason that a height correction factor produced from independently field measured sampled plots from the same ALS dataset was applied to all ALS trees. Other issues that should be noted are the potential for artifacts within individual tree crowns. The cumulative error of the ALS and DAP point cloud data must be considered when utilizing the data being presented. Although a predominant portion of the matched trees showed height growth and volume increases, some trees were slightly shorter and indicated less volume in 2015 than in 2013, which could be artifacts from both the CHM and P95 heights as well as DBH modelling. To more precisely quantify the decreases in height associated with natural occurrences such as leader breakage, manual field measurements would be needed.

The relatively short period from 2013 to 2015 between data set collections could also have introduced inaccuracy due to measurement and precision errors potentially being within the physical limits of tree growth (Wulder et al., 2008). In order to ameliorate the potential for these errors in future studies, a framework to consider could involve broad

scale ALS acquisition at 10 - 15 year intervals with regular 4 - 6 year UAS-DAP point cloud updates for mature stands (White et al., 2013a). Although much more frequent than current forest management standards, higher periodicity of inventory updates could help to improve growth and yield estimates, while also providing spatial and structural information related to areas of potential growth deficiency, competition concern, or treatment successes and failures.

Descriptive statistics for individual trees provide managers with data that allow for resource monitoring and guiding future harvest planning. Creation of conventional tabular information paired with the 3D point cloud in the form of an EFI can allow managers to better understand the development of composition, structure, and depending on sensors, potentially the health of the trees on their land base (Näsi et al., 2015). The ability to quickly operationalize UAS for DAP acquisitions also facilitates inventory updates in the event of an unforeseen disturbance or scheduled harvesting. The proposed inventory updating framework has the potential to maintain temporal and spatial accuracy of operational areas, allowing managers to have consistently reliable forest resource information (Lisein et al., 2013).

Estimating gross volume for individual trees increases the precision of forestry practices and provides a basis for estimating the economic value of timber that metrics such as tree height alone cannot. Managerial knowledge of how tree volume is changing from year to year across their land base not only facilitates an informed long term planning

process to maximize revenue from harvesting operations, but also allows the prioritization of where and when operations are conducted. Having multiple tactical plans for operations can reduce future economic uncertainty and help guide resource development. The combination of individual tree volumes, heights, and locations could be used to guide operational planning. Determining individual trees and areas that are suitable for harvesting now or in the near future increases economic and environmental sustainability while promoting progressive and precise forest stewardship and planning.

An inventory framework such as the one presented here has the potential to be used as an ecosystem-based management and monitoring tool (Zhang et al., 2016). Having a baseline and routinely updated EFI for a forest stand or harvested area may identify areas that are in need of treatments such as commercial thinning, and how they could respond post-treatment. Having accurate spatial knowledge of specific locations requiring treatments rather than a large-scale application of treatments will reduce application time and costs. By using UAS-DAP point clouds prior to, and after applications, managers can gauge successes and failures, and modify future actions based on their findings.

Similarly, a multi-temporal EFI framework could help guide decision-making about the location and characteristics of desirable timber. Such data can reduce the labour and time intensity of field reconnaissance so resources can be allocated more effectively. As technological advancements and reductions in cost for UAS compatible ALS sensors become more prevalent, the widespread collection of these data will become more

prominent (Zhang et al., 2016). The landscape level coverage of ALS data provides managers with spatially and temporally accurate models of operational areas. Block development and site plan information related to road and skid trail planning, presence and locations of streams and potential archaeological sites, stratification of stand types, and accurate estimates of fundamental tree parameters such as height and volume provide planning and operational information from which managers can make informed decisions on harvest methodologies and timing. Information on terrain and stand characteristics can help guide managers in optimizing harvest equipment being deployed to harvesting sites, thus reducing logging costs and improving the efficiency of operations. EFI information about log volumes prior to harvest can be used in conjunction with current market climates to allow for better planning in the appropriate allocation of timber to specialist mills for higher value end product generation. All of these operational decisions have significant effects on the overall cost, efficiency, and sustainability of operations.

Given that 70 % of trees were matched across datasets, further research into the improvement of tree detection and crown growing algorithms is needed to improve the accuracy and reliability of individual tree inventories. Of the individual trees that were matched, a majority were dominant in the canopy. For this reason research into refining the detection and matching of non-dominant stems within stands would help to improve overall detection and matching accuracies. The incorporation of spectral data from UAS orthoimagery, which is already used in the DAP process, along with CHMs could help to

refine tree detection and matching methodologies. Furthermore, acquiring high resolution visible as well as NIR imagery could help to improve accurate identification of individual tree species, health, and outline potential areas of management concern (Näsi et al., 2015). Accurate species identification will reduce uncertainty in applying species specific DBH and volume models in mixed stands, expanding the scope of our case study methodology.

8.4 Conclusions

This case study confirmed the potential of UAS-DAP as a forest inventory tool and illustrates an effective method to update pre-existing ALS EFIs. The ability to produce tree height and volume growth estimates using both ALS and DAP point clouds over time provides spatial and quantitative data that can guide future operational decisions. With ongoing research and development, generating and updating EFIs using ALS and UAS-DAP point clouds will likely become the standard for providing informative, cost-effective, and spatially accurate information in support of precision forest management.

Chapter 9:

Conclusions

9.1 Dissertation objectives

The objectives of this dissertation were to:

- Review, examine, and report on the successes and limitations of DAP for characterizing forests of varying structures.
- Determine possible use of DAP in generating, extrapolating, and updating EFI data.
- Assess DAP-derived inventory products and datasets for their potential to monitor, update, and expand inventory knowledge, as well as inform multi-level forest management initiatives.

These themes were addressed by answering each of my research questions (Figure 1) as detailed below.

"What is the state of DAP research with regard to enhancing forest inventories, and what is the capacity to create, update, and monitor EFIs in maturing stands using DAP?"

The in-depth literature review and discussion presented in Chapter 2 provides substantial justification for the integration of DAP to update landscape level, area-based EFIs. Chapter 7 and 8 reiterate these findings at the local operational scale, indicating that DAP is flexible in terms of its ability to provide multi-scale information. The amalgamation of a wealth of DAP literature providing comparisons to ALS data indicates that DAP data are more cost-effective and analogous in accuracy. The caveat to these statements is that a high resolution DTM must exist to facilitate DAP normalization, perhaps the largest

challenge to operational implementation of DAP. However, the literature also outlines its potential for synergy in updating ALS EFI baselines.

Chapters 7 and 8 demonstrate that DAP is effective at delineating the spatial distribution and magnitude of selection harvesting in harvest ready stands, as well as updating tree-level attributes. In general, these findings demonstrate that DAP is an effective multi-scale updating tool providing inventory data capable of informing operational, tactical, and strategic management strategies.

Peer-reviewed evidence related to DAP's accuracy, cost-effectiveness, and potential for estimation of standard and novel forest attributes indicates that these data should be strongly considered for integration into multi-temporal EFI frameworks. DAP is consistently shown to be a viable option for establishing linkages among forest inventories with varying objectives, helping to establish ecosystem-based management approaches.

"How does seasonal timing of DAP acquisitions influence its ability to provide accurate terrain information in sparsely forested openings?"

As described throughout this dissertation, a major challenge with using DAP is that it is often reliant on high resolution DTMs, such as those produced using ALS, to produce accurate and reliable EFI data. Outcomes from Chapter 4 indicated that DAP point clouds were capable of generating DTMs that were comparable with a reference ALS DTM in a deciduous dominated low canopy cover site. Accuracy of these DTMs decreased with increasing vegetation cover. DTMs acquired in spring, late-fall, and early-winter were the most accurate. This analysis confirmed that seasonal vegetation differences affected the

performance of DAP for producing DTMs, providing managerial insight into the timing of DTM generation for maximizing data utility and accuracy. The fundamental limitation of DAP for generating accurate terrain models outside of low cover, deciduous dominated sites still holds true. The methodology presented in Chapter 4 is opportunistic and entirely dependent upon site conditions. Results from this Chapter provide potential methodologies for managers to generate accurate terrain information in harvested areas that otherwise would require alternate technologies to generate accurate terrain information.

"Can temporal and spatial knowledge of forest regeneration be improved using DAP?"

In Chapter 5, DAP structural and spectral metrics were found to have potential to characterize post-harvest regeneration of various ages. Novel inventory attributes including the accurate classification of forest cover, their spatial distribution, and structural composition wall-to-wall provide effective tools for meeting silvicultural obligations and planning management strategies. These findings are timely in that silvicultural surveying is conducted over vast areas of forest annually, is time intensive, and requires further characterization to better integrate with growth and yield projections. Novel and informative silvicultural data products such as those presented in Chapter 5 provide a basis for linking data on early forest development with already established projection models. The inclusion of these data could help to establish linkages between inventories, and improve estimates of early forest growth.

"What are the values of DAP spectral and structural metrics for spatially modelling biotically disturbed stands and standard inventory attributes?"

Climate change is expected to alter the magnitude and spatial distribution of biotic disturbances. Chapter 6 focused on the need for spatially explicit, detailed information on the extent and severity of forest health issues, specifically cumulative eastern spruce budworm defoliation, to establish proactive, data-driven management approaches. While traditional methods of delineating forests affected by annual defoliation through sketch mapping surveys provide useful information, consistent and cost-effective approaches to forest health surveying and inventory management are needed. DAP spectral metrics were found to be effective at modeling the severity and distribution cumulative spruce budworm defoliation at a landscape level, providing a means of monitoring defoliation trends.

Chapter 5 and Chapter 6 outline the dual analytical potential of DAP data in that they provide both spectral and structural information. This is of importance for forest management firstly, because spectral metrics can accurately model the spatial distribution and magnitude of defoliation across a landscape, and secondly, because structural metrics are effective for estimating standard forest inventory attributes such as volume and basal area. This indicates that DAP data can serve dual purposes in providing both forest health information and improving inventory attribute estimates from a single image acquisition. A key point with reference to these acquisitions is that many jurisdictions already have established multi-year funding for the purpose of routine photo-interpretation. Therefore, the methodologies presented have promise for being integrated into existing and future

stereo-image surveys to capitalize on previously unrealized economic value, enhance spatial knowledge on forest health, and improve landscape-level inventory content.

"What are the drivers for acquiring DAP data using UAS?"

Although not the primary focus of this dissertation, UAS platforms were demonstrated to be effective for forestry stereo-image acquisitions at an operational scale. The literature review of UAS in Chapter 3 indicated their cost-effectiveness, potential for rapid operationalization, and propensity to acquire high resolution data at a local operational scale. Integration of these platforms into forest inventory and interdisciplinary ecological research is happening extremely rapidly. The use of these platforms can be described as the democratization of remote sensing in that data parameters are defined by user needs. There is no doubt that technological and legislative advances will continue, improving rationale for the use of these platforms in forest management. It is my opinion that UAS integration into forestry is a paradigm shift in conceptualizing and implementing management. It will soon become a survey tool as common as a compass or clinometer.

Cost is a major factor that influences the decision of commercial forest licensees to conduct routine forest inventory updates. The adoption of large scale ALS coverage over the past decade has proven informative, cost-effective, and efficient in providing information that characterizes forest structure and terrain while quantifying potential harvest volumes (Wulder et al., 2008). Given the results of Chapters 4, 5, 7, & 8, further economic benefits and improved inventory frameworks can be realized by supplementing traditional aerial vehicles using ALS with new, state-of-the-art UAS technologies (Lisein et

al., 2013; Tao et al., 2011). Apart from lower capital and operational costs when operating at local operational scales (< 100 ha), UAS have a rapid operationalization capacity, an enhanced ability to control spatial and temporal resolution of outputs, and a reduced potential for risks to flight crews (Tang and Shao, 2015).

An added benefit is that UAS development is ongoing, providing opportunity for producers and developers to continually improve system utility to match the needs of consumers such as the forest industry. Partnership and collaboration such as this should be welcomed to improve the overall efficiency and effectiveness of UAS and sensor development as well as forest management practices.

9.2 Research innovations

This dissertation provided key innovations for outlining the potential of DAP for characterizing forests and informing EFIs:

- Novel approaches that incorporate DAP acquisitions within an EFI updating framework are highlighted in Chapters 2, 4, 5, 7 and 8. This work has better informed the capacity of DAP to characterize forest structure and produced accurate methods of generating standard and novel inventory attributes to improve the spatial and temporal accuracy of EFIs.
- Chapter 4 established new insights into the significant relationship between vegetation phenology and the accuracy of DAP derived terrain models in low cover deciduous dominated stands. This information can support rationale for management and data acquisition decision-making, enhancing the utility and accuracy of desired terrain information. This method forms a means of generating EFI baselines for multi-temporal analysis.

- A reconceptualization of post-harvest regeneration inventories is presented in Chapter 5. The acquisition of high resolution DAP data shows significant promise for facilitating effective silvicultural management strategies, providing reliable estimates of spatial distribution and structural content, and consequent products that promote due-diligence. Continuation of research into this methodology is being actively pursued.
- Originality in the use of both the structural and spectral components of DAP, as well as developing insights into their comparative importance, was conducted in Chapters 5 and 6. The benefits of both data sets from a single DAP acquisition promote their cost-effectiveness and potential for further EFI product innovation.
- Substantial evidence of the potential to use UAS as a viable imagery acquisition platform is presented in Chapters 3, 4, 5, 7, and 8. These chapters are evidence of the early adoption of UAS technology for forest management, some of which (Chapters 5, 7 & 8) have been well referenced in the greater body of remote sensing of forestry literature.

9.3 Research limitations

9.3.1 Study locations and sample data

Study areas used in this dissertation are small in the context of global forests. All analytical chapters were focused on Canadian forests and forest management approaches. Studies were often conducted to determine methods for meeting and augmenting Canadian forest management objectives. These analyses do not directly relate to the diverse and variable forests in other nations. I acknowledge that not all structural compositions of these forests have been tested using DAP, and that transfer of methodological approaches and

achieved results should be conducted accordingly. Ongoing benchmarking and development of DAP forest inventory products in these areas is of great research interest.

Availability of sample data in the form of timber cruises and regeneration surveys was determined by available budget and time constraints. I acknowledge that sample sizes larger than those used in some chapters would be ideal for improving statistical relationships and confidence in results. However, I did make every effort to maximize sample data quality and quantity given limited time and budget.

9.3.2 Image matching algorithms and software

A secondary caveat to this research is that the generation of DAP point clouds and consequent analytical products are reliant on available image matching algorithms and processing suites. Software such as Pix4D, used in Chapters 5, 7, and 8, and Agisoft Photoscan used in Chapters 4 and 6 are proprietary, not specifically designed for 3D reconstruction of vegetation, and their image-matching algorithms are predominantly guarded from users. The internal workings of these software are black-boxes, limiting the ability of researchers to better understand how they work and fine tune parameters to test their influence on DAP products. Additionally, these software are in continual development, meaning that algorithm functionality is constantly changing, potentially leading to varying spectral and structural characterizations of forests. As algorithm capabilities progress, especially for reconstruction of vegetation, the methodologies employed in this dissertation may need to change alongside image-matching development.

Furthermore, there is no standard method for DAP point cloud generation and post-processing. The methodologies employed in this dissertation were chosen based on peer reviewed research, which often call for standardization of DAP processing and parameterization benchmarking.

9.3.3 DAP as a compromise technology

This dissertation outlines that DAP is a technology capable of integration into multiple aspects of forest inventories; however, I also believe that there is rationale for describing these data as a compromise technology. This description is largely based on the fact that DAP is a cost-effective alternative to state-of-the-art, often cost-restrictive, remote sensing technologies like ALS and hyperspectral imagery.

9.3.3.1 DAP and ALS

Chapter 1, 2, 7 & 8 outlined that ALS is capable of characterizing forests more comprehensively and accurately than DAP, and that ALS derived DTMs are often fundamental to using DAP for updating EFIs. While results in Chapters 4 and 5 indicated that DAP is capable of generating DTMs in regenerating forests that can be used in consequent multi-temporal analyses, DAP is still dependent on ALS DTMs for deriving accurate and meaningful inventory products in most stands.

Currently, DAP is not an ALS replacement. I advocate that the synergistic use of both technologies to form an effective inventory updating framework is promising. However, DAP is a compromise to ALS and it can provide analogous upper canopy

characterizations for a cheaper price, but it is unable to characterize forest structures that may be of interest to managers as effectively as ALS. For example, the characterization of forest understorey and other sub-canopy structures is never conducted in this dissertation largely because DAP is only able to characterize the outer canopy surface of forests. This does not mean that DAP is an inferior technology to ALS, but rather that it has limitations that must be acknowledged prior to its acquisition and use for informing forest management scenarios.

9.3.3.2 DAP and hyperspectral imagery

While DAP is a compromise to ALS in some aspects, it is also capable of characterizing forests in ways that ALS cannot. Most importantly, as outlined in Chapters 5 and 6, DAP can also provide spectral data from acquired imagery. Results in this dissertation indicated that DAP spectral data is effective for providing information on land cover and severity of cumulative spruce budworm defoliation, although the spectral resolution of this imagery is often limited. This is again an instance where DAP can be viewed as a compromise technology. The results within this dissertation indicate the future promise of being able to integrate DAP to provide cost-effective forest health data. However, other research has shown that using hyperspectral imagery provides more data rich spectral information that facilitates better spectral characterizations and modelling outcomes. As cost reductions for hyperspectral sensors become reality, perhaps their use for photogrammetric approaches will become more common.

Additionally, this dissertations use of DAP spectral metrics were limited to only two applications. Further research into the use of these data should continue, especially DAP's ability to characterize defoliation patterns and severity from different biotic agents, such as mountain pine beetle (*Dendroctonus ponderosae*), or stress responses from fungal disturbances.

9.3.4 UAS

This dissertation did not look to compare different UAS platforms or available sensors. I relied upon previous research for deriving information related to the cost/benefit of UAS and their operational feasibility. At the time of writing, commercially available UAS are limited to operational coverages, though changes in regulations and advances in hardware and software are expected to take place. The following section outlines the importance of ongoing research into UAS platforms and sensors for forest inventory applications.

9.4 Future directions

While incorporating DAP into EFI frameworks is clearly beneficial, there are also logistic and scientific justifications for continued research (Figure 42).

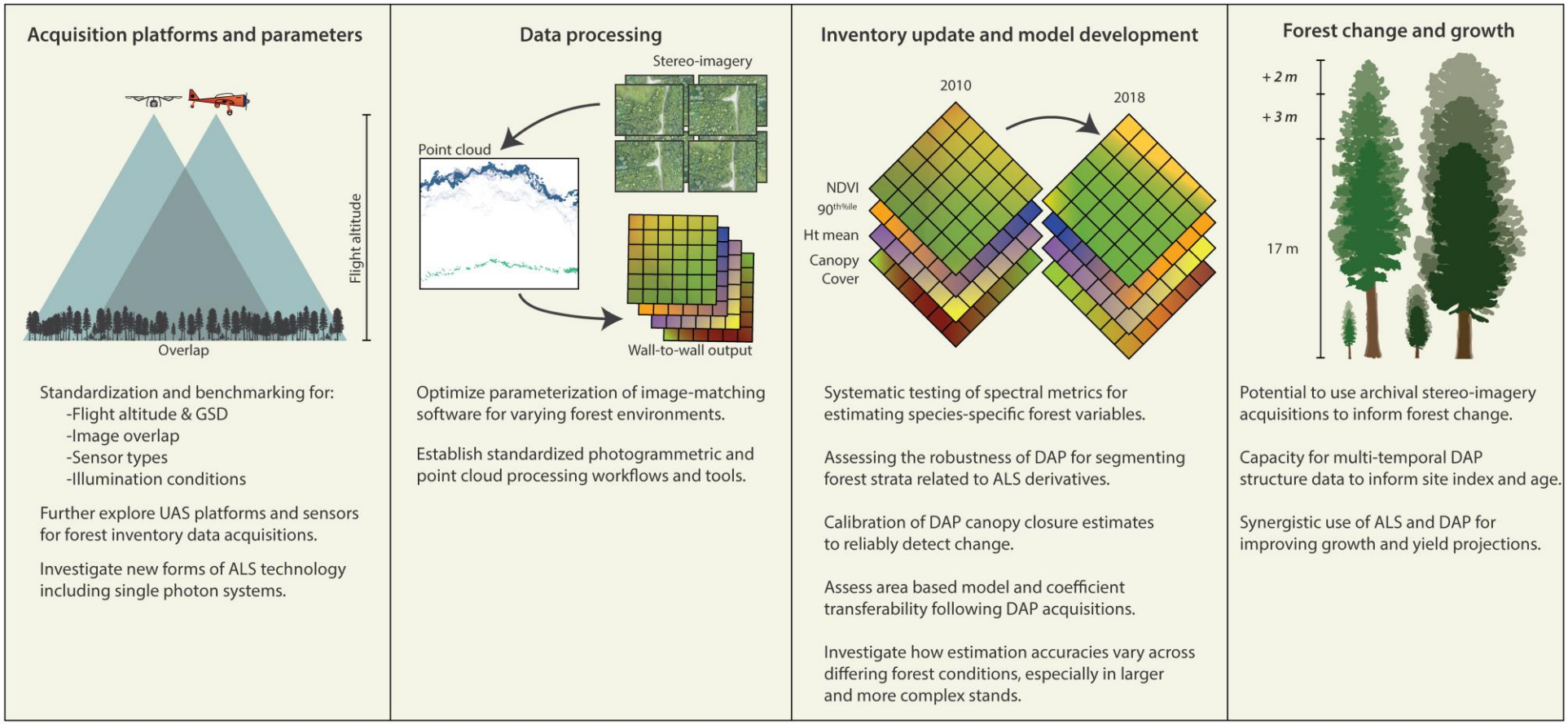

Figure 42: Summary of where additional research is warranted to improve the potential of DAP for characterizing forest structure and enhancing forest inventories.

9.4.1 Acquisition planning

- Standardization and benchmarking for flight altitude, image overlap, ground sample distance, sensor types, and illumination conditions.
- Further explore UAS platforms and sensors for forest inventory data acquisitions.
- Investigate new forms of ALS technology for characterizing terrain surfaces, including single photon systems.

An area that requires rigorous sensitivity analysis is with respect to how differences in acquisition parameters such as altitude, GSD, and across-track overlap influence the viability of produced point clouds for forest inventory applications. Some such studies in this area have been recently conducted (e.g., Bohlin et al., 2012; Granholm et al., 2015; Iqbal et al., 2018; Nurminen et al., 2013; Puliti, 2017); however more research is required to outline best practice approaches for different forested ecosystems. Forests varying in their vertical and horizontal structure could necessitate varying parameter levels to achieve best photogrammetric processing results.

One of the major inhibitors of conducting parameter benchmarking experiments is high cost. The use of UAS for quickly operationalized, cost-effective, and efficient image acquisition campaigns could help to illuminate how differences in acquisition and point cloud processing parameterization impact variation of modelling outcomes (Goodbody et al., 2017b; Puliti et al., 2015). Studies focusing on how UAS can be used to establish parametric benchmarking and standardization will help to improve the utility and value of data acquired using conventional manned aircraft. Some parameters such as flight altitude may be more difficult to benchmark due to regulatory restrictions and compatible sensor differences.

As described in Chapter 3, UAS platforms and their associated sensors are diverse in hardware and software. Rapid technological innovation in this field prompts the need to

continually test these systems to better understand how they can be used to achieve management requirements alongside evolving legislation. A manager needs to be able to confidently use a variety of UAS airframes and sensors to achieve reliability, cost-effectiveness, and consistency of inventory products.

The need for an ALS derived DTM is fundamental. The advent of new ALS technologies such as single photon lidar may enable cost effective landscape level characterization of the ground surface with sufficient accuracy to support DAP normalization. Single photon systems have the ability to fly at higher elevations and faster speeds, acquiring ALS data for less cost than currently standard systems (White et al., 2013a). This raises the potential for DAP data to be used to support forest inventory frameworks, especially in areas beyond existing EFI boundaries. This would allow EFIs to be used to update previous conventional photo-based inventories and modernize landscape level forest inventory assessments. Further inquiry into the potential of this technology is needed.

9.4.2 Data processing

- Optimize parameterization of image-matching software for varying forest environments.
- Establish standardized photogrammetric and point cloud processing workflows and tools.

Image-matching algorithms with a focus on forest vegetation reconstruction are needed. Current algorithms, although showing success, could be optimized for vegetated environments, helping to further enhance the capacity for area-based estimations using DAP.

Physical characteristics of forests and the local environment that pose problems to DAP point cloud generation also require a higher level of inquiry. Studies have found that shadowing and solar angle / illumination (Honkavaara et al., 2012; Rahlf et al., 2017; St-Onge et al., 2008; Stone et al., 2016; Vastaranta et al., 2013), occlusion from neighbouring tree canopies (St-Onge

et al., 2015), and tree swaying caused by wind (Dandois and Ellis, 2010; Näsi et al., 2015) have contributed to problems with point cloud generation (Iqbal et al., 2018). Robust analyses into these potential sources of variability in point cloud generation will help to establish best practice conditions, as well as outline potential sources of error and how to manage them effectively prior to stereo-image acquisitions.

Studies that describe how photogrammetric algorithm parameterization can influence point cloud utility for area-based estimates are needed. Iqbal et al., (2018) provided a detailed description of how processing parameterization within Agisoft Photoscan (2018) can influence point cloud outputs and found that differing levels of *Key Point Limits*, *Quality*, and *Depth Filtering* parameters were relatively robust to differences in processing strategies. These results demonstrate that parameterization differences using this particular software do not adversely influence point cloud utility. Given that processing speed is determined by hardware components, these results are encouraging for being able use parameters with lower processing requirements and still achieve point clouds capable of being used for generating EFI products. While promising, analyses that test parameterization in a range of commercially available and open-source photogrammetric software for the purposes of forest inventory applications such as Probst et al., (2018) are needed to help establish best practices parametrization routines.

9.4.3 Inventory update and model development

- Systematic testing of spectral metrics for estimating species-specific forest variables.
- Assessing the robustness of DAP for segmenting forest strata related to ALS derivatives.
- Calibration of DAP canopy closure estimates to reliably detect change.
- Assess potential for area-based model and coefficient transferability following DAP acquisitions.

- Investigate how estimation accuracies vary across differing forest conditions, especially in larger and more complex stands.

The provision of spectral information from stereo-imagery could play an important role in further deriving qualitative differences in the forested landscape. Investigations of the potential to utilize spectral indices in combination with structural metrics for area-based outcomes should continue.

The integration of these metrics for assessing how well DAP is able to stratify forest landscapes could also be important. Continued assessments of where DAP is successful or limited in stratifying landscapes are important steps for more seamless inventory integration. Landscape level investigations looking to determine DAP's effectiveness for stratifying forest types as well as stand-level assessments to outline canopy closure are needed. White et al. (2018) indicated that DAP did not accurately map canopy gaps compared to ALS, and called for further research into its ability to measure size and quantity of canopy gaps. They outline that DAP data are not capable of characterizing small canopy openings and are challenged by shadows and occlusions prevalent in mature forest canopies.

Using DAP to update previously established ALS EFI attributes requires investigation into the potential transferability of area-based models and their coefficients. Relationships between DAP and ALS metrics have been well described; however, details on the potential ubiquity of models across forest types has yet to be conducted in detail.

9.4.4 Forest change and growth

- Potential to use archival stereo-imagery acquisitions to inform forest change.
- Capacity for multi-temporal DAP structure data to inform site index and age.
- Synergistic use of ALS and DAP for improving growth and yield projections.

Synergistic uses of ALS and multi-temporal DAP acquisitions are showing increasing promise for accurately estimating growth and yield attributes such as height, site index, and age. Analyses capitalizing on the availability of long-term photo archives such as Vastaranta et al. (2016), who developed and tested an approach to estimate stand age, and Véga and St-Onge (2008, 2009), who showed the potential to estimate and spatially map site index and growth, present promising analytical frameworks. Stepper et al. (2014), who assessed forest height changes using regularly acquired aerial imagery, suggested that CHMs derived from repeat aerial image surveys can be a viable and cost-effective way to monitor forest height changes through time. Studies such as these indicate that the estimation of these attributes can be conducted using available stereo-imagery archives, improving the quality and completeness of forest inventory databases.

A template matching approach proposed in Tompalski et al. (2016) for integrating area-based inventories with growth and yield simulators is also promising. Methodologies propose the use of multiple attributes such as volume, basal area, and height to define a growth curve for a spatially explicit area. This method could provide improved and more spatially detailed results than using traditional polygon-based approaches. Adding to this work, Tompalski et al. (2018) also looked to determine whether improved growth curve assignments could be realized with the addition of a secondary DAP time-step. Other approaches to assimilating remote sensing data sets such as Nyström et al. (2015), who tested the ability to use a DAP-derived CHM time series in combination with growth models, showed promising results for incorporating multiple types of remote sensing data to provide spatial layers of up-to-date estimates of forest stand predictions. Further research into data assimilation approaches and multi-temporal modelling of growth and yield curves using DAP data sets is warranted.

9.5 Closing statement

The findings of this dissertation demonstrate that DAP point clouds and underlying technologies capable and effective at characterizing forest structure and enhancing forest inventories. Chapters presented herein have detailed that DAP point clouds, which can be generated using aerial imagery from a variety of sensors and platforms, are capable of providing quantifiable benefits to forest inventory programs. While DAP is often dependent on ALS data for its terrain information, the spatial, structural, and spectral data it provides over forested environments can help to enhance the value and utility of forest inventories. In my opinion, results presented in this thesis, as well as in the greater body of DAP forestry research, justify its integration into multi-temporal inventory frameworks. My hope is that the methodologies and discussion presented in this dissertation fairly describe the potential value of these data and underlying technologies, the need for further research into their limitations, and the opportunity they present for improving forest management decision making.

Bibliography

Agisoft, 2018. Agisoft PhotoScan Professional Edition.

Aguilar, F.J., Mills, J.P., 2008. Accuracy assessment of lidar-derived digital elevation models. Photogramm. Rec. 23, 148–169.

Alonzo, M., Morton, D.C., Cook, B.D., Andersen, H.E., Babcock, C., Pattison, R., 2017. Patterns of canopy and surface layer consumption in a boreal forest fire from repeat airborne lidar. Environ. Res. Lett. 12.

Andersen, H.E., Reutebuch, S.E., McGaughey, R.J., d'Oliveira, M.V.N., Keller, M., 2014. Monitoring selective logging in western amazonia with repeat lidar flights. Remote Sens. Environ. 151, 157–165.

Ashley, M., Rea, J., Wright, L., 1976. Spruce budworm damage evaluations using aerial photography. Photogramm. Eng. Remote Sensing 42, 1265–1272.

Balaguer-Beser, A., Ruiz, L.A., Hermosilla, T., Recio, J.A., 2013. Using semivariogram indices to analyse heterogeneity in spatial patterns in remotely sensed images. Comput. Geosci. 50, 115–127.

Balaguer, A., Ruiz, L.A., Hermosilla, T., Recio, J.A., 2010. Definition of a comprehensive set of texture semivariogram features and their evaluation for object-oriented image classification. Comput. Geosci. 36, 231–240.

Baltsavias, E., Gruen, A., Eisenbeiss, H., Zhang, L., Waser, L.T., 2008. High-quality image matching and automated generation of 3D tree models. Int. J. Remote Sens. 29, 1243–1259.

Baltsavias, E.P., 1999. Airborne laser scanning: Basic relations and formulas. ISPRS J. Photogramm. Remote Sens. 54, 199–214.

Baltsavias, E.P., 1999. A comparison between photogrammetry and laser scanning. ISPRS J.

Photogramm. Remote Sens. 54, 83–94.

Barrett, F., McRoberts, R.E., Tomppo, E., Cienciala, E., Waser, L.T., 2016. A questionnaire-based review of the operational use of remotely sensed data by national forest inventories. Remote Sens. Environ. 174, 279–289.

Baskerville, G., MacLean, D.A., 1979. Budworm-caused mortality and 20-year recovery in immature balsam fir stands - Rep. M-X-102. Fredericton, N.B.

BC Forest Service, 1976. Whole Stem Cubic Metre Volume Equations and Tables: Centimetre Diameter Class Merchantable Volume Factors. Forest Inventory Division, British Columbia Forest Service, Dept of Forests, Victoria, BC.

Bechtold, W.A., Patterson, P.L., 2005. The enhanced forest inventory and analysis program - national sampling design and estimation procedures.

Besl, P., McKay, N., 1992. A Method for Registration of 3-D Shapes. IEEE Trans. Pattern Anal. Mach. Intell.

Blais, J.R., 1958. Effects of Defoliation By Spruce Budworm (Choristoneura Fumbferana Clem.) on radial growth at breast height of balsam fir (Abies Balsamea (1 . 1 Mill .) and white spruce (Picea Glauca (Moench) Voss .). For. Chron. 34, 39–47.

Blais, J.R., 1961. Spruce budworm outbreaks in the Lower St. Lawrence and Gaspé regions. For. Chron. 37, 192–202.

Blaschke, T., 2010. Object based image analysis for remote sensing. ISPRS J. Photogramm. Remote Sens. 65, 2–16.

Blyenburgh & Co, 2014. R2014 RPAS Yearbook - RPAS: The Global Perspective, 12th ed. Blyenburgh & Co, Paris, France.

Bohlin, J., Bohlin, I., Jonzén, J., Nilsson, M., 2017. Mapping forest attributes using data from

stereophotogrammetry of aerial images and field data from the national forest inventory. Silva Fenn. 51, 1–18.

Bohlin, J., Wallerman, J., Fransson, J.E.S., 2012. Forest variable estimation using photogrammetric matching of digital aerial images in combination with a high-resolution DEM. Scand. J. For. Res. 27, 692–699.

Bollandsås, O. M., Gregoire, T. G., Næsset, E., & Øyen, B.-H., 2013. Detection of biomass change in a Norwegian mountain forest area using small footprint airborne laser scanner data. Stat. Methods Appt. 22, 113–129.

Bolton, D.K., White, J.C., Wulder, M.A., Coops, N.C., Hermosilla, T., Yuan, X., 2018. Updating stand-level forest inventories using airborne laser scanning and Landsat time series data. Int. J. Appl. Earth Obs. Geoinf. 66, 174–183.

Bonnor, G.M., Magnussen, S., 1987. Forest inventories in Canada: a framework for change. For. Chron. 63, 193–198.

Breidenbach, J., Næsset, E., Lien, V., Gobakken, T., Solberg, S., 2010. Prediction of species specific forest inventory attributes using a nonparametric semi-individual tree crown approach based on fused airborne laser scanning and multispectral data. Remote Sens. Environ. 114, 911–924.

Breiman, L., 1996. Out-of-bag estimation.

Breiman, L., 2001. Random forests. Mach. Learn. 45, 5–32.

Bush, B.L., Nachbar, R.B., 1993. Sample-distance partial least squares: PLS optimized for many variables, with application to CoMFA. J. Comput. Aided. Mol. Des. 7, 587–619.

Candau, J.-N., Fleming, R.., 2005. Landscape-scale spatial distribution of spruce budworm defoliation in relation to bioclimatic conditions. Can. J. For. Res. 35, 2218–2232.

Candau, J.-N., Fleming, R.., Hopkin, A., 1998. Spatiotemporal patterns of large-scale defoliation caused by the spruce budworm in Ontario since 1941. Can. J. For. Res. 28, 1733–1741.

Cao, L., Coops, N.C., Innes, J.L., Sheppard, S.R.J., Fu, L., Ruan, H., She, G., 2016. Remote Sensing of Environment Estimation of forest biomass dynamics in subtropical forests using multi-temporal airborne LiDAR data. Remote Sens. Environ. 178, 158–171.

Carrascal, L.M., Galván, I., Gordo, O., 2009. Partial Least Squares Regression as an Alternative to Current Regression Methods Used in Ecology. Oikos 118, 681–690.

Central Uplands Ecoregion, 2013. In: Our Landscape Heritage. Government of New Brunswick, Fredericton, N.B, pp. 145–150.

Chong, I.G., Jun, C.H., 2005. Performance of some variable selection methods when multicollinearity is present. Chemom. Intell. Lab. Syst. 78, 103–112.

Clarke, R., 2014. The regulation of civilian drones' impacts on behavioural privacy. Comput. Law Secur. Rev. 30, 286–305.

Clausi, D.A., 2002. An analysis of co-occurrence texture statistics as a function of grey level quantization. Can. J. Remote Sens. 28, 45–62.

Colomina, I., Molina, P., 2014. Unmanned aerial systems for photogrammetry and remote sensing : A review. ISPRS J. Photogramm. Remote Sens. 92, 79–97.

Corona, P., 2016. Consolidating new paradigms in large-scale monitoring and assessment of forest ecosystems. Environ. Res. 144, 8–14.

Corona, P., Fattorini, L., 2008. Area-based lidar-assisted estimation of forest. Can. J. For. Res. 38, 2911–2916.

Cramer, M., Haala, N., Stallmann, D., 2000. Direct Georeferencing Using GPS/Inertial Exterior Orientations for Photogrammetric Applications. IAPRS XXXIII.

Dale, V., Joyce, L., McNulty, S., Neilson, R., Ayres, M., Flannigan, M., Hanson, P., Irland, L., Lugo, A., Peterson, C., Simberloff, D., Swanson, F., Stocks, B., Wotton, B., 2001. Climate change and forest disturbances. Bioscience 51, 723–734.

Dall'Asta, E., 2016. Semi-Global techniques in Image Matching and Change Detection with applications to Civil and Environmental Engineering. Università degli Studi di Parma.

Dall'Asta, E., Roncella, R., 2014. A comparison of semiglobal and local dense matching algorithms for surface reconstruction. Int. Arch. Photogramm. Remote Sens. Spat. Inf. Sci. XL-5, 187–194.

Dandois, J.P., Ellis, E.C., 2010. Remote sensing of vegetation structure using computer vision. Remote Sens. 2, 1157–1176.

Dandois, J.P., Ellis, E.C., 2013. High spatial resolution three-dimensional mapping of vegetation spectral dynamics using computer vision. Remote Sens. Environ. 136, 259–276.

Dawson, R., Armleder, H., Bings, B., Peel, D., 2007. Management Strategy for Mule Deer Winter Ranges in the Cariboo-Chilcotin Part 1a: Management Plan for Shallow and Moderate Snowpack Zones 2007, Management.

Day, K.J., 2007. Management and working plan #3. Williams Lake, BC.

Debella-Gilo, M., 2016. Bare-earth extraction and dtm generation from photogrammetric point clouds with a partial use of an existing lower resolution dtm. Int. Arch. Photogramm. Remote Sens. Spat. Inf. Sci. - ISPRS Arch. 41, 201–206.

Dees, M., Straub, C., Koch, B., 2012. Can biodiversity study benefit from information on the vertical structure of forests? Utility of LiDAR remote sensing. Curr. Sci. 102, 1181–1187.

Dormann, C.F., Elith, J., Bacher, S., Buchmann, C., Carl, G., Carré, G., Marquéz, J.R.G., Gruber, B., Lafourcade, B., Leitão, P.J., Münkemüller, T., Mcclean, C., Osborne, P.E.,

Reineking, B., Schröder, B., Skidmore, A.K., Zurell, D., Lautenbach, S., 2013. Collinearity: A review of methods to deal with it and a simulation study evaluating their performance. Ecography (Cop.). 36, 27–46.

Dunford, R., Michel, K., Gagnage, M., Piégay, H., Trémelo, M.L., 2009. Potential and constraints of Unmanned Aerial Vehicle technology for the characterization of Mediterranean riparian forest. Int. J. Remote Sens. 30, 4915–4935.

Duryea, M.L., 2000. Forest Regeneration Methods : Natural Regeneration , Direct Seeding and Planting 1.

Dvořák, P., Müllerová, J., Bartaloš, T., Brůna, J., 2015. Unmanned Aerial Vehicles for Alien Plant Species Detection and Monitoring. ISPRS - Int. Arch. Photogramm. Remote Sens. Spat. Inf. Sci. XL-1/W4, 83–90.

Eltner, A., Baumgart, P., Maas, H.G., Faust, D., 2015. Multi-temporal UAV data for automatic measurement of rill and interrill erosion on loess soil. Earth Surf. Process. Landforms 40, 741–755.

Erdle, T.A., MacLean, D.A., 1999. Stand growth model calibration for use in forest pest impact assessment. For. Chron. 75, 141–152.

Fekety, P.A., Falkowski, M.J., Hudak, A.T., 2015. Temporal transferability of LiDAR-based imputation of forest inventory attributes. Can. J. For. Res. 45, 422–435.

Fiorella, M., Ripple, W.J., 1993. Analysis of Conifer Forest Regeneration Using Landsat Thematic Mapper Data. Photogramm. Eng. Remote Sens. 59, 1383–1388.

Forest, C.D., Forest, B.C.L., Dynamics, S., Wiley, J., 1990. Development Following Major Structure and Process II . Stem Exclusion 1–6.

Franklin, J.F., 1993. Preserving Biodiversity: Species, Ecosystems, or Landscapes? Ecol. Appl.

3, 202–205.

Franklin, S.E., 2001. Remote Sensing For Sustainable Forest Management, 1st Editio. ed. CRC Press, Boca Raton, Florida.

Franklin, S.E., Fan, H., Guo, X., 2008. Relationship between landsat TM and SPOT vegetation indices and cumulative spruce budworm defoliation. Int. J. Remote Sens. 29, 1215–1220.

Franklin, S.E., Waring, R.H., McCreight, R.W., Cohen, W.B., Fiorella, M., 1995. Aerial and Satellite Sensor Detection and Classification of Western Spruce Budworm Defoliation in a Subalpine Forest. Can. J. Remote Sens. 21, 299–308.

Frazer, G.W., Magnussen, S., Wulder, M.A., Niemann, K.O., 2011. Simulated impact of sample plot size and co-registration error on the accuracy and uncertainty of LiDAR-derived estimates of forest stand biomass. Remote Sens. Environ. 115, 636–649.

Frey, J., Kovach, K., Stemmler, S., Koch, B., 2018. UAV photogrammetry of forests as a vulnerable process. A sensitivity analysis for a structure from motion RGB-image pipeline. Remote Sens. 10.

Fridman, J., Holm, S., Nilsson, M., Nilsson, P., Ringvall, A.H., Ståhl, G., 2014. Adapting National Forest Inventories to changing requirements - The case of the Swedish National Forest Inventory at the turn of the 20th century. Silva Fenn. 48, 1–29.

Furze, S., Ogilvie, J., Arp, P.A., 2017. Fusing Digital Elevation Models to Improve Hydrological Interpretations. J. Geogr. Inf. Syst. 09, 558–575.

Gillis, M.D., Leckie, D.G., 1996. Forest inventory update in Canada. For. Chron. 72, 138–156.

Gobakken, T., Bollandsås, O.M., Næsset, E., 2015. Comparing biophysical forest characteristics estimated from photogrammetric matching of aerial images and airborne laser scanning data. Scand. J. For. Res. 30, 73–86.

Goodbody, T.R.H., Coops, N.C., Hermosilla, T., Tompalski, P., Crawford, P., 2017a. Assessing the status of forest regeneration using digital aerial photogrammetry and unmanned aerial systems. Int. J. Remote Sens. 39, 5246–5264.

Goodbody, T.R.H., Coops, N.C., Hermosilla, T., Tompalski, P., McCartney, G., MacLean, D.A., 2018a. Digital aerial photogrammetry for assessing cumulative spruce budworm defoliation and enhancing forest inventories at a landscape-level. ISPRS J. Photogramm. Remote Sens. 142, 1–11.

Goodbody, T.R.H., Coops, N.C., Hermosilla, T., Tompalski, P., Pelletier, G., 2018b. Vegetation Phenology Driving Error Variation in Digital Aerial Photogrammetrically Derived Terrain Models. Remote Sens. 10, 1554.

Goodbody, T.R.H., Coops, N.C., Marshall, P., Tompalski, P., Crawford, P., 2017b. Unmanned aerial systems for precision forest inventory purposes a review and case study. For. Chron. 93, 71–81.

Goodbody, T.R.H., Coops, N.C., Tompalski, P., Crawford, P., Day, K.J., 2016. Updating residual stem volume estimates using ALS- and UAV-acquired stereo-photogrammetric point clouds. Int. J. Remote Sens. 1161.

Granholm, A.H., Lindgren, N., Olofsson, K., Nyström, M., Allard, A., Olsson, H., 2017. Estimating vertical canopy cover using dense image-based point cloud data in four vegetation types in southern Sweden. Int. J. Remote Sens. 38, 1820–1838.

Granholm, A.H., Olsson, H., Nilsson, M., Allard, A., Holmgren, J., 2015. The potential of digital surface models based on aerial images for automated vegetation mapping. Int. J. Remote Sens. 36, 1855–1870.

Gray, D.R., 2008. The relationship between climate and outbreak characteristics of the spruce

budworm in eastern Canada. Clim. Change 87, 361–383.

Grenzdörffer, G., Engel, A., Teichert, B., 2008. The photogrammetric potential of low-cost UAVs in forestry and agriculture. Int. Arch. Photogramm. Remote Sens. Spat. Inf. Sci. 31, 1207–1214.

Gruen, A., Li, Z., 2002. Automatic DTM Generation from Three-Line-Scanner (TLS) Images. Int. Arch. Photogramm. Remote Sens. 34, 131–137.

Guerra-Hernández, J., González-Ferreiro, E., Monleón, V.J., Faias, S.P., Tomé, M., Díaz-Varela, R.A., 2017. Use of multi-temporal UAV-derived imagery for estimating individual tree growth in Pinus pinea stands. Forests 8, 1–19.

Guo, X., Coops, N.C., Tompalski, P., Nielsen, S.E., Bater, C.W., John Stadt, J., 2017. Regional mapping of vegetation structure for biodiversity monitoring using airborne lidar data. Ecol. Inform. 38, 50–61.

Haala, N., 2014. EuroSDR-Project Commission 2 - "Benchmark on Image Matching" Final Report. Wien, Austria.

Haala, N., Fritsch, D., Stallmann, D., Cramer, M., 2000. On the preformance of digital airborne pushbroom cameras for photogrammetric data processing – a case study. Int. Arch. Photogramm. Remote Sensing. Vol. XXXIII, Part B4. Amsterdam 2000. XXXIII, 324–331.

Haala, N., Hastedt, H., Wolf, K., Ressl, C., Baltrusch, S., 2010. Digital Photogrammetric Camera Evaluation – Generation of Digital Elevation Models. Photogramm. - Fernerkundung - Geoinf. 2010, 99–115.

Haala, N., Hastedt, H., Wolf, K., Ressl, C., Baltrusch, S., Stallmann, D., Cramer, M., 1998. Calibration Of Directly Measured Position And Attitude By Aerotriangulation Of Three-Line Airborne Imagery. Int. Arch. Photogramm. Remote Sens. 32, 23–30.

Haddow, K.A., King, D.J., Pouliot, D.A., Pitt, D.G., Bell, F.W., 2000. Early regeneration conifer identification and competition cover assessment using airborne digital camera imagery. For. Chron. 76, 915–928.

Hakala, T., Honkavaara, E., Saari, H., Mäkynen, J., Kaivosoja, J., Pesonen, L., Pölönen, I., 2013. Spectral Imaging From Uavs Under Varying Illumination Conditions. ISPRS - Int. Arch. Photogramm. Remote Sens. Spat. Inf. Sci. XL-1/W2, 189–194.

Hall, R. J., R. T. Morton, and R.N.N., 1989. A comparison of existing models for DBH estimation from large-scale photos. For. Chron. 65, 114–120.

Hall, R.J., Aldred, A.H., 1992. Forest regeneration appraisal with largescale aerial photographs. For. Chron. 68, 142–150.

Hardy, Y.J., Lafond, A., Hamel, L., 1983. The epidemiology of the current spruce budworm outbreak in Quebec. For. Sci. 29, 715–725.

Harris, J.W.., Dawson, A.F., Goodenough, D., 1978. Evaluation of LANDSAT data for forest pest detection and damage appraisal surveys in British Columbia. Report. Pacific For. Res. Cent.

Hawryło, P., Tompalski, P., Węzyk, P., 2017. Area-based estimation of growing stock volume in Scots pine stands using ALS and airborne image-based point clouds. Forestry 90, 686–696.

Hébert, F., 2016. Best Management Practices for Tolerant Hardwoods in New Brunswick. Volume I: Distribution, Silvics and Stand Attributes of Key Species Associated with Northern Hardwoods in New Brunswick. Edmunston, New Brunswick.

Hermosilla, T., Wulder, M.A., White, J.C., Coops, N.C., Hobart, G.W., 2015a. An integrated Landsat time series protocol for change detection and generation of annual gap-free surface reflectance composites. Remote Sens. Environ. 158, 220–234.

Hermosilla, T., Wulder, M.A., White, J.C., Coops, N.C., Hobart, G.W., 2015b. Regional detection, characterization, and attribution of annual forest change from 1984 to 2012 using Landsat-derived time-series metrics. Remote Sens. Environ. 170, 121–132.

Hilker, T., Wulder, M.A., Coops, N.C., 2008. Update of forest inventory data with lidar and high spatial resolution satellite imagery. Can. J. Remote Sens. 34, 5–12.

Hirschmüller, H., 2005. Accurate and efficient stereo processing by semi-global matching and mutual information. IEEE Comput. Soc. Conf. Comput. Vis. Pattern Recognit. 2, 807–814.

Hirschmüller, H., 2008. Stereo Processing by Semi-Global Matching and Mutual Information. Stereo Process. by Semi-Global Matching Mutual Inf. 30, 328–341.

Hirschmüller, H., 2011. Semi-Global Matching - Motivation, Developments and Applications. Photogramm. Week 11 173–184.

Holopainen, M., Vastaranta, M., Hyyppä, J., 2014. Outlook for the Next Generation's Precision Forestry in Finland. Forests 5, 1682–1694.

Holopainen, M., Vastaranta, M., Karjalainen, M., Karila, K., Kaasalainen, S., Honkavaara, E., 2015. Forest inventory attribute estimation using airborne laser scanning, aerial stereo imagery, radargrammetry and interferometry – finnish experiences of the 3d techniques. ISPRS Ann. Photogramm. Remote Sens. Spat. Inf. Sci. 2, 25–27.

Honkavaara, E., Arbiol, R., Markelin, L., Martinez, L., Cramer, M., Bovet, S., Chandelier, L., Ilves, R., Klonus, S., Marshal, P., Schläpfer, D., Tabor, M., Thom, C., Veje, N., 2009. Digital airborne photogrammetry-a new tool for quantitative remote sensing?-a state-of-the-art review on radiometric aspects of digital photogrammetric images. Remote Sens. 1, 577–605.

Honkavaara, E., Litkey, P., Nurminen, K., 2013. Automatic storm damage detection in forests

using high-altitude photogrammetric imagery. Remote Sens. 5, 1405–1424.

Honkavaara, E., Markelin, L., Rosnell, T., Nurminen, K., 2012. Influence of solar elevation in radiometric and geometric performance of multispectral photogrammetry. ISPRS J. Photogramm. Remote Sens. 67, 13–26.

Hunt, E.R., Doraiswamy, P.C., McMurtrey, J.E., Daughtry, C.S.T., Perry, E.M., Akhmedov, B., 2012. A visible band index for remote sensing leaf chlorophyll content at the Canopy scale. Int. J. Appl. Earth Obs. Geoinf. 21, 103–112.

Iqbal, I.A., Musk, R.A., Osborn, J., Stone, C., Lucieer, A., 2019. A comparison of area-based forest attributes derived from airborne laser scanner , small-format and medium-format digital aerial photography. Int J Appl Earth Obs Geoinf. 76, 231–241.

Iqbal, I.A., Osborn, J., Stone, C., Lucieer, A., Dell, M., McCoull, C., 2018. Evaluating the robustness of point clouds from small format aerial photography over a Pinus radiata plantation. Aust. For. 81, 162–176.

Isenburg, M., 2013. LASzip: lossless compression of LiDAR data. Photogramm. Eng. Remote Sens. 79, 209–217.

Isenburg, M., 2018. LAStools. Retrieved from http://lastools.org.

Jaakkola, A., Hyyppä, J., Kukko, A., Yu, X., Kaartinen, H., Lehtomäki, M., Lin, Y., 2010. A low-cost multi-sensoral mobile mapping system and its feasibility for tree measurements. ISPRS J. Photogramm. Remote Sens. 65, 514–522.

James, P.M.A., Robert, L.-E., Wotton, M., Martell, D.L., Fleming, R.A, 2017. Lagged cumulative spruce budworm defoliation affects the risk of fire ignition in Ontario, Canada. Ecol. Appl. 27, 532–544.

Järnstedt, J., Pekkarinen, A., Tuominen, S., Ginzler, C., Holopainen, M., Viitala, R., J. Järnstedt ,

A. Pekkarinen , S. Tuominen , C. Ginzler , M. Holopainen, R.V., Järnstedt, J., Pekkarinen, A., Tuominen, S., Ginzler, C., Holopainen, M., Viitala, R., 2012. Forest variable estimation using a high-resolution digital surface model. ISPRS J. Photogramm. Remote Sens. 74, 78–84.

Jin, S., Sader, S.A., 2005. MODIS time-series imagery for forest disturbance detection and quantification of patch size effects. In: New Brunswick Department of Natural Resources. pp. 462–470.

Kang, J., Park, J., Kim, M., Analysis, A., Map, D., 2008. Digital mapping using aerial digital camera imagery. Int. Arch. Photogramm. Remote Sens. Spat. Inf. Sci. XXXVII, 1275–1278.

Kangas, A., Gobakken, T., Puliti, S., Hauglin, M., Næsset, E., 2018. Value of airborne laser scanning and digital aerial photogrammetry data in forest decision making. Silva Fenn. 52, 1–19.

Kantola, T., Vastaranta, M., Yu, X., Lyytikainen-Saarenmaa, P., Holopainen, M., Talvitie, M., Kaasalainen, S., Solberg, S., Hyyppa, J., 2010. Classification of defoliated trees using tree-level airborne laser scanning data combined with aerial images. Remote Sens. 2, 2665–2679.

Ketcheson, M.V., Braumandl, T.F., Meidinger, D., Utzig, G., Demarchi, D.A., Wikeem, B.M., 1991. Interior Cedar — Hemlock Zone, Ecosystems of Bristish Columbia.

Khosravipour, A., Skidmore, A.K., Isenburg, M., Wang, T., Hussin, Y. a., 2014. Generating Pit-free Canopy Height Models from Airborne Lidar. Photogramm. Eng. Remote Sens. 80, 863–872.

King, D.J., 2000. Airborne Remote Sensing in Forestry: Sensors, Analysis and Applications. For. Chron. 76, 859–876.

Koh, L.P., Wich, S.A., 2012. Dawn of drone ecology : low-cost autonomous aerial vehicles for conservation. Trop. Conserv. Sci. 5, 121–132.

Koot, C., Day, K., Ewen, S., Skea, D., 2015. Harvesting on Mule Deer Winter Range under General Wildlife Measures for Shallow & Moderate Snowpack Zones : Approach and Lessons Learned following a Second Harvest Entry after 30 Years.

Kraus, K., 2004. Photogrammetrie, Seventh Ed. ed. Berlin-New York.

Kukkonen, M., Maltamo, M., Packalen, P., 2017. Image matching as a data source for forest inventory – Comparison of Semi-Global Matching and Next-Generation Automatic Terrain Extraction algorithms in a typical managed boreal forest environment. Int. J. Appl. Earth Obs. Geoinf. 60, 11–21.

Lausch, A., Erasmi, S., King, D.J., Magdon, P., Heurich, M., 2017. Understanding forest health with Remote sensing-Part II-A review of approaches and data models. Remote Sens. 9, 1–33.

Leberl, F., Irschara, A., Pock, T., Meixner, P., Gruber, M., Scholz, S., Wiechert, A., 2010. Point Clouds: Lidar versus 3D Vision. Photogramm. Eng. Remote Sens. 76, 1123–1134.

Leckie, D.G., Ostaff, D.P., 1988. Classification of airborne multispectral scanner data for mapping current defoliation caused by the spruce budworm. For. Sci. 34, 259–275.

Lemaire, C., 2005. Aspects of the Dsm Production With High Resolution Images. Int. Arch. Photogramm. Remote Sens. Spat. Inf. Sci. XXXVII, 1143–1146.

Lemmens, M., 2008. Digital Aerial Cameras: System Configurations and Sensor Architectures. GIM Int. 22.

Lim, K., Hopkinson, C., Treitz, P., 2008. Examining the effects of sampling point densities. For. Chron. 84, 876–885.

Lim, K., Lim, K., Treitz, P., Treitz, P., Wulder, M., Wulder, M., St-Onge, B., St-Onge, B., Flood, M., Flood, M., 2003. LiDAR remote sensing of forest structure. Prog. Phys. Geogr. 27, 88–106.

Lin, Y., Hyyppä, J., Jaakkola, A., 2011. Mini-UAV-borne LIDAR for fine-scale mapping. IEEE Geosci. Remote Sens. Lett. 8, 426–430.

Lin, Y., Jiang, M., Yao, Y., Zhang, L., Lin, J., 2015. Use of UAV oblique imaging for detection of individual trees in residential environments. Urban For. Urban Green. 14, 404–412.

Lisein, J., Pierrot-Deseilligny, M., Bonnet, S., Lejeune, P., 2013. A Photogrammetric Workflow for the Creation of a Forest Canopy Height Model from Small Unmanned Aerial System Imagery. Forests 4, 922–944.

Liu, X., 2008. Airborne LiDAR for DEM generation: Some critical issues. Prog. Phys. Geogr. 32, 31–49.

Löw, F., Prishchepov, A.V., Waldner, F., Dubovyk, O., Akramkhanov, A., Biradar, C., Lamers, J.P.A., 2018. Mapping Cropland abandonment in the Aral Sea Basin with MODIS time series. Remote Sens. 10.

Lowe, D.G., 2004. Distinctive Image Features from Scale-Invariant Keypoints. Int. J. Comput. Vis. 60, 91–110.

Lu, Y., Coops, N.C., Hermosilla, T., 2016. Regional assessment of pan-Pacific urban environments over 25 years using annual gap free Landsat data. Int. J. Appl. Earth Obs. Geoinf. 50, 198–210.

Lu, Y., Coops, N.C., Hermosilla, T., 2017. Chronicling urbanization and vegetation changes using annual gap free Landsat composites from 1984 to 2012. 2017 Jt. Urban Remote Sens. Event, JURSE 2017 1–4.

Luther, J.E., Franklin, S.E., Hudak, J., Meades, J.P., 1997. Forecasting the susceptibility and vulnerability of balsam fir stands to insect defoliation with Landsat thematic mapper data. Remote Sens. Environ. 59, 77–91.

MacDicken, K.G., 2015. Global Forest Resources Assessment 2015: What, why and how? For. Ecol. Manage. 352, 3–8.

MacLean, D.A., 1984. Effects of Spruce Budworm Outbreaks on the Productivity and Stability of Balsam Fir Forests. For. Chron. 60, 273–279.

MacLean, D.A., Erdle, T.A., MacKinnon, W.E., Porter, K.B., Beaton, K.P., Cormier, G., Morehouse, S., Budd, M., 2001. The Spruce Budworm Decision Support System: forest protection planning to sustain long-term wood supply. Can. J. For. Res. 31, 1742–1757.

MacLean, D.A., Lidstone, R.G., 1982. Defoliation by spruce budworm: estimation by ocular and shoot-count methods and variability among branches, trees, and stands. Can. J. For. Res. 12, 582–594.

Maclean, D.A., MacKinnon, W.E., 1996. Accuracy of aerial sketch-mapping estimates of spruce budworm defoliation in New Brunswick. Can. J. For. Res. 26, 2099–2108.

Maclean, D.A., MacKinnon, W.E., 1998. Sample Sizes Required to Estimate Defoliation of Spruce and Balsam Fir Cause by Spruce Budworm Accuratly. North. J. Appl. For. 15, 135–140.

Madding, R.P., Hogan, H.E., 1978. Detection and mapping of spruce budworm defoliation in northern Wisconsin using digital analysis of LANDSAT data. In: 44th Annu. Meet. Am. Soc. Photogram. Washington, D.C., pp. 285–300.

Magnussen, S., Næsset, E., Gobakken, T., Frazer, G., 2012. A fine-scale model for area-based predictions of tree-size-related attributes derived from LiDAR canopy heights. Scand. J.

For. Res. 27, 312–322.

Maltamo, M., T. Tokola, and M.L., 2003. Estimating stand characteristics by combining single tree pattern recognition of digital video imagery and a theoretical diameter distribution model. For. Sci. 49, 98–109.

Marceau, D.J., Howarth, P.J., Dubois, J.M., Gratton, D.J., 1990. Evaluation Of The Grey-level Co-occurrence Matrix Method For Land-cover Classification Using Spot Imagery. IEEE Trans. Geosci. Remote Sens. 28, 513–519.

Marshall, P., 1996. FRDA 242 - Response of uneven-aged douglas-fir to alternative spacing regimes: analysis of the initial impact of the spacing regimes.

McGlone, J., Mikhail, E., Bethel, J., Mullen, R., 2004. Manual of Photogrammetry, fifth. ed, American Society of Photogrammetry and Remote Sensing.

McKenna, P., Erskine, P.D., Lechner, A.M., Phinn, S., 2017. Measuring fire severity using UAV imagery in semi-arid central Queensland, Australia. Int. J. Remote Sens. 38, 4244–4264.

McRoberts, R.E., Chen, Q., Gormanson, D.D., Walters, B.F., 2018. The shelf-life of airborne laser scanning data for enhancing forest inventory inferences. Remote Sens. Environ. 206, 254–259.

McRoberts, R.E., Tomppo, E.O., 2007. Remote sensing support for national forest inventories. Remote Sens. Environ. 110, 412–419.

Mehtätalo, L., de-Miguel, S., Gregoire, T.G., 2015. Modeling height-diameter curves for prediction. Can. J. For. Res. 45, 826–837.

Meidinger, D., Pojar, J., Harper, W.L., 1991. Chapter 14 : Sub-Boreal Spruce Zone by. Ecosyst. Br. Columbia 209–221.

Melin, M., Korhonen, L., Kukkonen, M., Packalen, P., 2017. Assessing the performance of aerial

image point cloud and spectral metrics in predicting boreal forest canopy cover. ISPRS J. Photogramm. Remote Sens. 129, 77–85.

Meng, X., Currit, N., Zhao, K., 2010. Ground filtering algorithms for airborne LiDAR data: A review of critical issues. Remote Sens. 2, 833–860.

Meng, X., Zhang, A., Hu, S., Sun, W., Yang, J., 2012. A Method to Align POS Data and Linear Push-Broom Imaging Data. In: Lee, G. (Ed.), Advances in Automation and Robotics, Vol. 2. Springer Berlin Heidelberg, Berlin, Heidelberg, pp. 99–106.

MFLNRO, 2016. Silviculture Survey Procedures Manual.

Miller, C.A., 1977. The feeding impact of spruce budworm on balsam fir. Can. For. Serv. 7, 76–84.

Minore, D., Laacke, R.J., 1992. Reforestation practices in southwestern Oregon and northern California.

Mirijovskỳ, J., Langhammer, J., 2015. Multitemporal monitoring of the morphodynamics of a mid-mountain stream using UAS photogrammetry. Remote Sens. 7, 8586–8609.

Möckel, T., Dalmayne, J., Prentice, H.C., Eklundh, L., Purschke, O., Schmidtlein, S., Hall, K., 2014. Classification of Grassland Successional Stages Using Airborne Hyperspectral Imagery. Remote Sens. 6, 7732–7761.

Mohan, M., Silva, C.A., Klauberg, C., Jat, P., Catts, G., Cardil, A., Hudak, A.T., Dia, M., 2017. Individual tree detection from unmanned aerial vehicle (UAV) derived canopy height model in an open canopy mixed conifer forest. Forests 8, 1–17.

Mokroš, M., Výbošt'ok, J., Merganič, J., Hollaus, M., Barton, I., Koreň, M., Tomaštík, J., Čerňava, J., 2017. Early stage forest windthrow estimation based on unmanned aircraft system imagery. Forests 8, 1–17.

Montambault, S., Beaudry, J., Toussaint, K., Pouliot, N., 2010. On the Application of VTOL UAVs to the Inspection of Power Utility Assets. 1st Int. Conf. Appl. Robot. Power Ind. 1–7.

Mulverhill, C., Coops, N.C., White, J.C., Tompalski, P., Marshall, P.L., Bailey, T., 2018. Enhancing the estimation of stem-size distributions for unimodal and bimodal stands in a boreal mixedwood forest with airborne laser scanning data. Forests 9.

Murtha, P.A., 1973. Spruce Budworm Damage in Fundy National Park, New Brunswick. Ottawa, Ont.

Næsset, E., 2002a. Predicting forest stand characteristics with airborne scanning laser using a practical two-stage procedure and field data. Remote Sens. Environ. 80, 88–99.

Næsset, E., 2002b. Determination of mean tree height of forest stands by digital photogrammetry. Scand. J. For. Res. 17, 446–459.

Næsset, E., 2007. Airborne laser scanning as a method in operational forest inventory: Status of accuracy assessments accomplished in Scandinavia. Scand. J. For. Res. 22, 433–442.

Næsset, E., 2014. Area-Based Inventory in Norway -- From Innovation to an Operational Reality. In: Maltamo, M., Næsset, E., Vauhkonen, J. (Eds.), Forestry Applications of Airborne Laser Scanning: Concepts and Case Studies. Springer Netherlands, Dordrecht, pp. 215–240.

Næsset, E., Bjerknes, K.-O., 2001. Estimating tree heights and number of stems in young forest stands using airborne laser scanner data. Remote Sens. Environ. 78, 328–340.

Næsset, E., Bollandsås, O.M., Gobakken, T., 2005. Comparing regression methods in estimation of biophysical properties of forest stands from two different inventories using laser scanner data. Remote Sens. Environ. 94, 541–553.

Näsi, R., Honkavaara, E., Lyytikäinen-Saarenmaa, P., Blomqvist, M., Litkey, P., Hakala, T.,

Viljanen, N., Kantola, T., Tanhuanpää, T., Holopainen, M., Wang, C., Wynne, R.H., Thenkabail, P.S., 2015. Using UAV-Based Photogrammetry and Hyperspectral Imaging for Mapping Bark Beetle Damage at Tree-Level. Remote Sens 7, 15467–15493.

Natural Resources Canada, 2016. The State of Canada's Forests: Annual Report 2016.

Navarro, J.A., Fernández-Landa, A., Tomé, J.L., Guillén-Climent, M.L., Ojeda, J.C., 2018. Testing the quality of forest variable estimation using dense image matching: a comparison with airborne laser scanning in a Mediterranean pine forest. Int. J. Remote Sens. 39, 4744–4760.

Nevalainen, O., Honkavaara, E., Tuominen, S., Viljanen, N., Hakala, T., Yu, X., Hyyppä, J., Saari, H., Pölönen, I., Imai, N.N., Tommaselli, A.M.G., 2017. Individual tree detection and classification with UAV-Based photogrammetric point clouds and hyperspectral imaging. Remote Sens. 9.

Nex, F., Remondino, F., 2013. UAV for 3D mapping applications: a review. Appl. Geomatics 6, 1–15.

NFD, 2017. Forest Insects: Spruce Budworm, 1975-2015. URL http://nfdp.ccfm.org/data/graphs/graph_41_a_e.php (accessed 1.19.18).

Nilsson, M., 1996. Estimation of Tree Heights and Stand Volume Using an Airborne Lidar System. Remote Sens. Environ. 56, 1–7.

Nolan, M., Larsen, C.F., Sturm, M., 2015. Mapping snow-depth from manned-aircraft on landscape scales at centimeter resolution using Structure-from-Motion photogrammetry. Cryosph. Discuss. 9, 333–381.

Noss, R.F., 1999. Assessing and monitoring forest biodiversity: A suggested framework and indicators. For. Ecol. Manage. 115, 135–146.

Nurminen, K., Karjalainen, M., Yu, X., Hyyppä, J., Honkavaara, E., 2013. Performance of dense digital surface models based on image matching in the estimation of plot-level forest variables. ISPRS J. Photogramm. Remote Sens. 83, 104–115.

Nyström, M., Lindgren, N., Wallerman, J., Grafström, A., Muszta, A., Nyström, K., Bohlin, J., Willén, E., Fransson, J.E.S., Ehlers, S., Olsson, H., Ståhl, G., 2015. Data assimilation in forest inventory: First empirical results. Forests 6, 4540–4557.

Økseter, R., Bollandsås, O.M., Gobakken, T., Næsset, E., 2015. Modeling and predicting aboveground biomass change in young forest using multi-temporal airborne laser scanner data 30, 458–469.

Oliver, C.D., Larson, B.C., 1996. Temporal and Spatial Patterns of Tree Invasion. In: Forest Stand Dynamics: Updated Edition. John Wiley and Sons, pp. 171–193.

Ontiveros, C., Smith, S., Snape, S., Sua, J.C., 2005. Use of airborne LiDAR and aerial photography in the estimation of individual tree heights in forestry. Comput. Geosci. 31, 253–262.

Osborn, J., Dell, M., Stone, C., Iqbal, I.A., Lacey, M., Lucieer, A., Mccoull, C., 2017. Photogrammetry for forest inventory: Planning Guidelines.

Pádua, L., Hruška, J., Bessa, J., Adão, T., Martins, L.M., Gonçalves, J.A., Peres, E., Sousa, A.M.R., Castro, J.P., Sousa, J.J., 2018. Multi-temporal analysis of forestry and coastal environments using UASs. Remote Sens. 10, 1–21.

Pajares, G., 2015. Overview and Current Status of Remote Sensing Applications Based on Unmanned Aerial Vehicles (UAVs). Photogramm. Eng. Remote Sens. 81, 281–329.

Palermo, G., Piraino, P., Zucht, H.-D., 2009. Performance of PLS regression coefficients in selecting variables for each response of a multivariate PLS for omics-type data. Adv. Appl.

Bioinform. Chem. 2, 57–70.

Panagiotidis, D., Abdollahnejad, A., Surový, P., Chiteculo, V., Panagiotidis, D., Abdollahnejad, A., Surový, P., Chiteculo, V., 2017. Determining tree height and crown diameter from high-resolution UAV imagery Determining tree height and crown diameter from high-resolution UAV imagery. Int. J. Remote Sens. 00, 1–19.

Pasquarella, V.J., Bradley, B.A., Woodcock, C.E., 2017. Near-real-time monitoring of insect defoliation using Landsat time series. Forests 8.

Patias, P., Giagkas, F., Georgiadis, C., Mallinis, G., Kaimaris, D., Tsioukas, V., 2017. Evaluating horizontal positional accuracy of low-cost UAV orthomosaics over forest terrain using ground control points extracted from different sources. Proc. SPIE - Int. Soc. Opt. Eng. 10444.

Peasgood, S., Valentin, M., 2015. Drones: A Rising Market.

Penner, M., Woods, M., Pitt, D.G., 2015. A comparison of airborne laser scanning and image point cloud derived tree size class distribution models in Boreal Ontario. Forests 6, 4034–4054.

Pepe, M., Fregonese, L., Scaioni, M., 2018. Planning airborne photogrammetry and remote-sensing missions with modern platforms and sensors. Eur. J. Remote Sens. 51, 412–435.

Petrie, G., Walker, A.S., 2007. Airborne digital imaging technology: a new overview. Photogramm. Rec. 22, 203–225.

Pickell, P.D., Hermosilla, T., Frazier, R.J., Coops, N.C., Wulder, M.A., 2016. Forest recovery trends derived from Landsat time series for North American boreal forests Forest recovery trends derived from Landsat time series for North American boreal forests. Int. J. Remote Sens. 1161, 138–149.

Pitt, D.G., Wagner, R.G., Hall, R.J., Douglas, J.K., Leckie, D.G., Runesson, U., 1997. Use of remote sensing for forest vegetation management : A problem analysis. For. Chron. 73, 459–477.

Pitt, D.G., Woods, M., Penner, M., 2014. A comparison of point clouds derived from stereo imagery and airborne laser scanning for the area-based estimation of forest inventory attributes in boreal Ontario. Can. J. Remote Sens. 40, 214–232.

Pix4D, 2018a. Sequoia Pix4D [WWW Document]. URL https://pix4d.com/sequoia-faq/ (accessed 8.3.18).

Pix4D, 2018b. Pix4D [WWW Document]. URL https://www.pix4d.com/ (accessed 1.9.19).

Power, J.M., 1991. National data on forest pest damage. In: Proceedings of a National Conference on Canada's Timber Resources, June 3-5, 1990, Victoria, British Columbia. Victoria, British Columbia, pp. 119–129.

Powers, R.P., Hermosilla, T., Coops, N.C., Chen, G., 2015. Remote sensing and object-based techniques for mapping fine-scale industrial disturbances. Int. J. Appl. Earth Obs. Geoinf. 34, 51–57.

Probst, A., Gatziolis, D., Strigul, N., 2018. Intercomparison of photogrammetry software for three-dimensional vegetation modelling. R. Soc. Open Sci. 5.

Puliti, S., 2017. Use of photogrammetric 3D data for forest inventory.

Puliti, S., Gobakken, T., Ørka, H.O., Næsset, E., 2017. Assessing 3D point clouds from aerial photographs for species-specific forest inventories. Scand. J. For. Res. 32, 68–79.

Puliti, S., Ørka, H.O., Gobakken, T., Næsset, E., 2015. Inventory of small forest areas using an unmanned aerial system. Remote Sens. 7, 9632–9654.

Puliti, S., Saarela, S., Gobakken, T., Ståhl, G., Næsset, E., 2018a. Combining UAV and Sentinel-

2 auxiliary data for forest growing stock volume estimation through hierarchical model-based inference. Remote Sens. Environ. 204, 485–497.

Puliti, S., Talbot, B., Astrup, R., 2018b. Tree-Stump Detection, Segmentation, Classification, and Measurement Using Unmanned Aerial Vehicle (UAV) Imagery. Forests 9, 102.

Rahlf, J., 2017. Forest resource mapping using 3D remote sensing: Combining national forest inventory data and digital aerial photogrammetry.

Rahlf, J., Breidenbach, J., Solberg, S., Astrup, R., 2015. Forest parameter prediction using an image-based point cloud: A comparison of semi-ITC with ABA. Forests 6, 4059–4071.

Rahlf, J., Breidenbach, J., Solberg, S., Næsset, E., Astrup, R., 2014. Remote Sensing of Environment Comparison of four types of 3D data for timber volume estimation. Remote Sens. Environ. 155, 325–333.

Rahlf, J., Breidenbach, J., Solberg, S., Næsset, E., Astrup, R., 2017. Digital aerial photogrammetry can efficiently support large-area forest inventories in Norway. Forestry 90, 710–718.

Régnière, J., Nealis, V.G., 2007. Ecological mechanisms of population change during outbreaks of the spruce budworm. Ecol. Entomol. 32, 461–477.

Remondino, F., Del Pizzo, S., Kersten, T.P., Troisi, S., 2012. Low-Cost and Open-Source Solutions for Automated Image Orientation -- A Critical Overview. In: Ioannides, M., Fritsch, D., Leissner, J., Davies, R., Remondino, F., Caffo, R. (Eds.), Progress in Cultural Heritage Preservation. Springer Berlin Heidelberg, Berlin, Heidelberg, pp. 40–54.

Remondino, F., Menna, F., 2008. Image-based surface measurement for close-range heritage documentation. Int. Arch. Photogramm. Remote Sens. Spat. Inf. Sci. XXXVII, 199–206.

Remondino, F., Spera, M.G., Nocerino, E., Menna, F., Nex, F., 2014. State of the art in high

density image matching. Photogramm. Rec. 29, 144–166.

Reutebuch, S.E., Andersen, H., Mcgaughey, R.J., Forest, L., 2005. Light Detection and Ranging (LIDAR): An Emerging Tool for Multiple Resource Inventory. J. For. 103, 286–292.

Rickbeil, G.J.M., Hermosilla, T., Coops, N.C., White, J.C., Wulder, M.A., 2017. Barren-ground caribou (Rangifer tarandus groenlandicus) behaviour after recent fire events; integrating caribou telemetry data with Landsat fire detection techniques. Glob. Chang. Biol. 23, 1036–1047.

Robinson, D.J., Redding, N.J., Crisp, D.J., 2002. Implementation of a Fast Algorithm for Segmenting SAR Imagery. Salisbury, Australia.

Rossini, M., Di Mauro, B., Garzonio, R., Baccolo, G., Cavallini, G., Mattavelli, M., De Amicis, M., Colombo, R., 2018. Rapid melting dynamics of an alpine glacier with repeated UAV photogrammetry. Geomorphology 304, 159–172.

Royama, T., 1984. Population Dynamics of the Spruce Budworm Choristoneura Fumiferana. Ecol. Monogr. 54, 429–462.

Ruiz, L.A., Recio, J.A., Fernández-Sarría, A., Hermosilla, T., 2011. A feature extraction software tool for agricultural object-based image analysis. Comput. Electron. Agric. 76, 284–296.

Rusnák, M., Sládek, J., Kidová, A., Lehotský, M., 2018. Template for high-resolution river landscape mapping using UAV technology. Meas. J. Int. Meas. Confed. 115, 139–151.

Schmidtlein, S., Feilhauer, H., Bruelheide, H., 2012. Mapping plant strategy types using remote sensing. J. Veg. Sci. 23, 395–405.

Šedina, J., Pavelka, K., Raeva, P., 2017. UAV remote sensing capability for precision agriculture, forestry and small natural reservation monitoring. In: Proceedings Volume

10213, Hyperspectral Imaging Sensors: Innovative Applications and Sensor. p. 102130L–10213–12.

Senf, C., Seidl, R., Hostert, P., 2017. Remote sensing of forest insect disturbances: Current state and future directions. Int. J. Appl. Earth Obs. Geoinf. 60, 49–60.

Shadish, W.R., Zuur, A.F., Sullivan, K.J., 2014. Using generalized additive (mixed) models to analyze single case designs. J. Sch. Psychol. 52, 149–178.

Siebert, S., Teizer, J., 2014. Mobile 3D mapping for surveying earthwork projects using an Unmanned Aerial Vehicle (UAV) system. Autom. Constr. 41, 1–14.

Singh, K.K., Frazier, A.E., 2018. A meta-analysis and review of unmanned aircraft system (UAS) imagery for terrestrial applications. Int. J. Remote Sens. 00, 1–21.

Sippell, W.L., 1983. A review of the spruce budworm and its outbreak history. In: Carrow, C.J.S. and J.R. (Ed.), The Spruce Budworm Problem in Ontario -- Read or Imaginary? Proceedings of a Symposium Sponsored by the Ontario Ministry of Natural Resources and the Great Lakes Forest Research Centre under the Auspices of the Canada-Ontario Joint Forestry Research Commi. pp. 17–25.

Smith, M.W., Carrivick, J.L., Quincey, D.J., 2015. Structure from motion photogrammetry in physical geography. Prog. Phys. Geogr. 40, 247–275.

Sobel, I., Feldman, G., 1968. A 3x3 isotropic gradient operator for image processing.

Spurr, S.H., 1954. The Forests of Itasca in the Nineteenth Century as Related to Fire Published. Ecology 35, 21–25.

St-Onge, B., Audet, F.-A., Bégin, J., 2015. Characterizing the Height Structure and Composition of a Boreal Forest Using an Individual Tree Crown Approach Applied to Photogrammetric Point Clouds. Forests 6, 3899–3922.

St-Onge, B., Véga, C., Fournier, R.A., Hu, Y., Vega, C., Fournier, R.A., Hu, Y., 2008. Mapping canopy height using a combination of digital stereo-photogrammetry and lidar. Int. J. Remote Sens. 29, 3343–3364.

Stephens, G.L., Ellingson, R.G., Jr, J.., Bolton, W., Tooman, T.P., Valero, F.P.J., 2000. The Department of Energy's Atmospheric Radiation Measurement (ARM) Unmanned Aerospace Vehicle (UAV) Program. Bull. Am. Meteorol. Soc. 81, 2915–2937.

Stepper, C., Straub, C., Immitzer, M., Pretzsch, H., 2017. Using canopy heights from digital aerial photogrammetry to enable spatial transfer of forest attribute models: a case study in central Europe. Scand. J. For. Res. 32, 748–761.

Stepper, C., Straub, C., Pretzsch, H., 2014. Assessing height changes in a highly structured forest using regularly acquired aerial image data. Forestry 88, 304–316.

Sterner, T.E., Davidson, A.., 1982. Forest insect and disease conditions in Canada. Ottawa, Ont.

Stone, C., Webster, M., Osborn, J., Iqbal, I., 2016. Alternatives to LiDAR-derived canopy height models for softwood plantations: a review and example using photogrammetry. Aust. For. 79, 271–282.

Straub, C., Stepper, C., Seitz, R., Waser, L.T., 2013. Potential of UltraCamX stereo images for estimating timber volume and basal area at the plot level in mixed European forests. Can. J. For. Res. 43, 731–741.

Stroppiana, D., Villa, P., Sona, G., Ronchetti, G., Candiani, G., Pepe, M., Busetto, L., Migliazzi, M., Boschetti, M., 2018. Early season weed mapping in rice crops using multi-spectral UAV data. Int. J. Remote Sens. 00, 1–21.

Strunk, J., Temesgen, H., Andersen, H.E., Flewelling, J.P., Madsen, L., 2012. Effects of lidar pulse density and sample size on a model-assisted approach to estimate forest inventory

variables. Can. J. Remote Sens. 38, 644–654.

Tang, L., Shao, G., 2015. Drone remote sensing for forestry research and practices. J. For. Res. 26, 791–797.

Tanhuanpää, T., Saarinen, N., Kankare, V., Nurminen, K., Vastaranta, M., Honkavaara, E., Karjalainen, M., Yu, X., Holopainen, M., Hyyppä, J., 2016. Evaluating the performance of high-altitude aerial image-based digital surface models in detecting individual tree crowns in mature boreal forests. Forests 7.

Tao, W., Lei, Y., Mooney, P., 2011. Dense point cloud extraction from UAV captured images in forest area. ICSDM 2011 - Proc. 2011 IEEE Int. Conf. Spat. Data Min. Geogr. Knowl. Serv. 389–392.

The American Society for Photogrammetry & Remote Sensing, 2011. LAS 1.4 Draft Specification. ASPRS, Am. Soc. Photogramm. Remote Sens. 1–18.

Thrower, J.S., Goudie, J.W., 1992. Development of height-age and site-index functions for even-aged interior Douglas-fir in British Columbia, BC Ministry of Forests.

Tiede, D., Lang, S., Hoffmann, C., Ag, D., 2006. Supervised and forest type-specific multi-scale segmentation for a one-level-representation of single trees. In: 1st International Conference on Object-Based Image Analysis.

Tomaštík, J., Mokroš, M., Saloš, S., Chudỳ, F., Tunák, D., 2017. Accuracy of photogrammetric UAV-based point clouds under conditions of partially-open forest canopy. Forests 8.

Tompalski, P., Coops, N.C., White, J.C., Wulder, M.A., 2014. Simulating the impacts of error in species and height upon tree volume derived from airborne laser scanning data. For. Ecol. Manage. 327, 167–177.

Tompalski, P., Coops, N.C., White, J.C., Wulder, M.A., 2016. Enhancing forest growth and yield

predictions with airborne laser scanning data: Increasing spatial detail and optimizing yield curve selection through template matching. Forests 7, 1–20.

Tompalski, P., Coops, N.C., White, J.C., Wulder, M.A., Pickell, P.D., Tompalski, P., Coops, N.C., White, J.C., Wulder, M.A., Tompalski, P., Coops, N.C., White, J.C., Michael, A., Pickell, P.D., 2015. Estimating Forest Site Productivity Using Airborne Laser Scanning Data and Landsat Time Series 8992.

Tompalski, P., Coops, N.C., White, J.C., Wulder, M.A., Yuill, A., 2017. Characterizing streams and riparian areas with airborne laser scanning data. Remote Sens. Environ. 192, 73–86.

Tompalski, P., Coops, N.C., Wulder, M.A., Bailey, T., 2018. Combining Multi-Date Airborne Laser Scanning and Digital Aerial Photogrammetric Data for Forest Growth and Yield Modelling. Remote Sens. 10, 1–21.

Tompalski, P., Wężyk, P., Weidenbach, M., Kok, R. De, Hawryło, P., 2014. a Comparison of Lidar and Image-Derived Canopy Height Models for Individual Tree Crown Segmentation With Ob- Ject Based Image Analysis. South-Eastern Eur. J. Earth Obs. Geomatics 3, 1–4.

Tomppo, E., Gschwantner, T., Lawrence, M., McRoberts, R.E., 2010. National Forest Inventories Pathways for Common Reporting. Springer Netherlands.

Transport Canada, 2014. Guidance Material for Operating Unmanned Air Vehicle Systems under an Exemption.

Trumbore, S., Brando, P., Hartmann, H., 2015. Forest health and global change. Science (80-.). 349, 814–818.

Tuominen, S., Pitkänen, T., Balázs, A., Kangas, A., 2017. Improving finnish multi-source national forest inventory by 3D aerial imaging. Silva Fenn. 51, 1–21.

Turner, M.G., 2010. Disturbance and landscape dynamics in a changing world. Ecology 91,

2833–2849.

Ullah, S., Dees, M., Datta, P., Adler, P., Koch, B., 2017. Comparing airborne laser scanning, and image-based point clouds by semi-global matching and enhanced automatic terrain extraction to estimate forest timber volume. Forests 8.

van den Berg, R.A., Hoefsloot, H.C.J., Westerhuis, J.A., Smilde, A.K., van der Werf, M.J., 2006. Centering, scaling, and transformations: improving the biological information content of metabolomics data. BMC Genomics 7, 142.

van Leeuwen, M., Nieuwenhuis, M., 2010. Retrieval of forest structural parameters using LiDAR remote sensing. Eur. J. For. Res. 129, 749–770.

Vastaranta, M., Kantola, T., Lyytikäinen-Saarenmaa, P., Holopainen, M., Kankare, V., Wulder, M.A., Hyyppä, J., Hyyppä, H., 2013a. Area-based mapping of defoliation of scots pine stands using airborne scanning LiDAR. Remote Sens. 5, 1220–1234.

Vastaranta, M., Niemi, M., Wulder, M.A., White, J.C., Nurminen, K., Litkey, P., Honkavaara, E., Holopainen, M., Hyyppä, J., 2016. Forest stand age classification using time series of photogrammetrically derived digital surface models. Scand. J. For. Res. 31, 194–205.

Vastaranta, M., Wulder, M. a., White, J.C., Pekkarinen, A., Tuominen, S., Ginzler, C., Kankare, V., Holopainen, M., Hyyppä, J., Hyyppä, H., 2013b. Airborne laser scanning and digital stereo imagery measures of forest structure: Comparative results and implications to forest mapping and inventory update. Can. J. Remote Sens. 39, 382–395.

Vauhkonen, J., Ene, L., Gupta, S., Heinzel, J., Holmgren, J., Pitkänen, J., Solberg, S., Wang, Y., Weinacker, H., Hauglin, K.M., Lien, V., Packalén, P., Gobakken, T., Koch, B., Næsset, E., Tokola, T., Maltamo, M., 2012. Comparative testing of single-tree detection algorithms under different types of forest. Forestry 85, 27–40.

Véga, C., St-Onge, B., 2009. Mapping site index and age by linking a time series of canopy height models with growth curves. For. Ecol. Manage. 257, 951–959.

Véga, C., St. Onge, B., 2008. Height growth reconstruction of a boreal forest canopy over a period of 58 years using a combination of photogrammetric and lidar models. Remote Sens. Environ. 112, 1784–1794.

Vega, F.A., Ramírez, F.C., Saiz, M.P., Rosúa, F.O., 2015. Multi-temporal imaging using an unmanned aerial vehicle for monitoring a sunflower crop. Biosyst. Eng. 132, 19–27.

Vincent, L., Vincent, L., Soille, P., 1991. Watersheds in Digital Spaces: An Efficient Algorithm Based on Immersion Simulations. IEEE Trans. Pattern Anal. Mach. Intell.

Vogelmann, J.E., Tolk, B., Zhu, Z., 2009. Monitoring forest changes in the southwestern United States using multitemporal Landsat data. Remote Sens. Environ. 113, 1739–1748.

Wallace, L., Lucieer, A., Watson, C., Turner, D., 2012a. Development of a UAV-LiDAR system with application to forest inventory. Remote Sens. 4, 1519–1543.

Wallace, L., Lucieer, A., Watson, C.S., 2012b. Assessing the Feasibility of UAV-Based Lidar for High Resolution Forest Change Detection. ISPRS - Int. Arch. Photogramm. Remote Sens. Spat. Inf. Sci. 38, 499–504.

Wallace, L., Lucieer, A., Watson, C.S., 2014a. Evaluating tree detection and segmentation routines on very high resolution UAV LiDAR ata. IEEE Trans. Geosci. Remote Sens. 52, 7619–7628.

Wallace, L., Musk, R., Lucieer, A., 2014b. An assessment of the repeatability of automatic forest inventory metrics derived from UAV-borne laser scanning data. IEEE Trans. Geosci. Remote Sens. 52, 7160–7169.

Waser, L.T., Baltsavias, E., Ecker, K., Eisenbeiss, H., Feldmeyer-Christe, E., Ginzler, C.,

Küchler, M., Zhang, L., 2008. Assessing changes of forest area and shrub encroachment in a mire ecosystem using digital surface models and CIR aerial images. Remote Sens. Environ. 112, 1956–1968.

Wehr, A., Lohr, U., 1999. Airborne laser scanning—an introduction and overview. ISPRS J. Photogramm. Remote Sens. 54, 68–82.

Westoby, M.J., Brasington, J., Glasser, N.F., Hambrey, M.J., Reynolds, J.M., 2012. "Structure-from-Motion" photogrammetry: A low-cost, effective tool for geoscience applications. Geomorphology 179, 300–314.

White, J., Tompalski, P., Vastaranta, M., Wulder, M.A., Saarinen, N., Stepper, C., Coops, N.C., 2017. A model development and application guide for generating an enhanced forest inventory using airborne laser scanning data and an area-based approach. Victoria, British Columbia, Canada.

White, J.C., Coops, N.C., Wulder, M.A., Vastaranta, M., Hilker, T., Tompalski, P., 2016. Remote Sensing Technologies for Enhancing Forest Inventories: A Review. Can. J. Remote Sens. 42, 619–641.

White, J.C., Stepper, C., Tompalski, P., Coops, N.C., Wulder, M.A., 2015. Comparing ALS and Image-Based Point Cloud Metrics and Modelled Forest Inventory Attributes in a Complex Coastal Forest Environment. Forests 6, 3704–3732.

White, J.C., Tompalski, P., Coops, N.C., Wulder, M.A., 2018. Comparison of airborne laser scanning and digital stereo imagery for characterizing forest canopy gaps in coastal temperate rainforests. Remote Sens. Environ. 208, 1–14.

White, J.C., Wulder, M.A., Varhola, A., Vastaranta, M., Coops, N.C., Cook, B.D., Pitt, D., Woods, M., 2013a. A best practices guide for generating forest inventory attributes from

airborne laser scanning data using an area-based approach. For. Chron. 89, 50.

White, J.C., Wulder, M.A., Vastaranta, M., Coops, N.C., Pitt, D., Woods, M., 2013b. The Utility of Image-Based Point Clouds for Forest Inventory: A Comparison with Airborne Laser Scanning. Forests 4, 518–536.

Wold, S., 1995. PLS for multivariate linear modeling. In: Waterbeemd, H. van de (Ed.), QSAR: Chemometric Methods in Molecular Design, Methods and Principles in Medicinal Chemistry. Verlag Chemie, Weinheim, Germany, p. 195.

Wold, S., Johansson, E., Cocci, M., 1993. 3D QSAR in Drug Design; Theory, Methods, and Applications. ESCOM, Leiden, Holland.

Wold, S., Sjöström, M., Eriksson, L., 2001. PLS-regression: A basic tool of chemometrics. Chemom. Intell. Lab. Syst. 58, 109–130.

Wolter, P.T., Townsend, P.A., Sturtevant, B.R., Kingdon, C.C., 2008. Remote sensing of the distribution and abundance of host species for spruce budworm in Northern Minnesota and Ontario. Remote Sens. Environ. 112, 3971–3982.

Wood, S.N., 2011. Fast stable restricted maximum likelihood and marginal likelihood estimation of semiparametric generalized linear models. J. R. Stat. Soc. Ser. B Stat. Methodol. 73, 3–36.

Woods, M., Pitt, D., Penner, M., Lim, K., Nesbitt, D., Etheridge, D., Treitz, P., 2011. Operational implementation of a LiDAR inventory in Boreal Ontario. For. Chron. 87, 512–528.

Wulder, M.A., White, J.C., Nelson, R.F., Næsset, E., Ørka, H.O., Coops, N.C., Hilker, T., Bater, C.W., Gobakken, T., 2012. Lidar sampling for large-area forest characterization: A review. Remote Sens. Environ. 121, 196–209.

Wulder, M.A., Bater, C., Coops, N.C., Hilker, T., White, J., 2008. The role of LiDAR in sustainable forest management. For. Chron. 84, 807–826.

Wulder, M.A., White, J.C., Loveland, T.R., Woodcock, C.E., Belward, A.S., Cohen, W.B., Fosnight, E.A., Shaw, J., Masek, J.G., Roy, D.P., 2016. The global Landsat archive: Status, consolidation, and direction. Remote Sens. Environ. 185, 271–283.

Xiang, J., Chen, J., Sofia, G., Tian, Y., Tarolli, P., 2018. Open-pit mine geomorphic changes analysis using multi-temporal UAV survey. Environ. Earth Sci. 77, 1–18.

Yu, X., Hyyppa, J., Kaartinen, H., Maltamo, M., 2004. Automatic detection of harvested trees and determination of forest growth using airborne laser scanning. Remote Sens. Environ. 90, 451–462.

Yu, X., Hyyppä, J., Karjalainen, M., Nurminen, K., Karila, K., Vastaranta, M., Kankare, V., Kaartinen, H., Holopainen, M., Honkavaara, E., Kukko, A., Jaakkola, A., Liang, X., Wang, Y., Hyyppä, H., Katoh, M., 2015. Comparison of laser and stereo optical, SAR and InSAR point clouds from air- and space-borne sources in the retrieval of forest inventory attributes. Remote Sens. 7, 15933–15954.

Yu, X., Hyyppä, J., Vastaranta, M., Holopainen, M., Viitala, R., 2011. Predicting individual tree attributes from airborne laser point clouds based on the random forests technique. ISPRS J. Photogramm. Remote Sens. 66, 28–37.

Zahawi, R.A., Dandois, J.P., Holl, K.D., Nadwodny, D., Reid, J.L., Ellis, E.C., 2015. Using lightweight unmanned aerial vehicles to monitor tropical forest recovery. Biol. Conserv. 186, 287–295.

Zakrzewski, W.T., Penner, M., 2013. A comparison of tree stem taper models for use in Ontario. Sault Ste Marie, Canada.

Zarco-Tejada, P.J., Diaz-Varela, R., Angileri, V., Loudjani, P., 2014. Tree height quantification using very high resolution imagery acquired from an unmanned aerial vehicle (UAV) and automatic 3D photo-reconstruction methods. Eur. J. Agron. 55, 89–99.

Zhang, J., Sohn, G., & Brédifb, M., 2013. Single Tree Detection From Airbone Lase Scanning Data: A Stochastic Approach. ISPRS Ann. Photogramm. Remote Sens. Spat. Inf. Sci. 1, 41–46.

Zhang, B., 2006. Next Generation Automatic Terrain Extraction © 2006. Image (Rochester, N.Y.).

Zhang, J., Hu, J., Lian, J., Fan, Z., Ouyang, X., Ye, W., 2016. Seeing the forest from drones: Testing the potential of lightweight drones as a tool for long-term forest monitoring. Biol. Conserv. 198, 60–69.

Zhao, K., Suarez, J.C., Garcia, M., Hu, T., Wang, C., Londo, A., 2018. Utility of multitemporal lidar for forest and carbon monitoring: Tree growth, biomass dynamics, and carbon flux. Remote Sens. Environ. 204, 883–897.

Zitová, B., Flusser, J., 2003. Image registration methods: A survey. Image Vis. Comput. 21, 977–1000.

Zuur, A., Ieno, E.N., Meesters, E., 2009. A Beginner's Guide to R. Springer Science & Business Media.

Appendices

Appendix A

	Bohlin et al., (2012)	Jarnstedt et al., (2012)	Nurminen (2013)	Vastaranta et al., 2013	Straub et al., 2013	Rahlf et al., 2014	Pitt et al., 2014	Gobakken et al., 2015	White et al., 2015	Yu et al., 2015	Puliti et al., 2017	Kukkonen et al., 2017	Hawrylo et al., 2017	Ullah et al., 2017	Caccamo et al., 2018	Navarro et al., 2018	Iqbal et al. 2019
Camera	Lantmäteriet DMC	UltraCamXP	UltraCamD	UltraCamXP	UltraCamX	UltraCamX	Leica ADS40	UltraCamXP	UltraCamX	Z/I Imaging DMC	UltraCamXP	UltraCamXP	UltraCamXP	UltraCamXP	Canon EOS 5D Mark II	Leica RCD30	Canon EOS 5D Mark II / PhaseOne P65+
Altitude	1200 / 4800 m agl	400 m agl	1700 m asl	400 m agl	not reported	not reported	not reported	2850 m agl	4187 m agl	5000 agl	2850 agl	6000 agl	not reported	2950 m asl	600 m agl	3600 m agl	600 / 1100 m agl
Image acquisition date	September 2009	August 2009	Autumn 2007	August 2009	April 2009	Summer 2007	July & August 2007	July 2010	August, Sptember, October 2012	May 2014	July 2010	June 2013	June 2012	August 2009	February 2015	Novermber 2016	February 2015
Along-track overlap	60 / 80%	70%	60 / 80%	70%	65%	60%	100%	80%	60%	80%	60% / 80%	80%	60%	60%	75%	70%	75 / 80%
Across-track overlap	30%	30%	not reported	30%	30%	20%	30%	30%	20%	64%	30% / 40%	45%	25%	30%	60%	60%	60 / 30%
GSD (m)	0.48	0.25	0.15	0.25	0.20	0.20	0.16	0.17	0.3	0.5	0.17 / 0.51	0.35	0.25	0.1	not reported	0.35	0.11 / 0.13
Image match software	Match-T DSM 5.3.1	SocetSet NGATE	SocetSet NGATE	SocetSet NGATE	LPS eATE	SocetSet NGATE	not reported (SGM)	MATCH-T DSM	RSG	SocetSet NGATE	Agisoft Photoscan	ERDAS (SGM) / BAE (NGATE)	Agisoft Photoscan	ERDAS eATE / SGM	Agisoft Photoscan	Agisoft Photoscan	Agisoft Photoscan
Study location	Southern Sweden	Southern Finland	Central Finland	Southern Finland	Bavaria, Germany	Southeastern Norway	Central Ontario, Canada	Southeastern Norway	Western Canada	Southern Finland	Southeastern Norway	Southern Finland	Southeastern Poland	Southeastern Germany	Tasmania	Central Spain	Tasmania
Modelling approach	LM	k-NN	RF	k-NN	LM	LM	RF	LM	RF	RF	LM	LM	LM	k-NN, SVM, and LM	RF / k-NN	RF	RF
Predictors	Standard area-based metrics plus height-based texture metrics	Standard area-based predictors; varied by target attribute	23 typical metrics (height percentiles)	Standard area-based predictors; varied by target	Standard height and cover metrics, plus surface roughness	Standard height and canopy density metrics	Standard height and canopy density metrics	Standard height and canopy density metrics	Standard height and canopy density metrics	Standard height and canopy density metrics	Standard height and canopy density metrics, spectral metrics	Standard height and canopy density metrics, spectral metrics	Standard height and canopy density metrics	Standard height and canopy density metrics	Standard height and canopy density metrics	Standard height and canopy density metrics	Standard height and canopy density metrics

Appendix A: Summary of parameters used in studies comparing ALS and DAP for forest inventory attribute estimation. See Figure 7 for % RMSE comparisons.